NBS

Technical Note *No. 300*

CHARACTERISTICS OF THE EARTH-IONOSPHERE WAVEGUIDE FOR VLF RADIO WAVES

J. R. Wait and K. P. Spies

THE NATIONAL BUREAU OF STANDARDS

The National Bureau of Standards is a principal focal point in the Federal Government for assuring maximum application of the physical and engineering sciences to the advancement of technology in industry and commerce. Its responsibilities include development and maintenance of the national standards of measurement, and the provisions of means for making measurements consistent with those standards; determination of physical constants and properties of materials; development of methods for testing materials, mechanisms, and structures, and making such tests as may be necessary, particularly for government agencies; cooperation in the establishment of standard practices for incorporation in codes and specifications; advisory service to government agencies on scientific and technical problems; invention and development of devices to serve special needs of the Government; assistance to industry, business, and consumers in the development and acceptance of commercial standards and simplified trade practice recommendations; administration of programs in cooperation with United States business groups and standards organizations for the development of international standards of practice; and maintenance of a clearinghouse for the collection and dissemination of scientific, technical, and engineering information. The scope of the Bureau's activities is suggested in the following listing of its four Institutes and their organizational units.

Institute for Basic Standards. Electricity. Metrology. Heat. Radiation Physics. Mechanics. Applied Mathematics. Atomic Physics. Physical Chemistry. Laboratory Astrophysics.* Radio Standards Laboratory: Radio Standards Physics; Radio Standards Engineering.** Office of Standard Reference Data.

Institute for Materials Research. Analytical Chemistry. Polymers. Metallurgy. Inorganic Materials. Reactor Radiations. Cryogenics.** Office of Standard Reference Materials.

Central Radio Propagation Laboratory. ** Ionosphere Research and Propagation. Troposphere and Space Telecommunications. Radio Systems. Upper Atmosphere and Space Physics.

Institute for Applied Technology. Textiles and Apparel Technology Center. Building Research. Industrial Equipment. Information Technology. Performance Test Development. Instrumentation. Transport Systems. Office of Technical Services. Office of Weights and Measures. Office of Engineering Standards. Office of Industrial Services.

---

* NBS Group, Joint Institute for Laboratory Astrophysics at the University of Colorado.
** Located at Boulder, Colorado.

NATIONAL BUREAU OF STANDARDS

Technical Note 300

Issued December 30, 1964

CHARACTERISTICS OF THE EARTH-IONOSPHERE
WAVEGUIDE FOR VLF RADIO WAVES

J. R. Wait and K. P. Spies
Central Radio Propagation Laboratory
National Bureau of Standards
Boulder, Colorado

CONTENTS   Page

CHARACTERISTICS OF THE EARTH-IONOSPHERE
WAVEGUIDE FOR VLF RADIO WAVES

J. R. Wait and K. P. Spies

The principal results of this technical note are
graphical presentations of the attenuation rates, phase
velocities, and excitation factors for the dominant modes
in the earth-ionosphere waveguide. The frequency range
considered is 8 kc/s to 30 kc/s. The model adopted for
the ionosphere has an exponential variation for both the
electron density and the collision frequency, and the effect
of the earth's magnetic field is considered. Comparison
with published experimental data confirms that the minimum
attenuation of VLF radio waves in daytime is approximately at
18 kc/s, while at night it is somewhat lower. The directional
dependences of propagation predicted by the theory are also
confirmed by experimental data.

1. Introduction

It is the purpose of this technical note to present calculated
results, based on mode theory, for the attenuation, phase velocity,
and excitation factors of VLF radio waves. While a great deal of
attention has been given to the subject, quantitative information on
the modal characteristics is relatively scarce. The theory itself
is not simple and approximations must be made with care. Never-
theless, it was felt that a serious effort to produce quantitative re-
sults using a realistic model would be worthwhile.

The technical note is broken up into a number of sections which
are more or less independent. In section 2 the available information
on the D-region of the ionosphere is surveyed in a rather sketchy
manner which, however, is sufficient to select a reasonable analyti-
cal model. In section 3, reflection coefficients for the adopted ex-
ponential model are presented with a view to demonstrate concisely

the role of certain profile parameters. In section 4, the necessary
formulas of mode theory, as developed for a spherical earth-
ionosphere waveguide are given, and in section 5, the corresponding
approximations for a flat earth are discussed. In section 6, the
method for solving the spherical earth mode equation is outlined,
while section 7 contains the main numerical results which are in
graphical form. Then, in section 8, a short discussion of relevant
experimental data is given. Finally, to add a finishing touch, a
group of waveguide contour plots are appended at the end of this
technical note. These plots show the relation between the boundary
impedance of the waveguide and the propagation characteristics.

2. Selection of a Model for the Lower Ionosphere

Propagation of VLF radio waves to very great distances is made possible by the high reflectivity of the lower ionosphere at oblique incidence. The latter is due to the relatively sharp gradient of the electron density in the D-region of the ionosphere. In fact, for many purposes, the assumption of an abrupt lower edge of the ionized region has permitted an analytical approach to the problem, which has produced useful results. In the main, these are confirmed experimentally. However, a number of systematic discrepancies have been observed which suggest that the sharply bounded model is not entirely adequate.

In recent years, evidence from a number of independent experimental approaches has indicated that the profile of the electron density in the undisturbed lower ionosphere can be approximately described by an exponential function of height. Some of this evidence is indicated briefly below.

One of the best techniques currently available for the study of D-layer ionization is the partial reflection method [Belrose and Burke, 1964]. Typically, for the daytime, the profile shows two ledges of ionization which are not particularly well defined. The electron density rises fairly steeply in the region 60 km to 70 km (reaching values of the order 10^2 electrons cm^{-3}) and then does not change appreciably until the onset of the upper ledge in the height range 72 km to 76 km. The electron density increases further above this to merge with the base of the E-layer at about 85 km. Similar profiles have been measured by using the method of pulse cross modulation [Barrington, et al., 1963].

The production of the normal D-layer of the form described above is probably the combined result of Lyman-α radiation for

heights above 70 km and cosmic rays for heights below 70 km. On this basis, Nicolet and Aikin [1960] have derived theoretical profiles which seem to fit the observed profiles quite closely.

A convenient quantity to describe the characteristics of the lower ionosphere is the "conductivity parameter" ω_r which is defined by

$$\omega_r = \omega_o^2/\nu \quad , \tag{1}$$

where ω_o is the (angular) plasma frequency of the electrons and ν is the effective collision frequency.[†] The plasma frequency at a particular height is determined directly by the electron density profile. The appropriate profile for the collision frequency must also be specified. Using laboratory data for electron collisions with nitrogen Phelps and Pack [1959] have calculated the expected profile of collision frequency ν as a function of height. A curve based on his results is shown in figure 1. An average experimental curve of the collision profile deduced from partial reflection data [Belrose, 1964] and from rocket data [Kane, 1961] is also shown in figure 1. It is evident that both the theoretical and the experimental profiles are nearly exponential in form (noting that the scale is log-linear). In fact, the analytical form

$$\nu = 5 \times 10^6 \exp[-0.15(z-70)] \tag{2}$$

is a very adequate representation of the facts. This curve, which plots as a straight line on log-linear scale, is also shown in figure 1.

Using the daytime electron density data described above and the assumed exponential formula for ν, profiles of ω_r as a function of height z were calculated. These are shown in figure 2. The exponential approximation for ω_r, given by

---

[†] In this way, the effect of the energy dependence of the collision frequency is accounted for in an implicit fashion (e.g., pg. 258, Wait, 1962a].

$$\omega_r = (2.5 \times 10^5) \exp [0.3 (z - 70)] \quad , \tag{3}$$

is also shown in figure 2.

Typically, the electron density profile will change from day to day even during magnetically quiet periods. As a consequence, the profile of the conductivity parameter ω_r will be somewhat variable. This is illustrated in figure 3 where the ω_r profiles for three sucessive days in winter are shown. Here, the electron density data from Belrose [1964] are used in conjunction with (2) to deduce the ω_r values. To indicate a comparison, the exponential form given by (3) is also shown in figure 3. It is evident that the experimentally deduced profiles have some departures from the ideal form.

A very marked change in the electron density in the ionosphere is caused by solar flares. In particular, within the polar cap region (i. e., latitudes greater than 60°), effects may last up to 14 days following a large flare. These events are usually called PCA's (polar cap absorption) because of the associated effects observed at VHF. Using some data obtained from Belrose [1964] on the partial reflection method, curves of ω_r as a function of height are deduced during PCA's. These are shown in figure 4 where it is indicated that the corresponding absorptions are 0.9 and 3.0 db for 30 Mc/s transmission through the ionosphere. The upper portion of the curve for the 3-db absorption event is deduced from rocket data [Kane, 1961]. The lowermost curve in figure 4 is a typical normal midday profile which is again deduced from Belrose's [1964] partial reflection data at Ottawa.

The gross characteristics of the three experimentally deduced ω_r profiles in figure 4 are well approximated by three exponential curves as indicated in the figure. In the important height region

from 60 km to 80 km, it is evident that the difference in the curves is primarily one of a vertical shift of the ordinate. In other words, the ionosphere disturbance, apart from whatever its physical causes may be, does not lead to a significant change in the shape of the ω_r profile. The effect is a bodily lowering of the profile, which means that the reflecting height is lowered by about 10 km during a moderately strong PCA.

The polar cap-type disturbances mentioned above are caused primarily by the arrival of solar proton radiation and the associated effects are mainly restricted to regions whose magnetic latitudes are greater than 60°. Also, there are disturbances associated with magnetic impulses limited to the auroral zone which influence the level of ionization in the lower ionosphere. In addition, there are effects associated with X-radiation during a solar flare. These effects are usually short-lived and reach a maximum in a matter of minutes and persist for up to a few hours and, of course, they are confined to the sunlit hemisphere. For further details, the reader should refer to the excellent survey article by Belrose [1964] which gives many references.

Geographical variations of the electron densities are known to exist from limited measurements at different latitudes. Also, the diurnal variations at equatorial and polar latitudes differ markedly. A comprehensive picture of the global and temporal variations of the undisturbed lower ionosphere has been courageously put forth by Pierce and Arnold [1963]. They work with the balance equations which govern the production and disappearance of electrons and ions in the ionosphere. Various particle densities and rate coefficients entering into these equations must be ascertained either from direct measurements or laboratory data. After summarizing a large body of information of this kind, Pierce and Arnold [1963] are able to deduce expected electron density profiles for an undisturbed ionosphere during equinox and

and during winter solstice. These results, plotted in the form of con-
tours of equal values of ω_r, are shown in figures 5 and 6, respectively.
The ordinate in figure 5 is the height above the earth's surface and the
abscissa is the relative longitude along the equator with noon being
chosen arbitrarily as $0°$. The situation is simlar in figure 6 except
that the abscissa is the latitude for a path along a meridian.

Height profiles of the conductivity parameter ω_r corresponding
to the conditions of figures 5 and 6 are shown in figures 7a and 7b,
respectively. For the equatorial path at equinox, various profiles
for different longitudes are indicated in figure 7a. The dashed
straight lines correspond to an exponential representation for ω_r
given by

$$\omega_r = (2.5 \times 10^5) \exp \left[\beta (z - h') \right] \quad ,$$

where β is a constant and h' is a reference height. It appears
that for daytime the curve for $\beta = 0.3$ is a reasonable approximation
although some departures are certainly evident. On the other hand,
at night, a value of $\beta = 0.5$ is more representative in the important
height region where VLF waves are mainly reflected. The situation
in figure 7b is quite similar. Here, for convenience, both the latitude
and solar zenith angle χ are shown for each profile during day. At
night only the latitude is shown, of course.

In view of recent work by Arnold [1964] and Belrose, et al. [1964],
there may be some question concerning the validity of the lower portions
of the nighttime N profiles deduced by Pierce and Arnold [1963] which
are abstracted here in figures 5, 6, 7a, and 7b. However, these levels
(i. e. , heights less than 70 km) do not materially influence the re-
flection of VLF radio waves although they have a significant effect for
LF radio waves at oblique incidence. This latter statement is borne
out by a theoretical study of perturbed exponential N profiles
[Wait and Walters, 1963].

In this brief introductory survey, a large number of salient topics have not been even mentioned, such as, for example, spatial irregularities and man-made effects. Nevertheless, it is not unreasonable to suggest that a suitable analytical model for the lower ionosphere is described by an effective conductivity which varies exponentially with height. It would then seem fruitful to regard more realistic models as a perturbation about the exponential form such as investigated analytically by Wait and Walters [1963]. It might also be mentioned that heavy ions will contribute to the effective value of ω_r. In fact, provided the frequency ω is much less than ν_i (the collision frequency for the ions), the lower ionosphere may still be represented by an effective conductivity which is numerically equal to $\epsilon_o \omega_r$ (e.g., see chapter VII in Wait, 1962a).
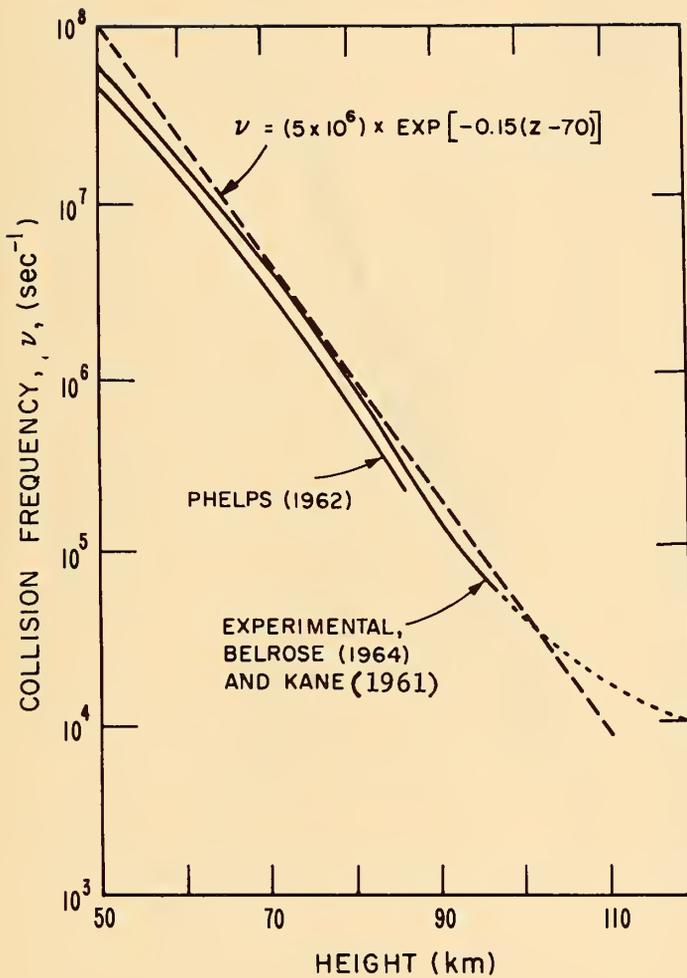
Collision frequency as a function of height in the lower ionosphere (the curve denoted Phelps [1962] was calculated by Belrose [1964] using a formula communicated by A. V. Phelps.)

FIGURE 1
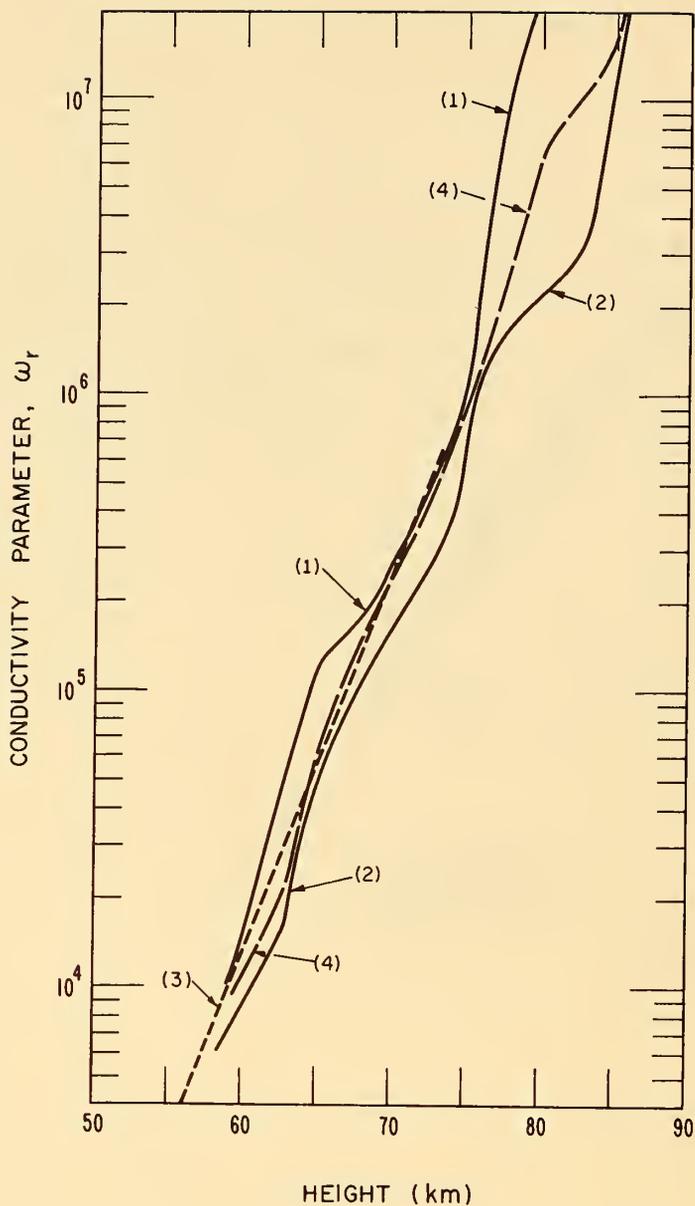
CONDUCTIVITY PARAMETER AS A FUNCTION OF HEIGHT

1) N DATA FROM BARRINGTON, THRANE AND BJELLAND [1963],
   PULSE CROSS MODULATION, 1000-1400 LST, MAR.-APR. 1960,
   KJELLER, NORWAY.

2) N DATA FROM BELROSE AND BURKE [1964], PARTIAL REFLECTION,
   1030 LST, 1 MAY 1961.

3) $\omega_r = (2.5 \times 10^5) \exp[0.3 (z-70)]$

4) N DATA FROM THEORY [NICOLET AND AIKIN, 1960] $X = 30°$
   AND MAG. LAT. $= 50°$.

FOR ABOVE CURVES, $\nu = (5 \times 10^6) \exp[-0.15 (z-70)]$

FIGURE 2
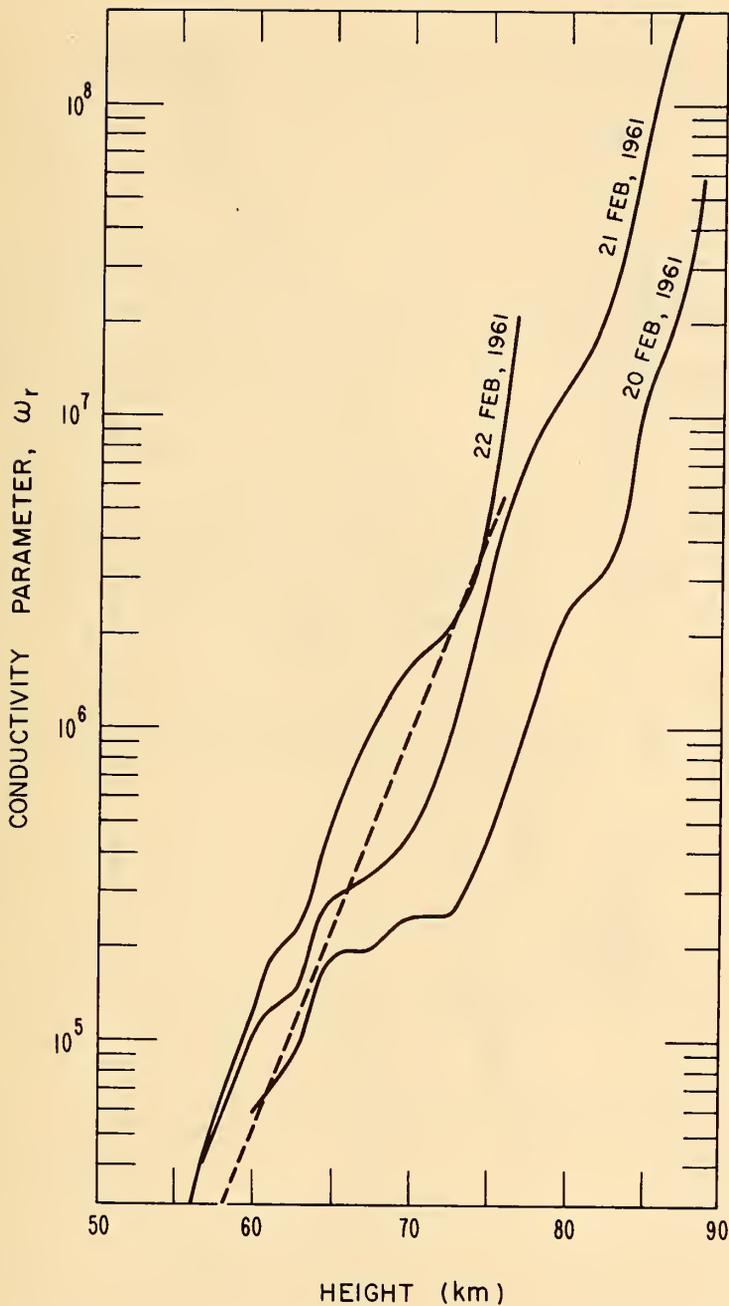
CONDUCTIVITY PARAMETER AS A FUNCTION OF HEIGHT
N DATA FOR THESE CURVES FROM BELROSE'S [1964]
PARTIAL REFLECTION EXPERIMENT ON MAGNETICALLY
QUIET DAYS IN OTTAWA ON DATES INDICATED. THE
DASHED LINE CORRESPONDS TO

$$\omega_r = (2.5 \times 10^5) \exp [0.3 (z-65)]$$

FIGURE 3
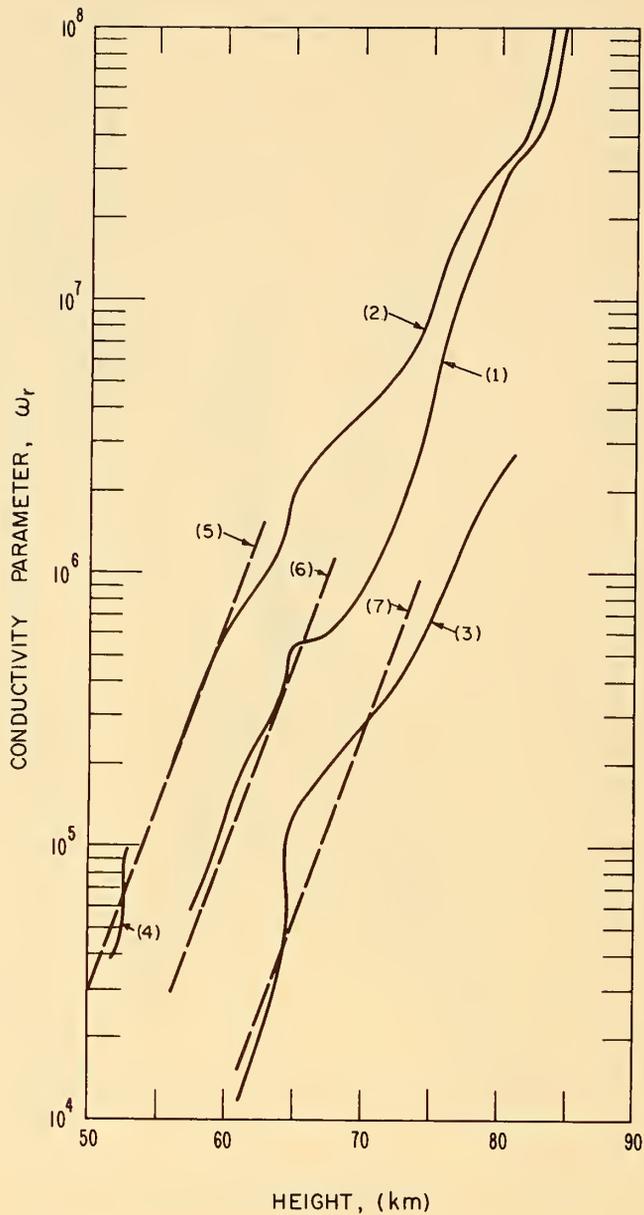
CONDUCTIVITY PARAMETER AS A FUNCTION OF HEIGHT

1)   N DATA FROM BELROSE [1964], PARTIAL REFLECTION DURING PCA
     (0.9 db AT 30 Mc/s) AT OTTAWA, 1045-1115 LST, JULY 14, 1961.

2)   N DATA FROM KANE [1961], ROCKET EXPERIMENT DURING PCA AT
     CHURCHILL (3 db AT 30 Mc/s), 1216 LST, JULY 4, 1957.

3)   N DATA FROM BELROSE [1964], PARTIAL REFLECTION, NORMAL
     MIDDAY AT OTTAWA.

4)   N DATA DURING PCA (3.0 db AT 30 Mc/s) AT OTTAWA, 1540-1600 LST.

5) $\omega_r = (2.5 \times 10^5) \exp[0.3 (z-56.5)]$

6) $\omega_r = (2.5 \times 10^5) \exp[0.3 (z-63)]$

7) $\omega_r = (2.5 \times 10^5) \exp[0.3 (z-70)]$

FOR ABOVE CURVES, $\nu = (5 \times 10^6) \exp[-0.15 (z-70)]$
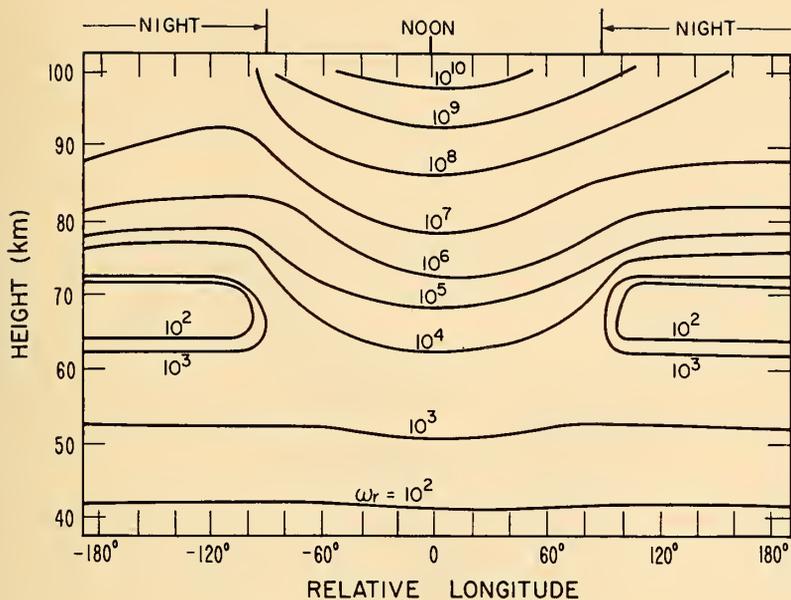
FIGURE 4

EQUATORIAL PATH AT EQUINOX -- CALCULATED ω_r CONTOURS AFTER
PIERCE AND ARNOLD [1963]

FIGURE 5
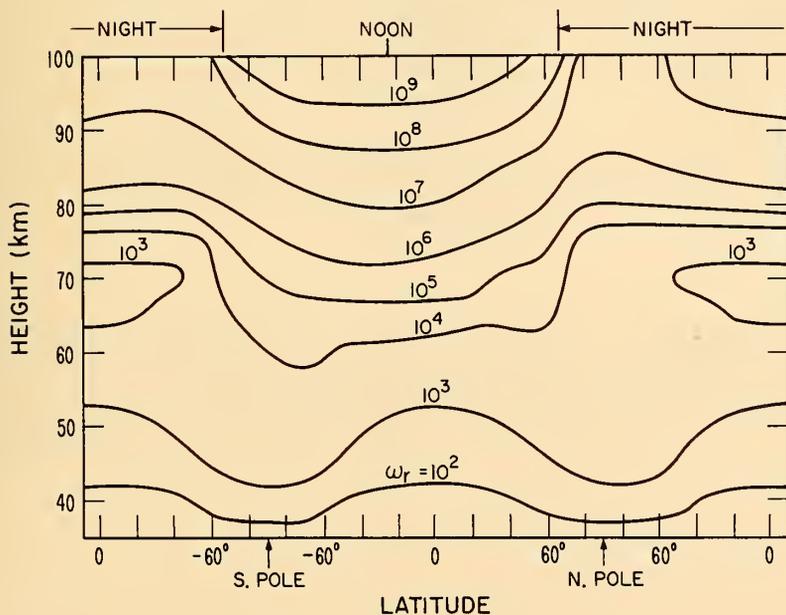
MERIDIONAL PATH AT WINTER SOLSTICE -- CALCULATED ω_r CONTOURS AFTER
PIERCE AND ARNOLD [1963]

FIGURE 6
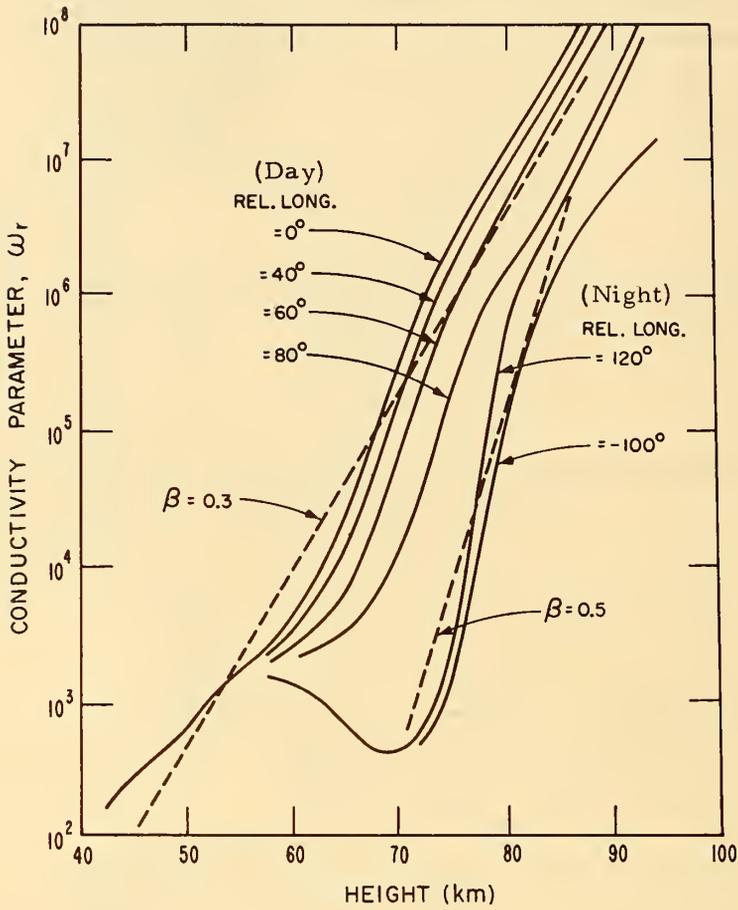
EQUATORIAL PATH AT EQUINOX -- CALCULATED ω_r PROFILES AFTER PIERCE AND ARNOLD [1963] AND IDEALIZED EXPONENTIAL CURVES

FIGURE 7a
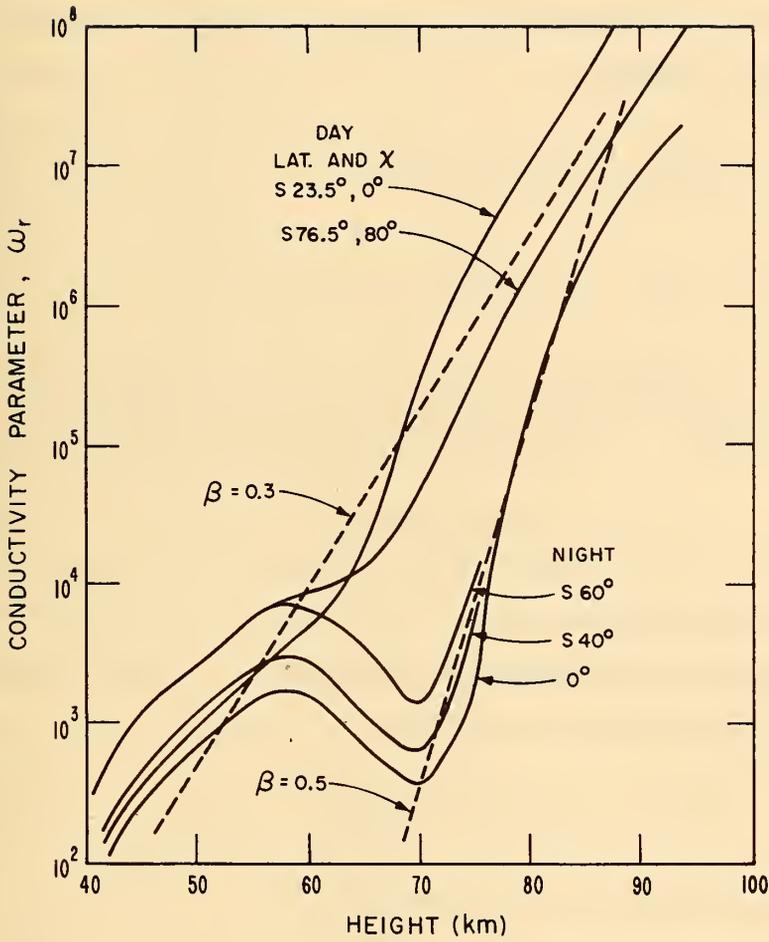
MERIDIONAL PATH AT WINTER SOLSTICE -- CALCULATED ω_r PROFILES
AFTER PIERCE AND ARNOLD [1963] AND IDEALIZED EXPONENTIAL CURVES

FIGURE 7b

3. Some Reflection Coefficients

As indicated in the previous section, both the electron density N(z) and the collision frequency $\nu(z)$ vary approximately in an exponential manner with height z above some reference level designated as z = 0. For example, in the undisturbed daytime ionosphere, we may assume

$$N(z) = N(0) \exp(bz) \tag{4}$$

and

$$\nu(z) = \nu(0) \exp(-az) \quad , \tag{5}$$

where a and b are positive constants. As a consequence, the conductivity parameter, as a function of height, has the form

$$\omega_r(z) = \omega_r(0) \exp(\beta z) \quad , \tag{6}$$

where $\omega_r(0) = \omega_o^2/\nu(0)$ and $\beta = b + a$.

Here, ω_o is the plasma frequency at the reference level z = 0 and is related to the electron density by

$$\omega_o^2 = 3.18 \times 10^9 \times N(0) \quad , \tag{7}$$

where N(0) is expressed in electrons per cm^3.

In a calculation of plane wave reflection coefficients for an exponential ionosphere of the form assumed above, it is required that the earth's magnetic field be considered. This introduces a major complexity into the problem. By using numerical techniques full wave solutions may be obtained following the methods of Budden [1961]. Another approach is to regard the ionosphere as composed of a large number of homogeneous slabs. The latter method has been exploited by Ferraro and Gibbons [1959], Johler [1963], Wait and Walters [1963, 1964], and others. If sufficient care is given to the finite

difference approximations in the full-wave method and provided fine enough slabs are chosen in the multi-slab technique, the two approaches yield identical results. A possible exception exists in the case of zero collisions which is really only of academic interest.

For the results given in this technical note, it is assumed that the terrestrial magnetic field is purely transverse. In other words, the results apply strictly only to propagation along the magnetic equator. This results in a major simplification to the calculations. Furthermore, the results are not quite as restrictive as they might seem. For arbitrary directions of propagation, it has been indicated that the transverse component of the earth's magnetic field is most important for reflection of VLF radio waves at highly oblique incidence. [Wait, 1962a]. Thus, these results may be used, at least in an approximation for arbitrary directions of propagation.

Using the method described by Wait and Walters [1964], which is essentially a multi-slab approach, some reflection coefficients were calculated for a vertically polarized plane wave at oblique incidence for an exponential model of the lower ionosphere. The earth's magnetic field was taken to be purely transverse to the direction of propagation. A convenient parameter to describe the relative importance of the earth's magnetic field is designated Ω and is defined by

$$\Omega = \omega_T / \nu(0) \quad , \tag{8}$$

where ω_T is the (angular) gyrofrequency of electrons in the earth's magnetic field. This quantity is negative for propagation from the WEST TOWARDS THE EAST, while it is positive for propagation from the EAST TOWARDS THE WEST. This magnetic field parameter Ω is used consistently in this technical note.

Specific numerical results for the reflection coefficient R are shown in figures 8a and 8b. The collision frequency profile is fixed by the constant $a = 0.15 \text{ km}^{-1}$. The exponential electron density profile is specified by the parameter b which ranges from 0.1 km^{-1} to 0.5 km^{-1}. The cosine of the angle of incidence, denoted by C, is assigned the value 0.1 corresponding to highly oblique incidence. The two sets of curves correspond to wavelengths of $\lambda = 10$ and 30 km (i.e., frequencies of 30 kc/s and 10 kc/s, respectively). The phase of the reflection coefficient R is referred to the level where $\omega_r = 2.5 \times 10^5 \text{ sec}^{-1}$. Other details of the computation and further discussion of the reflection coefficients are found in the referenced paper [Wait and Walters, 1964].

The abscissa in these figures is the magnetic parameter Ω which is the ratio of the gyrofrequency to the collision frequency at the reference height. Under typical daytime conditions, Ω would have a magnitude of about 1. It is immediately evident that the magnitude of the reflection coefficient is consistently greater for propagation from west towards the east than in the reverse direction. This nonsymmetry (i.e., nonreciprocity) is more pronounced for the large values of b corresponding to the more rapidly varying ionosphere. There is some evidence that the longer wavelengths are associated with greater nonreciprocal effects.

It may be seen in figure 8b that the phase of the reflection coefficient suffers some nonreciprocity although the effect is not great. The phase is quite sensitive to changes in the electron density gradient. In fact, for $\lambda = 10$ km, the phase shift is considerably modified when b is reduced from 0.5 to 0.1. Physically, this corresponds to a lowering of the effective reflection height. The general upward trend of the phase curves for increasing values of Ω corresponds to a

further lowering of the reflection height for propagation from east to west (as compared with propagation in the reverse direction).

It is interesting to note that the nonreciprocal characteristics of the reflection coefficient curves described here are quite similar to those deduced from the sharply bounded model with a purely transverse field [Barber and Crombie, 1959; Wait, 1962a]. In both cases, the amplitude of the reflection coefficient is higher for west-to-east propagation than in the reverse direction. However, there is one important distinction; the sharply bounded model would predict that the earth's magnetic field increases the phase shift on reflection for propagation from the west towards the east. This is just opposite to the behavior for the exponentially varying ionosphere. In both cases the nonreciprocal phase shifts are quite small relative to the magnitude of other effects. Nevertheless, it is quite important to understand these nonreciprocal phase phenomena in carrying out the interpretation of two-way experiments.

Calculations of the reflection coefficient under slightly different conditions have been carried out by Johler and Harper [1963]. In their case the earth's magnetic field was not purely transverse, but had a dip angle $I = 60^{\circ}$. Although their daytime "quiescent" model was only qualitatively similar to the exponential model, the nonreciprocal behavior of the phase was the same. For example, for 20 kc/s at a range of 1000 miles, they show that the phase shift in the west-to-east direction is greater than that in the east-to-west direction by about 6°. Recognizing that the effective transverse component of the gyrofrequency is reduced in their case, the agreement with calculations for the exponential model is quite good.

Some similar calculations have been carried out by Gossard [1963] whose daytime profile of electron density is almost exponential

in form (with $b \sim 0.15$ km^{-1}). Furthermore, his assumed collision frequency profile was nearly exponential (with $a \sim 0.15$ km^{-1}). He also considered the dip angle equal to 60°. With this model the non-reciprocal behavior of both the amplitude and the phase curves for 16 kc/s were very close to the calculations using a purely transverse component of the field. In particular, the same trend in the azimuthal dependence in the phase was observed.

For applications to mode calculations discussed in later sections, it proves to be convenient to express the reflection coefficient R in the following form

$$R = - \exp(\alpha C) \quad , \tag{9}$$

where α is, in general, a complex function of C. The latter may be written

$$\alpha = \alpha_1 + i\alpha_2 \quad , \tag{10}$$

where α_1 and α_2 are real. To illustrate the behavior of α as a function of C, the quantities α_1 and α_2 are plotted in figures 9a and 9b as a function of C in the range 0.05 to 0.30 for values of Ω from $+3$ to -3. The wavelength here was taken as 15 km (i. e., a frequency of 20 kc/s). The collision profile is again fixed by the parameter a which is 0.15 km^{-1} and the electron density profile is also fixed such that $b = 0.15$ km^{-1} (i. e., $\beta = b + a = 0.3$ km^{-1}).

It is clearly evident from the curves in figures 9a and 9b that the variation of α_1 and α_2 as a function of C, even over this wide range, is quite small. Furthermore, in the applications to mode calculations, the important range of C is from 0.1 to 0.2. Here, the total variation of α_1 is not more than two percent for Ω in the range of $+1$ to -1. The corresponding variation of α_2 is not more than eight percent.

The near constancy of α as a function of C permits calcu-
lations, for real angle of incidence, to be analytically continued
into the complex plane of C (for values of interest, C is in the
vicinity of the real axis where $\text{Re } C$ is in the range from 0.1 to 0.2).
Further justification for this procedure is given an extensive treat-
ment of the sharply bounded ionosphere where it is more convenient
to obtain higher order approximations [Spies and Wait, 1961].

The variation of α_1 and α_2 as a function of wavelength λ (in
kilometers) is shown in figures 10a and 10b where the individual
curves cover the range from -3 to +3. Here, $C = 0.1$,
$\beta = b + a = 0.3 \text{ km}^{-1}$, and $a = 0.15 \text{ km}^{-1}$, as indicated. It is
particularly interesting to note that the dependence on the magnetic
field parameter Ω is quite noticeable for the longer wavelengths.
It is also evident that the quantity α_1, which is primarily related
to attenuation, depends more strongly on Ω than does α_2, which
is primarily related to phase.

The reflection coefficients described in this section are intended
primarily as an introduction to the extensive presentation of mode
theory calculations which follows.
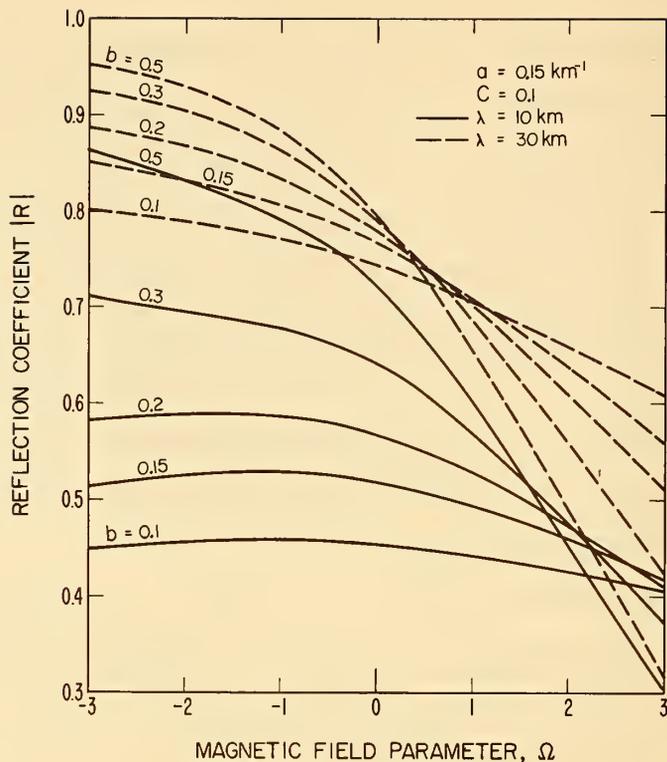
FIGURE 8a
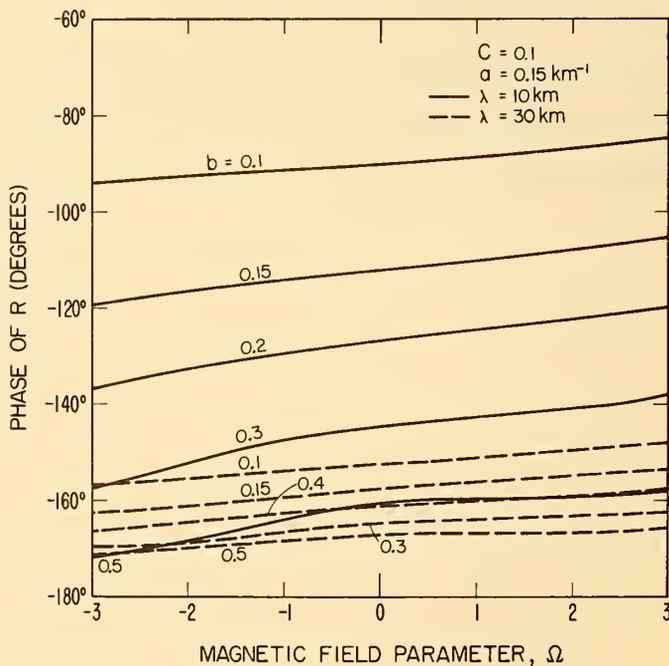
FIGURE 8b

REFLECTION COEFFICIENT R FOR A VERTICALLY POLARIZED
PLANE WAVE INCIDENT OBLIQUELY ONTO AN EXPONENTIALLY
VARYING IONOSPHERE. THE COLLISION PROFILE IS FIXED BY
$a = 0.15$ km^{-1}, WHILE THE ELECTRON DENSITY PROFILE N
IS DETERMINED BY THE PARAMETER b.

3-7
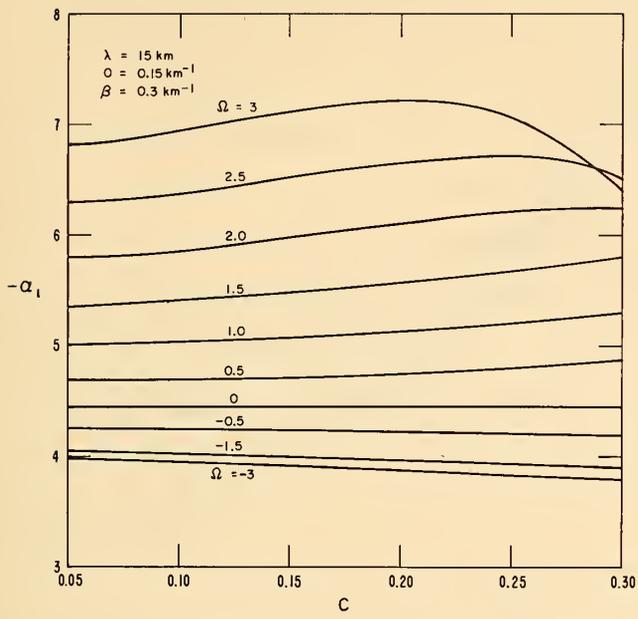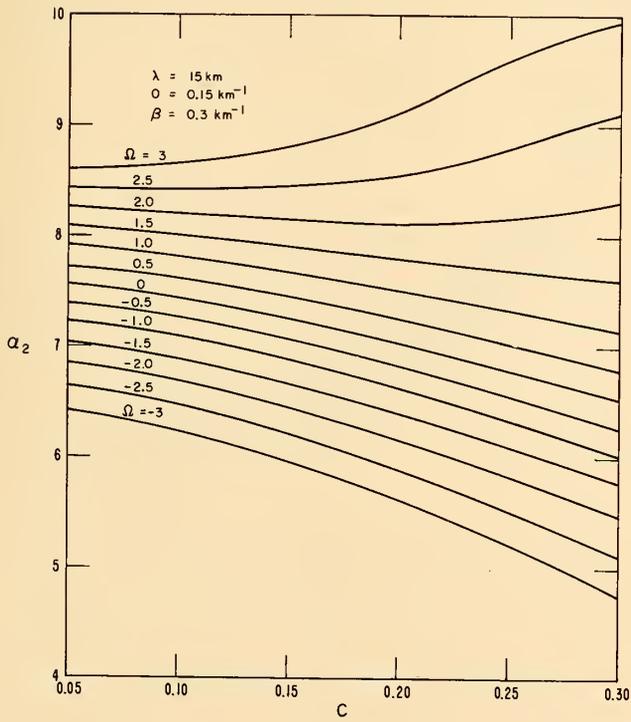
FIGURE 9a

FIGURE 9b

PARAMETERS IN THE REFLECTION COEFFICIENT
$R = - \exp\left[(\alpha_1 + i\,\alpha_2)C\right]$ SHOWING THE INFLUENCE
OF THE ANGLE OF INCIDENCE AND THE MAGNETIC
FIELD PARAMETER.
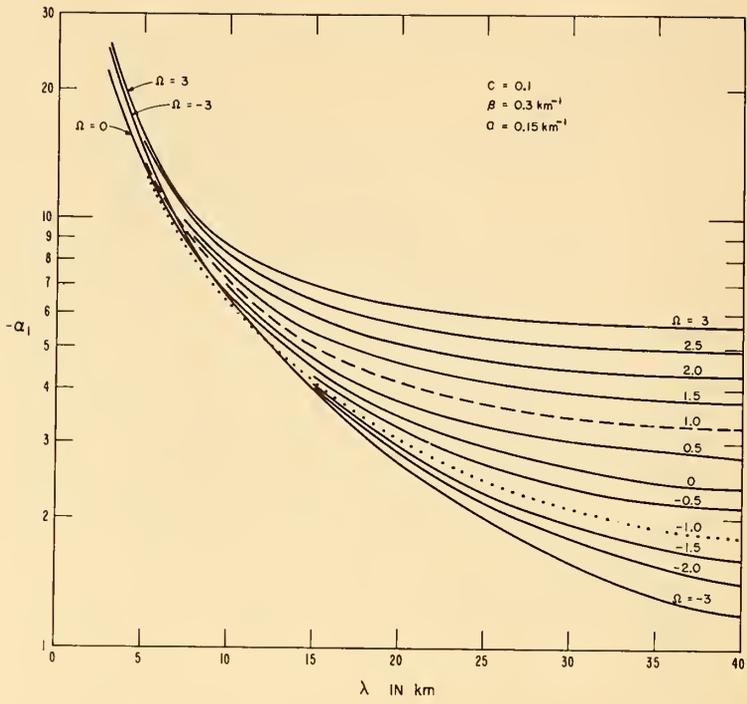
FIGURE 10a
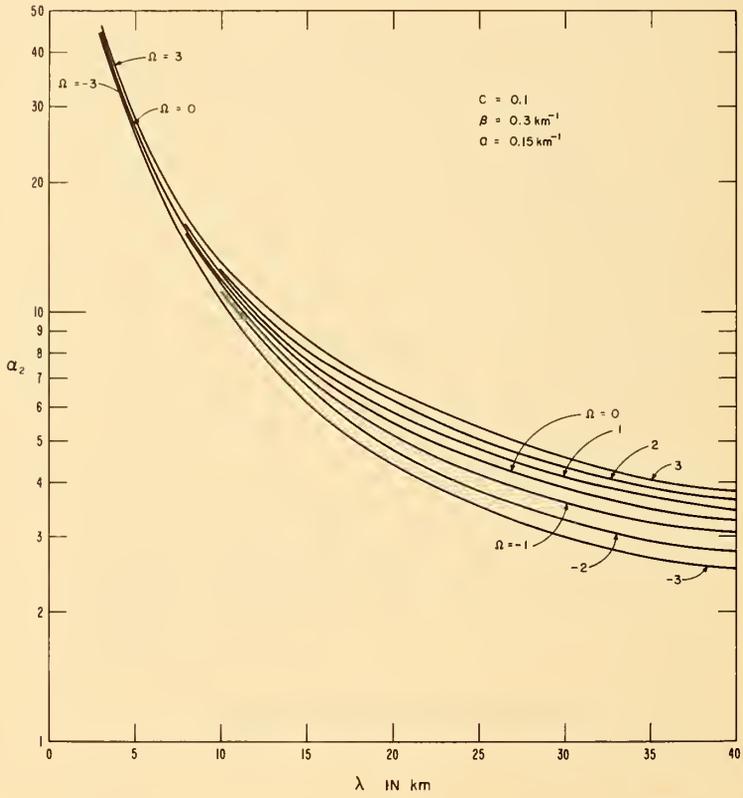
FIGURE 10b

PARAMETERS IN THE REFLECTION COEFFICIENT

$R = -\exp\left[(a_1 + i\,a_2)\,C\right]$ SHOWING THE INFLUENCE

OF THE WAVELENGTH AND THE MAGNETIC FIELD

PARAMETER.

3-9

4. Relevant Mode Theory and Some Simplifications

The model used and the derivation of the field expressions have been reported in the literature before. An accessible reference is chapter VII of a text book on the subject of waves in stratified media [Wait, 1962a]. For convenience of the reader, the relevant formulas are listed here along with explicit definitions of the pertinent factors.

The source is regarded as a vertical electric dipole on the surface of a smooth spherical earth of radius a and conductivity σ_g, and dielectric constant ϵ_g. Spherical coordinates are chosen with the dipole located at $r = a + z_o$ and $\theta = 0$. For the moment, the ionosphere is represented by a reflecting layer at $r = a + h$. The electrical properties of this shell are not specified except to say that the tangential electric and magnetic fields are related at the level $r = a + h$ by a surface impedance Z.

For harmonic time dependence, the radial component of the resultant electric field is written

$$E_r \cong \frac{e^{-ika\theta}}{a(\theta \sin \theta)^{\frac{1}{2}}} V e^{+i\omega t} \tag{11}$$

apart from a constant factor. An expression for V was derived previously [Wait, 1961] as the sum of waveguide modes. It may be written conveniently in the following form

$$V = \frac{4(\pi x)^{\frac{1}{2}}}{y_o} e^{-i\pi/4} \sum_n e^{-ixt_n} G_n(\hat{y}) G_n(y) \Lambda_n \quad , \tag{12}$$

where $x = (ka/2)^{\frac{1}{3}} \theta$, $\hat{y} = (2/ka)^{\frac{1}{3}} k z_o$, and $y = (2/ka)^{\frac{1}{3}} k(r-a)$. The other factors in this equation are discussed below.

The complex values t_n are solutions of the equation

$$1 - A(t) B(t) = 0 \quad , \tag{13}$$

where

$$A(t) = -\left[\frac{w_1'(t - y_o) + q_i\, w_1(t - y_o)}{w_2'(t - y_o) + q_i\, w_2(t - y_o)}\right] , \tag{14}$$

$$B(t) = -\left[\frac{w_2'(t) - q\, w_2(t)}{w_1'(t) - q\, w_1(t)}\right] , \tag{15}$$

$$q_i = -i(ka/2)^{\frac{1}{3}} Z/\eta_o, \qquad \eta_o = 120\,\pi, \qquad q \cong -i(ka/2)^{\frac{1}{3}}\left(\frac{i\,\epsilon_o\,\omega}{\sigma_g + i\,\epsilon_g\,\omega}\right)^{\frac{1}{2}}$$

$$\times \left(1 - \frac{i\,\epsilon_o\,\omega}{\sigma_g + i\,\epsilon_g\,\omega}\right)^{\frac{1}{2}}, \qquad \text{and} \qquad y_o = (2/ka)^{\frac{1}{3}} kh .$$

The functions $w_1(t)$ and $w_2(t)$ are Airy integral functions and the primes indicate a derivative with respect to the argument.

The functions G_n are height-gain functions and they are normalized to unity for y or y_o equal to zero. Explicitly,

$$G_n(y) = \frac{f(t_n, y)}{f(t_n, 0)} \tag{16}$$

where

$$f(t_n, y) = w_1(t_n - y) + A(t_n) w_2(t_n - y) . \tag{17}$$

The function Λ_n is a modal excitation factor [Wait, 1961]. Here it is normalized such that, in the limit of zero curvature and perfectly reflecting boundaries, it becomes unity for all modes. Under this condition

$$\Lambda_n = \frac{y_o}{2}\left[(t_n - q^2) - \frac{(t_n - y_o - q_i^2)\,[w_2'(t_n) - q\, w_2(t_n)]^2}{[w_2'(t_n - y_o) + q_i\, w_2(t_n - y_o)]^2}\right]^{-1} . \tag{18}$$

In some applications at VLF, the ionosphere may be described in terms of an effective conductivity parameter ω_r which is assumed to be constant above a certain height. On neglecting the terrestrial magnetic field and assuming that $\omega << \nu$ where ν is the collision frequency, it follows that $\omega_r = \omega_o^2/\nu$ where ω_o is the (angular) plasma frequency. Then, to within a good approximation, the surface impedance is given by [Wait, 1962a].

$$\frac{\eta_o}{Z} \cong \left(1 + \frac{\omega_r}{i\omega}\right)\left(\frac{i\omega}{\omega_r}\right)^{\frac{1}{2}} , \qquad (19)$$

being essentially independent of angle of incidence (or mode number) for grazing modes.

The use of an effective conductivity parameter ω_r which does not vary with height is strictly only valid for a sharply bounded homogeneous ionosphere. As indicated in the introduction, a more realistic ionospheric model is one in which ω_r is regarded as an exponential function of height. Then, instead of regarding $r = h$ as the height of a sharp boundary we specify that $r = h$ is the reference level in the ionosphere where the reflection coefficients are referred to. For example, it was shown before [Wait and Walters, 1963] that the oblique reflection of plane waves from a planar exponentially stratified medium could always be characterized in terms of an equivalent free-space problem. This equivalent situation could be imagined as a reflecting plane with a specified impedance boundary condition. The location of this plane is the reference surface which is referred to as $z = 0$ in the previous section.

The idea of a reference height for mode calculations in the earth-ionosphere waveguide yields a great simplification and it provides a means to adapt previous results for planar models to the more realistic spherical earth geometry. However, it is only fair to say

that there is a certain arbitrariness here in that the choice of the reference height must be selected at a level in the ionosphere where the bulk of the energy is being reflected. In other words, $r = h$ must be chosen to be effectively the upper boundary of the earth-ionosphere waveguide. Fortunately, there is some leeway in choosing this reference level. Variations by as much as ± 5 km do not materially influence the final results, provided the appropriate value of the normal surface impedance is used.

From a study of the reflection process for an isotropic exponentially stratified ionosphere [Wait and Walters, 1963], it is determined that a satisfactory choice for the reference level at VLF is where ω_r has the value 2.5×10^5 sec^{-1}. For the sake of consistency, this convention is followed for all models considered in this technical note.

To adapt previous numerical results for planar reflection coefficients to be used in conjunction with the mode equation (13), some further manipulations are needed. The procedure is outlined in what follows.

As indicated in the previous section and from earlier work [Wait, 1962a; Wait and Walters, 1963], the reflection coefficient R for a rather broad class of inhomogeneous media may be written in the form

$$R \cong - \exp(\alpha C') \quad , \tag{20}$$

where C' is the cosine of the angle of incidence and α, to a first order, is independent of C'. (Here, a prime is added to C in order to avoid confusion with the corresponding C for the ground reflection.) The result is particularly accurate at highly oblique incidence where C' is of the order of 0.1. Of course, it does not

apply at steep incidence, which is not a serious limitation for applications to mode theory. The beauty of this exponential simple form is that it provides a means to analytically continue R into the complex plane of C' once the complex value of α has been determined. It is these complex values of R which are used implicitly in mode theory. This procedure is valid since R has no poles in the vicinity of the real axis of C'.

The next step is to note that R may also be written in the form

$$R = \frac{C' - \Delta}{C' + \Delta} \quad , \tag{21}$$

which is always exact if Δ is a normalized impedance (or admittance) function which is a function of C'. For highly oblique incidence, it turns out that Δ is almost independent of C' for a broad class of continuously stratified media [Wait, 1962a]. This form for R is particularly convenient for application to the mode equation for the spherical earth-ionosphere waveguide. Now, it is not difficult to show that R as given by (21) may be written in the form

$$R = -e^{-2x} + \frac{2}{3} x^3 - \frac{4}{3} x^4 + \ldots \quad , \tag{22}$$

where $x = -\alpha C'/2$. Thus, if $|x^3|$ or $|(\alpha C')^3/8| << 1$, the two forms for R, given by (20) and (21), are equivalent. For highly oblique incidence and small values of α (i.e., R near -1), this will be a particularly good approximation.

Unfortunately, in certain areas of practical interest, the product $\alpha C'$ may be comparable with unity. However, even then, the error introduced in assuming an equivalence between the two forms for R is not great. To reduce this error still further, a correction is made as follows. The two expressions as given by (20) and (21) are equated.

Thus,

$$- \exp(\alpha C') = \frac{C' - \Delta}{C' + \Delta} \,, \tag{23}$$

which is deceptively simple. The numerical reflection coefficient
data are given in terms of complex values of α. For application
to the mode equation, the corresponding complex value of Δ is
needed. As indicated by (22), one simply has $\Delta = -2/\alpha$ if
$|(\alpha C')^3/8| << 1$.

For low order or grazing-type modes, C' may be approximated
by the real quantity $(2h/a)^{\frac{1}{2}}$ where h is the reference reflecting
height. Then, the identity given by (23) now may be written

$$- \exp\left[\alpha(2h/a)^{\frac{1}{2}}\right] \cong \frac{(2h/a)^{\frac{1}{2}} - \Delta}{(2h/a)^{\frac{1}{2}} + \Delta} \,. \tag{24}$$

This should be a definite improvement on using the simple connection
mentioned in the previous paragraph, despite the fact that C' is
crudely approximated.

The exponential ionospheric models used in the present technical
note were described in section 3. For purely transverse
propagation (i.e., along the magnetic equator), complex values of
α are taken directly from the work of Wait and Walters [1964]. They
are listed in table 1 for frequencies from 8 kc/s to 30 kc/s, where
the entries α_1 and α_2 are real and defined by $\alpha = \alpha_1 + i\alpha_2$. The
corresponding values of Δ are given in tables 2, 3, 4, and 5 for the
reference heights h, as indicated. The entries A and B are
real and defined by

$$\Delta = -2(iA - B)^{-1} \tag{25}$$

or

$$A + iB = 2i/\Delta \,. \tag{26}$$

The entries in tables 1 to 5 are accurate to the number of digits indicated. The method of calculation is discussed in the quoted reference [Wait and Walters, 1964].

In summary, the calculations given in this technical note are strictly correct for an earth-ionosphere waveguide which is bounded by a homogeneous smooth earth and a reflecting layer at height h with a normalized surface impedance Δ. The applicability of the results to an actual diffusely bounded ionosphere requires a number of approximations which are justified mainly on physical grounds. The principal assumption is that Δ is assumed at the outset and then the mode equation is solved to yield the propagation characteristics. A fundamental question may arise in that the angle of incidence is complex for modes in a lossy waveguide. However, it is fortunate that the cosine C' of the angle of incidence at the ionosphere is approximately equal to $(2h/a + C^2)^{\frac{1}{2}}$ where C is related to the parameter t, in (13), by

$$(ka/2)^{1/3} C = (-t)^{\frac{1}{2}} .$$

For all the important modes, $|C^2| << 2h/a$ and, thus, C' is approximately equal to $(2h/a)^{\frac{1}{2}}$ as assumed above. A small refinement is to use the above form for C' to obtain a modified value of Δ (or α) which is then employed in conjunction with the contour plots in section 12 to yield corrected values of the propagation parameters. The resulting corrections appear to be negligible for any situation considered in this technical note.

Tabulated Reflection Coefficient Data

Table 1

f (kc/s)	Isotropic Model ($\beta = 0.5$ km⁻¹)		Anisotropic Model $\Omega = -1$ ($\beta = 0.3$ km⁻¹) ($a = 0.15$ km⁻¹)		Isotropic Model ($\beta = 0.3$ km⁻¹)		Anisotropic Model $\Omega = +1$ ($\beta = 0.3$ km⁻¹) ($a = 0.15$ km⁻¹)	
	α_1	α_2	α_1	α_2	α_1	α_2	α_1	α_2
8	-2.280	2.497	-1.860	3.127	-2.448	3.403	-3.294	3.618
10	-2.306	2.538	-2.130	3.580	-2.676	3.903	-3.493	4.169
12	-2.378	2.654	-2.462	4.121	-2.965	4.481	-3.745	4.788
14	-2.488	2.821	-2.837	4.731	-3.298	5.117	-4.037	5.455
16	-2.625	3.025	-3.245	5.395	-3.664	5.801	-4.362	6.157
18	-2.785	3.258	-3.669	6.103	-4.052	6.523	-4.713	6.888
20	-2.965	3.558	-4.106	6.843	-4.456	7.274	-5.085	7.642
22	-3.161	3.796	-4.551	7.610	-4.872	8.048	-5.473	8.414
24	-3.369	4.143	-4.999	8.395	-5.295	8.839	-5.875	9.199
26	-3.589	4.408	-5.450	9.194	-5.723	9.642	-6.287	9.995
28	-3.817	4.794	-5.901	10.002	-6.155	10.454	-6.707	10.798
30	-4.051	5.079	-6.353	10.816	-6.589	11.272	-7.134	11.606

Table 2
Isotropic Model - Exponential Profile
($\beta = 0.5$ km⁻¹)

f (kc/s)	h = 60 km		h = 70 km		h = 80 km		h = 90 km	
	B	A	B	A	B	A	B	A
8	2.327	2.460	2.335	2.453	2.343	2.447	2.351	2.440
10	2.356	2.498	2.364	2.492	2.372	2.485	2.380	2.478
12	2.435	2.611	2.444	2.604	2.454	2.596	2.463	2.588
14	2.556	2.772	2.567	2.763	2.578	2.755	2.589	2.746
16	2.708	2.967	2.722	2.957	2.735	2.947	2.749	2.937
18	2.889	3.190	2.906	3.177	2.923	3.165	2.939	3.152
20	3.098	3.475	3.120	3.460	3.142	3.445	3.163	3.430
22	3.322	3.695	3.349	3.677	3.375	3.658	3.400	3.639
24	3.577	4.021	3.611	3.998	3.645	3.975	3.678	3.951
26	3.839	4.259	3.879	4.230	3.919	4.201	3.958	4.171
28	4.135	4.613	4.186	4.578	4.237	4.542	4.287	4.504
30	4.429	4.859	4.489	4.816	4.548	4.771	4.607	4.724

NOTE:

$$q_i = i2\left(\frac{ka}{2}\right)^{\frac{1}{3}}\frac{1}{-B+iA} = 2\left(\frac{ka}{2}\right)^{\frac{1}{3}}\frac{1}{A+iB}$$

Table 3
Anisotropic Model - Exponential Profile
($\Omega = -1$, $\beta = 0.3$ km⁻¹, $a = 0.15$ km⁻¹)

f (kc/s)	h = 60 km		h = 70 km		h = 80 km		h = 90 km	
	B	A	B	A	B	A	B	A
8	1.937	3.122	1.950	3.121	1.962	3.120	1.975	3.119
10	2.245	3.572	2.264	3.570	2.283	3.568	2.303	3.565
12	2.639	4.106	2.669	4.102	2.699	4.098	2.729	4.093
14	3.106	4.704	3.152	4.696	3.198	4.688	3.244	4.678
16	3.647	5.346	3.716	5.332	3.785	5.316	3.854	5.298
18	4.255	6.019	4.355	5.994	4.456	5.966	4.557	5.933
20	4.936	6.707	5.078	6.664	5.221	6.615	5.363	6.559
22	5.696	7.395	5.892	7.323	6.088	7.240	6.282	7.146
24	6.542	8.063	6.804	7.948	7.063	7.814	7.317	7.661
26	7.480	8.692	7.819	8.512	8.150	8.302	8.468	8.063
28	8.514	9.259	8.939	8.985	9.343	8.667	9.722	8.306
30	9.644	9.736	10.155	9.332	10.627	8.867	11.047	8.347

Table 4

Isotropic Model - Exponential Profile

$(\beta = 0.3 \text{ km}^{-1})$

f	h = 60 km		h = 70 km		h = 80 km		h = 90 km	
(kc/s)	B	A	B	A	B	A	B	A
8	2.558	3.365	2.577	3.358	2.595	3.351	2.613	3.343
10	2.838	3.858	2.865	3.849	2.893	3.839	2.920	3.829
12	3.206	4.423	3.247	4.411	3.288	4.398	3.328	4.384
14	3.654	5.041	3.714	5.023	3.774	5.004	3.834	4.983
16	4.179	5.696	4.266	5.669	4.353	5.639	4.440	5.606
18	4.781	6.374	4.904	6.332	5.028	6.286	5.151	6.234
20	5.465	7.061	5.636	6.996	5.807	6.923	5.976	6.840
22	6.237	7.741	6.467	7.640	6.696	7.525	6.921	7.395
24	7.102	8.394	7.405	8.241	7.701	8.063	7.989	7.861
26	8.067	9.001	8.452	8.770	8.822	8.501	9.173	8.197
28	9.134	9.535	9.607	9.194	10.050	8.799	10.455	8.354
30	10.300	9.968	10.859	9.477	11.361	8.914	11.794	8.289

Table 5

Anisotropic Model - Exponential Profile

$(\Omega = +1, \quad \beta = 0.3 \text{ km}^{-1}, \quad a = 0.15 \text{ km}^{-1})$

f	h = 60 km		h = 70 km		h = 80 km		h = 90 km	
(kc/s)	B	A	B	A	B	A	B	A
8	3.437	3.500	3.459	3.479	3.482	3.458	3.504	3.436
10	3.707	4.030	3.741	4.004	3.775	3.978	3.808	3.951
12	4.060	4.620	4.112	4.587	4.162	4.553	4.212	4.518
14	4.494	5.247	4.568	5.204	4.641	5.159	4.714	5.111
16	5.007	5.897	5.112	5.839	5.216	5.777	5.318	5.710
18	5.604	6.556	5.749	6.475	5.891	6.387	6.031	6.292
20	6.288	7.209	6.483	7.096	6.673	6.970	6.858	6.833
22	7.064	7.841	7.319	7.679	7.565	7.499	7.802	7.300
24	7.936	8.433	8.260	8.203	8.569	7.944	8.858	7.658
26	8.907	8.963	9.306	8.637	9.676	8.270	10.012	7.866
28	9.975	9.405	10.447	8.950	10.870	8.440	11.233	7.884
30	11.132	9.732	11.667	9.110	12.119	8.419	12.475	7.679

5. The Flat-Earth Limit

Because of the complexity of the working formulas for the field expressions, it is desirable to examine the limiting behavior for a flat earth. In this way, some physical insight into the general results are obtained.

The flat-earth mode theory is obtained as a special case of the spherical-earth mode theory when the following approximations hold:

$$\left| C_n \left(\frac{ka}{2} \right)^{\frac{1}{3}} \right| >> 1 \quad \text{and} \quad \left| C_n^2 \right| >> \frac{h}{a} \quad ,$$

where

$$C_n = (-t_n)^{\frac{1}{2}} [2/(ka)]^{\frac{1}{3}}$$

is the cosine of a complex angle associated with the n'th-order mode in a parallel-plate waveguide.

In this limiting case, it is found that C_n are roots of the mode equation

$$R_i(C) \, R_g(C) \, \exp(-i \, 2kh\,C) = \exp(-i \, 2\pi n) \quad , \tag{27}$$

where

$$R_i(C) = \frac{C - \Delta}{C + \Delta} \quad , \quad \Delta = Z/\eta_o \quad , \tag{28}$$

and

$$R_g(C) = \frac{C - \Delta_g}{C + \Delta_g} \quad , \quad \Delta_g = \left(\frac{i \epsilon_o \omega}{\sigma_g + i \epsilon_g \omega} \right)^{\frac{1}{2}} \left(1 - \frac{i \epsilon_o \omega}{\sigma_g + i \epsilon_g \omega} \right)^{\frac{1}{2}} \quad . \tag{29}$$

As in the spherical-earth problem, the normalized surface impedance is a function of C but for highly oblique incidence (i.e., low-order modes) it may be regarded as a constant.

The excitation factor may now be written in the following
form:

$$\Lambda_n = \delta_n \frac{C_n^2}{C_n^2 - \Delta_g^2} \quad , \tag{30}$$

where

$$\delta_n = \left[1 + i \frac{\partial(R_i R_g)/\partial C}{2 k h R_i R_g}\right]^{-1}_{C = C_n} . \tag{31}$$

The above result [Wait, 1962a] for Λ_n can be obtained as a limiting
case of (18) for $a \to \infty$ or it can be derived directly using a flat-
earth model at the outset [Wait, 1962a].

We now make the exponential approximation to the reflection co-
efficient, namely,

$$R_i \cong - \exp(\alpha C) \tag{32}$$

where α may be regarded as a complex quantity. The approximate
solutions of (27) are then given by [Wait, 1962a]

$$C_n \cong \frac{\pi(2n - 1) + 2 \exp(i 3\pi/4) G^{\frac{1}{2}}(C_n^o)^{-1}}{2 k h + i \alpha} \quad , \tag{33}$$

where

$$G = \frac{\epsilon_o \omega}{\sigma_g + i \epsilon_g \omega} \quad ,$$

and

$$C_n^o = \frac{\pi(2n - 1)}{k h} \quad .$$

The attenuation in nepers per unit distance is then equal to $- k \, \text{Im} \, S_n$
where $S_n = (1 - C_n^2)^{\frac{1}{2}} \cong 1 - C_n^2/2$. In a similar fashion, it is
seen that the phase velocity, relative to c, is $1/[\text{Re} \, S_n]$. The latter

quantity, designated v/c, is close to unity.

A relatively simple flat-earth formula for Λ_n is obtained from (30) under the assumption that Δ and Δ_g are independent of C. Thus,

$$\Lambda_n \cong \cfrac{1}{1 + i\cfrac{\Delta}{kh\left(C_n^2 - \Delta^2\right)} + i\cfrac{\Delta_g}{kh\left(C_n^2 - \Delta_g^2\right)}} \; \cfrac{C_n^2}{C_n^2 - \Delta_g^2} \qquad (34)$$

or, even more simply,

$$\Lambda_n \cong \cfrac{1}{1 + i\cfrac{\alpha}{2kh} + i\cfrac{\Delta_g}{kh\,C_n^2}} \quad , \qquad (35)$$

when

$$\left| \Delta_g^2 \right| << \left| C_n^2 \right| \quad .$$

The resulting formulas given in this section are directly applicable to ELF (extremely low frequency) studies [Wait, 1962b]. However, they serve as a useful check on the curved earth VLF calculations since, at frequencies below 10 kc/s, the flat-earth approximations are not seriously violated.

6. Method of Solving the Spherical-Earth Mode Equation

The principal task of this work was the determination of the roots of the mode equation

$$1 - A(t) \, B(t) \; = \; 0 \quad , \tag{36}$$

where $A(t)$ and $B(t)$ are given by (14) and (15). These roots were found by an application of the well-known Newton's method, the numerical calculations being performed on a high-speed digital computer (IBM 7090).

According to Newton's method, if t_o is an approximate root of (36), the next approximation is given by $t_o + \Delta t$ where

$$\Delta t \; = \; - \left[\frac{A(t) \, B(t) - 1}{\frac{\partial}{\partial t} \, [A(t) \, B(t)]} \right]_{t = t_o} . \tag{37}$$

By making use of the Wronskian relation

$$w_1'(Z) \, w_2(Z) \; - \; w_1(Z) \, w_2'(Z) \; = \; 2 \, i \quad , \tag{38}$$

it is not difficult to show that

$$\Delta t \; = \; \frac{A(t_o) \, B(t_o) - 1}{\dfrac{2 \, i \, (t_o - q^2)}{[w_1'(t_o) - q \, w_1(t_o)]^2} \, A(t_o) \; + \; \dfrac{(2 \, i \, q_i^2 - t_o + y_o)}{[w_2'(t_o - y_o) + q_i \, w_2(t_o - y_o)]^2} \, B(t_o)} . \tag{39}$$

Repeated applications of the method were used until $|\Delta t| \leq 10^{-5}$.

Successful use of Newton's technique requires a sufficiently good choice for the first approximation to the root of the mode equation.

This problem was solved in the following way. The first step was finding roots of the mode equation when $q = 0$ and $q_i = \infty$, i.e., for perfectly reflecting boundaries of the earth-ionosphere waveguide. Under these conditions, mode equation (36) reduces to

$$\frac{w_2'(t)}{w_1'(t)} \frac{w_1(t - y_o)}{w_2(t - y_o)} = 1 \ . \tag{40}$$

The only modes of physical interest are those which propagate without attenuation; these correspond to <u>real</u> roots of (40). For real arguments, it turns out that

$$\frac{w_2'(t)}{w_1'(t)} = \exp\left[2 i \tan^{-1}\left(\frac{A i'(t)}{B i'(t)}\right)\right] \tag{41}$$

and

$$\frac{w_1(t - y_o)}{w_2(t - y_o)} = \exp\left[- 2 i \tan^{-1}\left(\frac{A i(t - y_o)}{B i(t - y_o)}\right)\right] \ , \tag{42}$$

where the inverse tangents are continuous functions of t such that

$$\tan^{-1}\left(\frac{A i'(0)}{B i'(0)}\right) = -\frac{\pi}{6} \quad \text{and} \quad \tan^{-1}\left(\frac{A i(0)}{B i(0)}\right) = \frac{\pi}{6} \ . \tag{43}$$

Noting that $e^{-i 2 n \pi} = 1$, mode equation (40) for perfectly reflecting boundaries may be written as

$$\tan^{-1}\left(\frac{A i'(t)}{B i'(t)}\right) - \tan^{-1}\left(\frac{A i(t - y_o)}{B i(t - y_o)}\right) = -n\pi \ (n = 1, 2, 3, \dots) \ . \tag{44}$$

By plotting the left-hand member of (44) versus t, one may obtain approximate solutions of the mode equation for perfectly reflecting boundaries. Note that these solutions are functions only of frequency

and ionospheric height (since $y_o = \left(\dfrac{2}{ka}\right)^{\frac{1}{3}} kh$).

The second step was finding roots of the mode equation for perfectly conducting ground (i.e., q = 0) and specified values of the (complex) parameter Δ (which depends on the ionospheric model, as well as on frequency and ionospheric height). To accomplish this, a sequence of Δ values was chosen, starting with $\Delta = \infty$ (corresponding to perfectly reflecting boundaries) and ending with the desired value of Δ. (As a practical matter, this sequence was chosen so that the real and imaginary parts of $(1/\Delta)$ changed by about 0.5 from one element of the sequence to the next.) Starting with the approximate roots obtained by graphical means, Newton's method was used to find roots of the mode equation for the first Δ value in the sequence. These roots were, in turn, used as starting values in finding roots for the second Δ value in the sequence, and so on until roots corresponding to the final Δ value were found.

The final step consisted of solving the mode equation for specified finite values of ground conductivity and specified values of the parameter Δ. This was accomplished by choosing a sequence of ground conductivity values starting with a large value and ending with the desired value. (As a practical matter, the values used were 100, 50, 20, 10, 5, 2, and 1 millimho/meter.) Starting with roots corresponding to $\sigma_g = \infty$ and specified values of frequency, height and Δ, Newton's method was used to find roots of the mode equation for the first σ_g value in the sequence. These roots were next used as starting values in finding roots for the second σ_g value in the sequence, and so on until roots corresponding to the final σ_g value were found. The relative dielectric constant ϵ_g/ϵ_o of the ground was taken to be 15.

7. Graphical Presentation of Mode Characteristics

Using the method outlined in section 6, a fairly extensive set of calculations was prepared for a selected range of the pertinent parameters. A sampling of these results is shown here in graphical form in figures 11a to 38. The specific quantities considered are the attenuation rate in decibels per 1000 km of path length, the departure of the phase velocity ratio v/c from unity, and the excitation factor Λ. These quantities are plotted consistently as a function of frequency from 8 kc/s to 30 kc/s. In most cases, the results are shown both for mode numbers $n = 1$ and 2, which are the modes of lowest attenuation for the frequency range indicated.

For the curves shown in figures 11a to 38,

a) ω_r (or ω_o^2/v) profile varies as $\exp(\beta z)$ as a function of height z,

b) h is the height of the reference level above the earth's surface (i.e., where ω_r takes the value $2.5 \times 10^5 \text{ sec}^{-1}$).

c) σ_g is the conductivity of the ground and is expressed in milli-mhos/m.

Under the isotropic assumption (i.e., neglect of earth's magnetic field), only the ω_r (or ω_o^2/v) profile need be specified. Thus, in figures 11a to 30b, the profile is fully specified by the parameter β which is assigned to be 0.5 km^{-1}. However, for the anisotropic model, the collision profile v, in addition to the ω_r profile must be considered. Noting that these vary as $\exp(\beta z)$ and $\exp(-az)$, respectively, it is necessary to specify both β and a. For the curves shown in figures 31a to 38, β is assigned the value 0.3 km^{-1}, while a is assigned the value 0.15 km^{-1}. The magnetic field parameter Ω assumes the values -1 and $+1$ which correspond to propagation along the magnetic equator from

WEST-TO-EAST and from EAST-TO-WEST, respectively.[†] In this case, the gyrofrequency ω_T for the transverse d-c magnetic field is equal to the collision frequency ν at the reference height (since $|\Omega| = \omega_T/\nu$). Of course, when $\Omega = 0$ for the middle set of curves in figures 31a to 38, the earth's magnetic field is zero. Thus, these curves differ from figures 11a to 30b only in that β is 0.3 km^{-1} in place of 0.5 km^{-1}.

There is a considerable amount of information in the curves in figures 11a to 38 and it would be possible to discourse on these at length. However, many of the features are self evident and the interested reader might find it worthwhile to glance at these one by one. If he is reasonably perceptive he will notice a number of interesting points. For example:

a) The lowest attenuation of mode 1 in the daytime (i.e., h $\simeq$ 70 km) is at a frequency of 18 kc/s for both $\beta = 0.3$ km^{-1} and 0.5 km^{-1}.

b) The lowest attenuation of mode 1 at nighttime (i.e., h $\sim$ 90 km) is around 12 kc/s for both $\beta = 0.3$ km^{-1} and 0.5 km^{-1}.

c) In general, attenuation is lower for propagation from WEST-TO-EAST than from EAST-TO-WEST.

d) For daytime heights (h $\sim$ 70 km), the attenuation rate of mode 1 is always less than the attenuation rate of mode 2. At nighttime, (h $\sim$ 90 km), the attenuation rates may be of the same order.

e) In general, the attenuation rates for $\beta = 0.3$ and 0.5 are of the same order except at the higher end of the frequency range where the $\beta = 0.3$ curves show a decisive upward trend.

f) The magnitude of the excitation factor of mode 1 diminishes with increasing frequency with the effect being more pronounced at night.

_____

[†] At nighttime the effective value of Ω may be considerably greater than one.

g)   The phase velocity ratio v/c of mode 1, in daytime, is greater
      than one for frequencies less than about 14 kc/s and less
      than one for higher frequencies.   At nighttime, the cross-over
      point is more like 10 kc/s.

h)   The effect of finite ground conductivity is to increase the attenu-
      ation rates, particularly for mode 2.

i)   Finite ground conductivity results in a slightly decreased phase
      velocity for both modes 1 and 2.

j)   Finite ground conductivity tends to increase the magnitude of
      the excitation factor,

and so on.

   The results shown graphically in figures 11a to 38 are based on
the full solution of the spherical-earth mode equation.   The results
are believed to be accurate for the model specified to well within
one's ability to read numerical values from the graphs.   While the
parameters and adopted conventions are slightly different, the curves
may be compared in a few cases with other published work [Wait and
Spies, 1960; Spies and Wait, 1961; Krasnushkin, 1962; Wait, 1963;
Galejs, 1964].   In particular, the work of Galejs [1964] corresponds
to an exponential ionosphere where β = 0.291 which is sufficiently
close to our value of β = 0.3 to permit a useful comparison even
though the reference heights do not coincide.   As Galejs points out,
our choice of a reference height (i.e., where ω_r = 2.5 × 10^5) is
somewhat arbitrary.   This reference height is really the upper
boundary of the equivalent sharply bounded waveguide.   Ideally,
changes of this parameter with appropriate modification of the equiv-
alent surface impedance should not change the final results.   A
reference height chosen to have this property may be described as
optimum.   A study of this question, which is confirmed by the re-
sults of Galejs' calculations indicates that our choice is not far from
optimum.
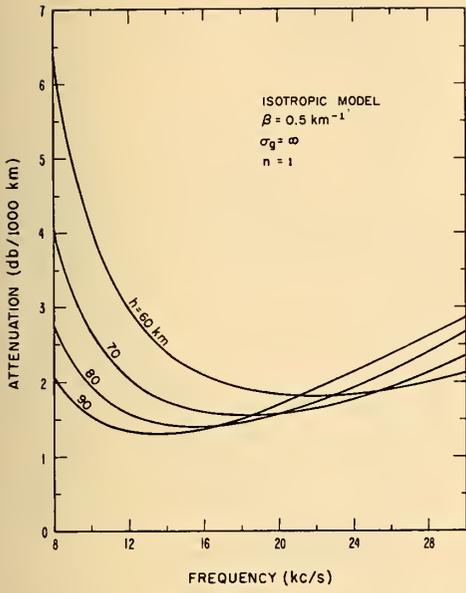
FIGURE 11a
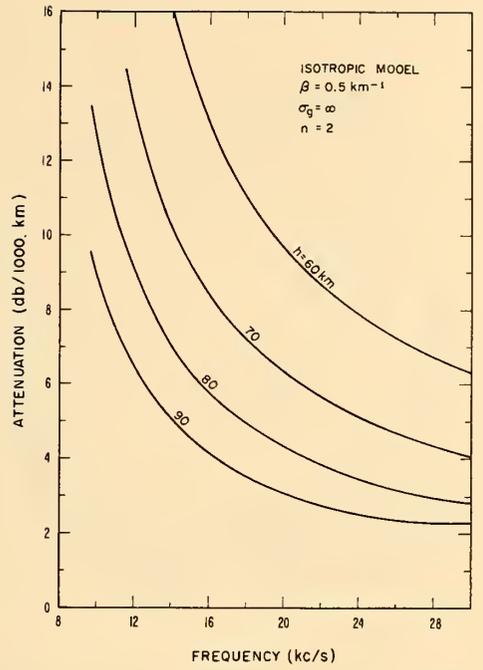
FIGURE 11b
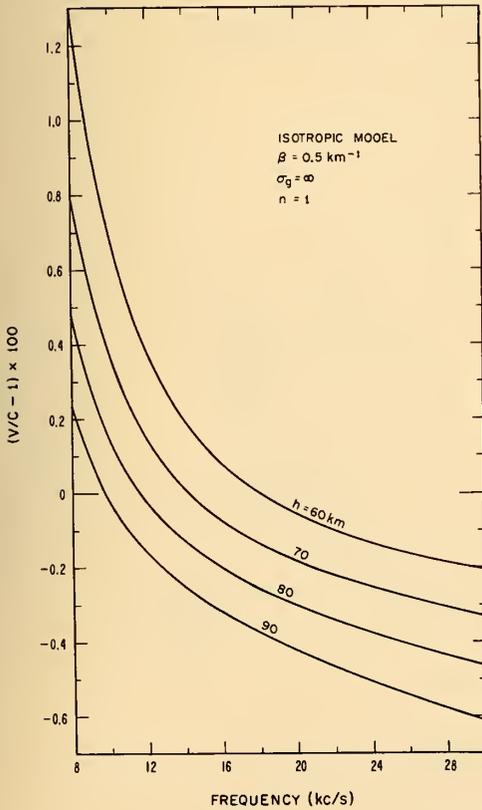
FIGURE 12a
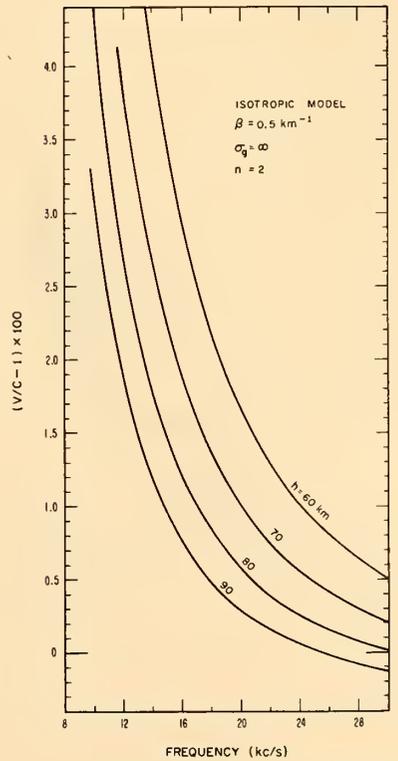
FIGURE 12b

ATTENUATION AND PHASE VELOCITY AS A FUNCTION OF
FREQUENCY SHOWING EFFECT OF REFLECTING HEIGHT

7-4
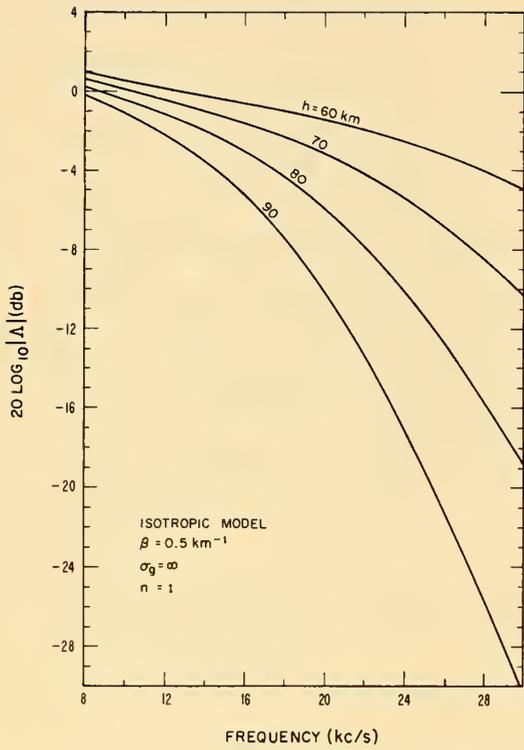
FIGURE 13a

FIGURE 14a
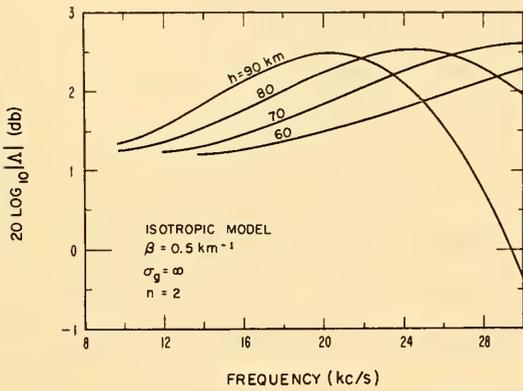
FIGURE 13b
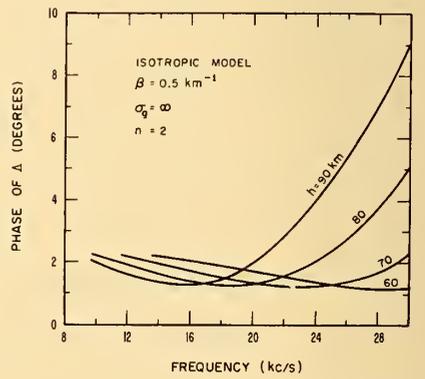
FIGURE 14b

EXCITATION FACTOR AS A FUNCTION OF FREQUENCY
SHOWING EFFECT OF REFLECTING HEIGHT
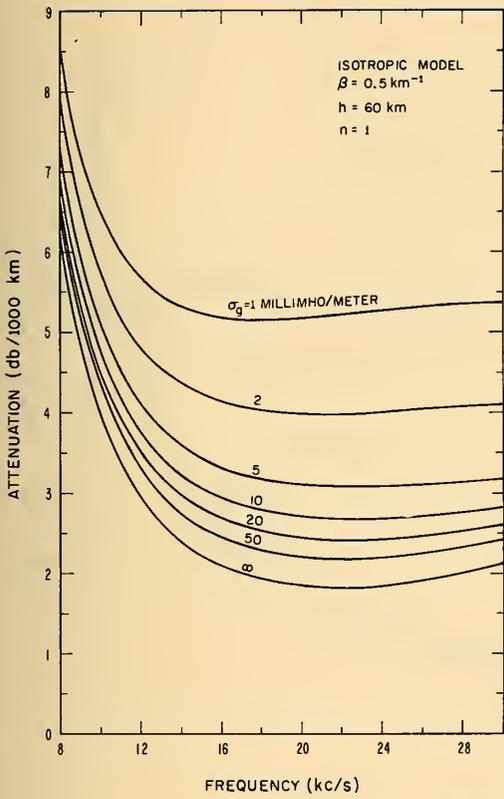
FIGURE 15a
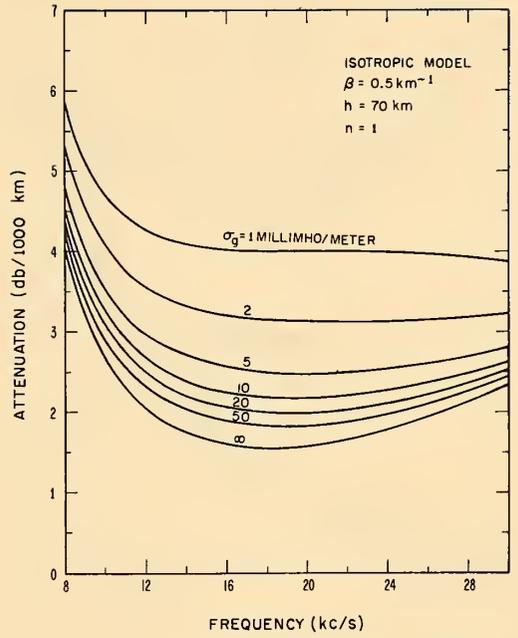
FIGURE 16a
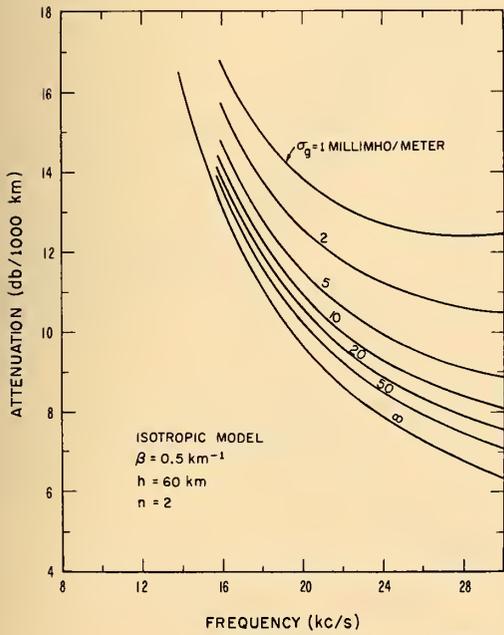
FIGURE 15b
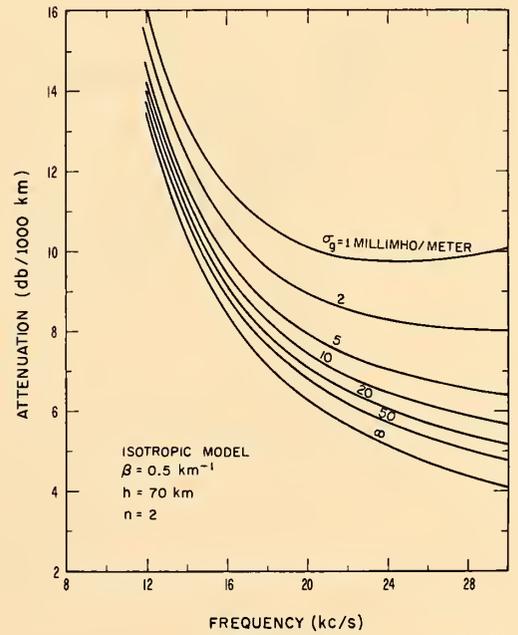
FIGURE 16b

ATTENUATION AS A FUNCTION OF FREQUENCY
SHOWING INFLUENCE OF GROUND CONDUCTIVITY

7-6
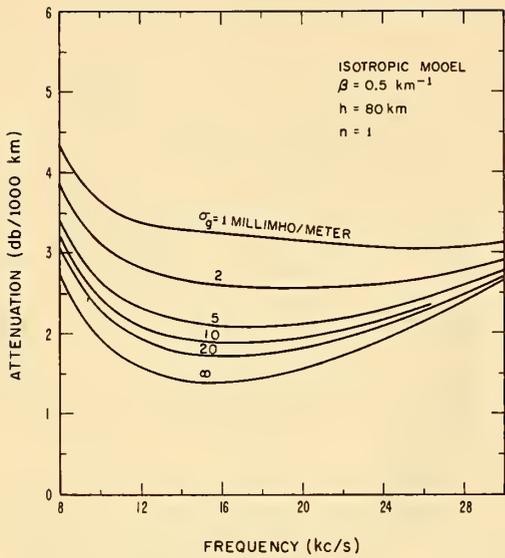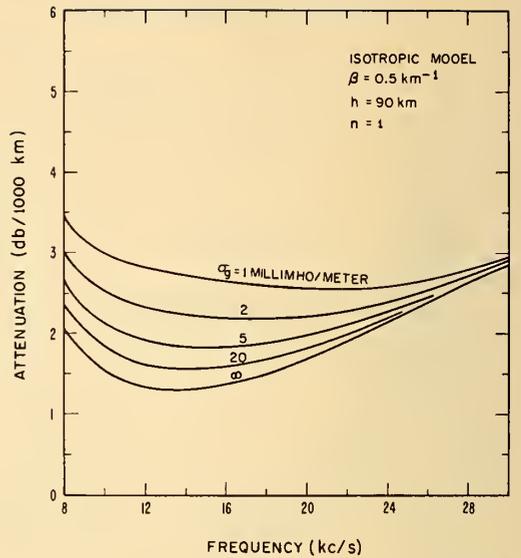
FIGURE 17a

FIGURE 18a
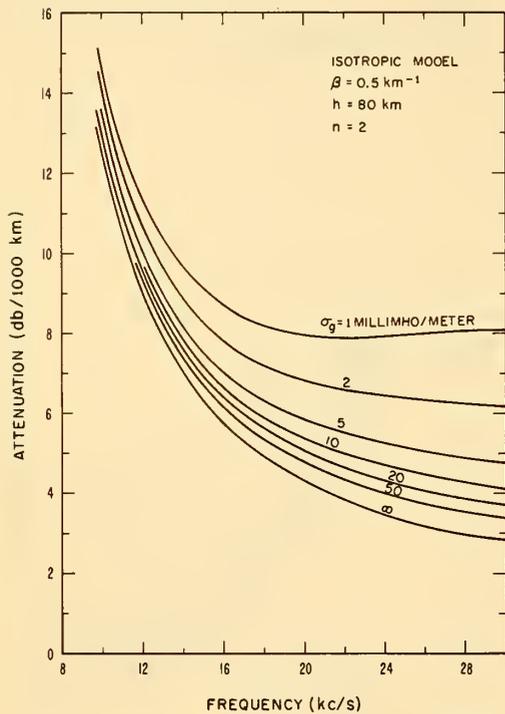
FICURE 17b
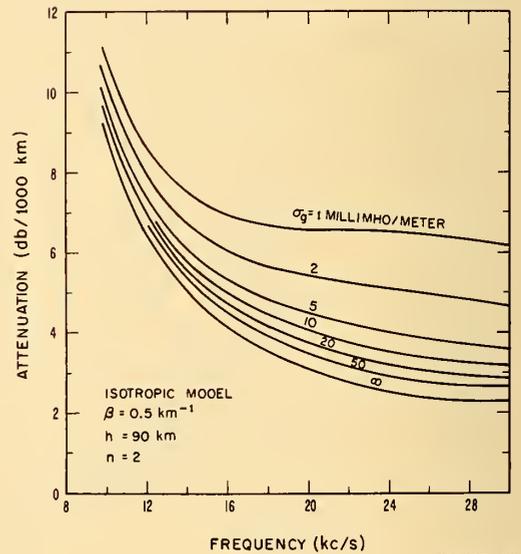
FIGURE 18b

ATTENUATION AS A FUNCTION OF FREQUENCY
SHOWING EFFECT OF GROUND CONDUCTIVITY

7-7
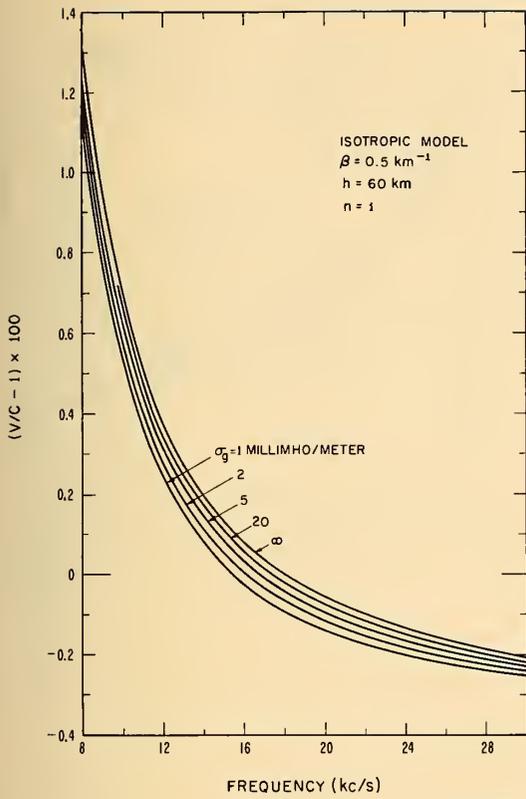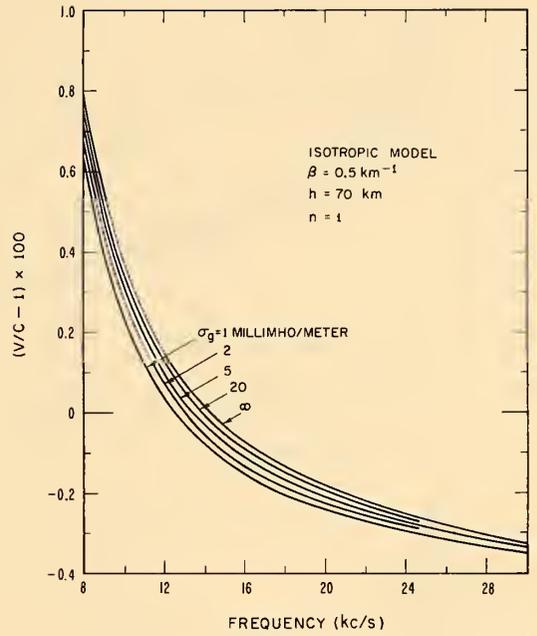
FIGURE 19a

FIGURE 20a
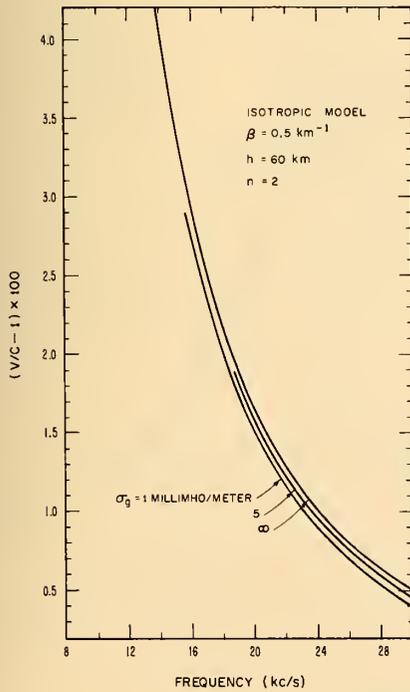
FIGURE 19b
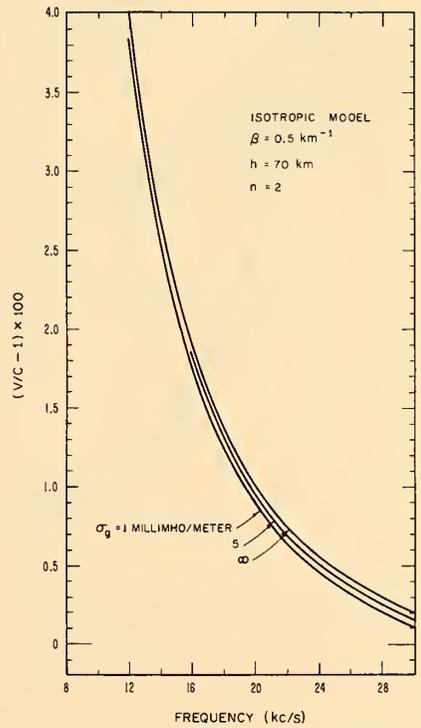
FIGURE 20b

PHASE VELOCITY AS A FUNCTION OF FREQUENCY
SHOWING EFFECT OF GROUND CONDUCTIVITY
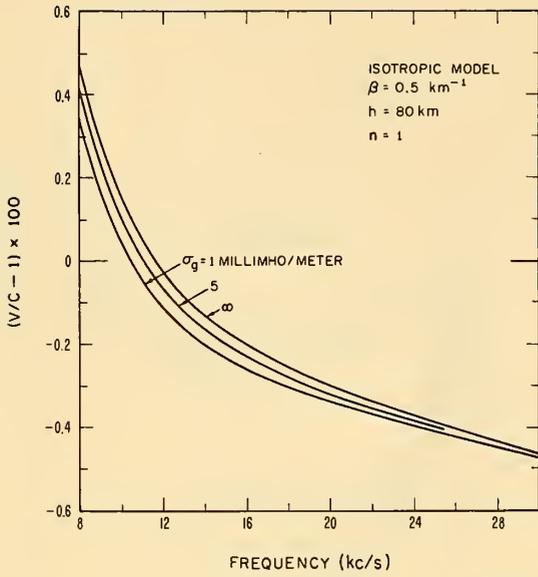
FIGURE 21a
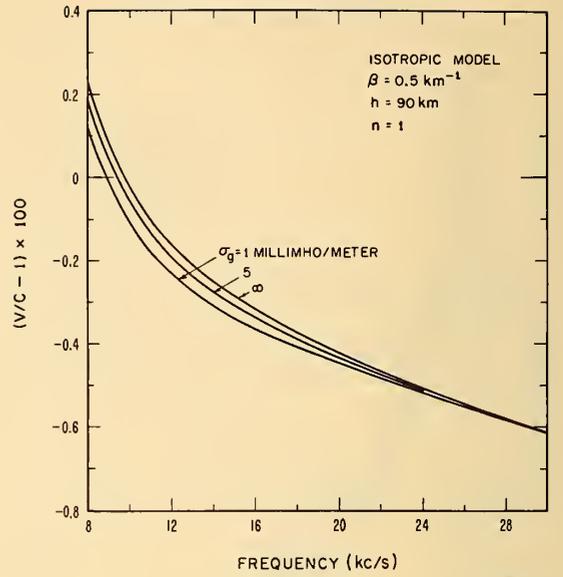
FIGURE 22a
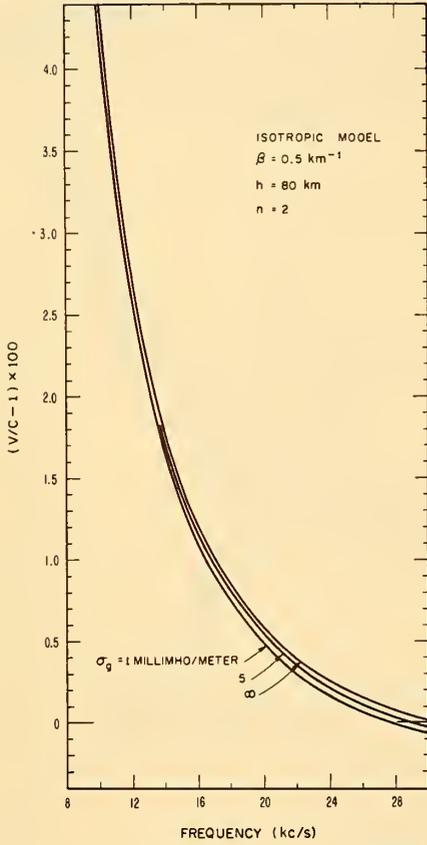
FIGURE 21b
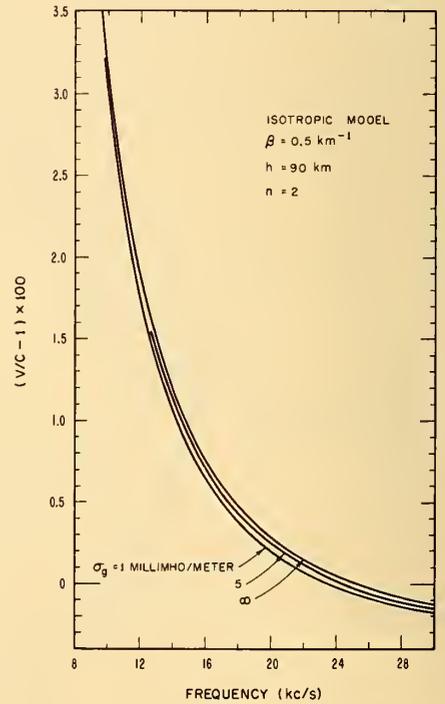
FIGURE 22b

PHASE VELOCITY AS A FUNCTION OF FREQUENCY
SHOWING EFFECT OF GROUND CONDUCTIVITY
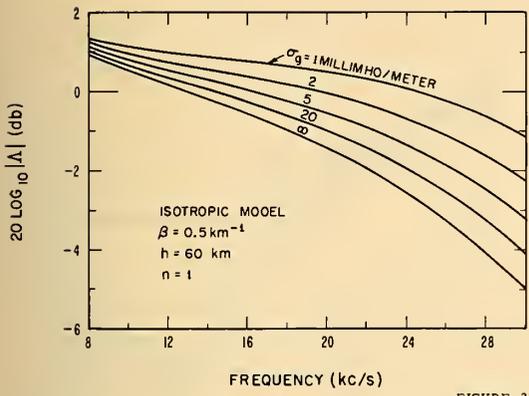
FIGURE 23a
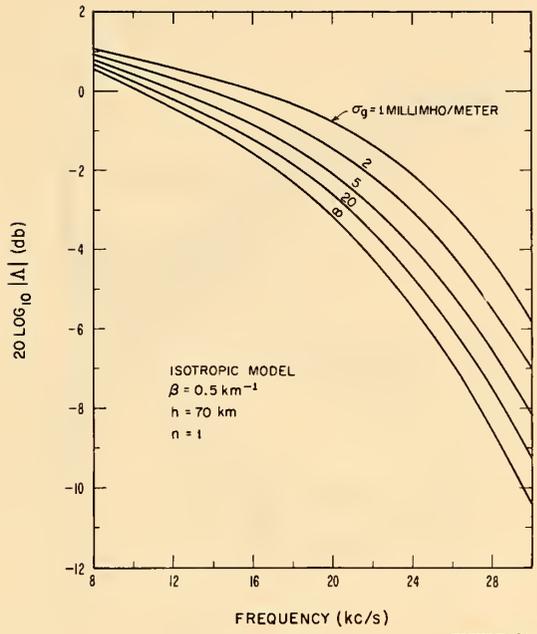
FIGURE 24a
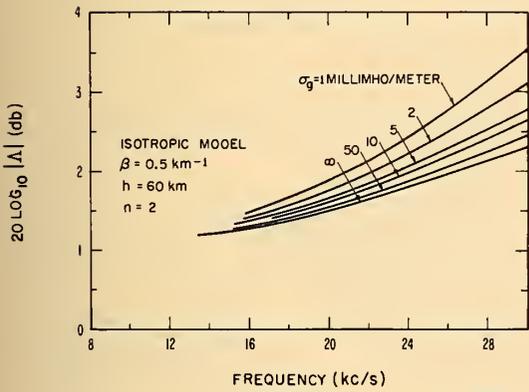
FIGURE 23b
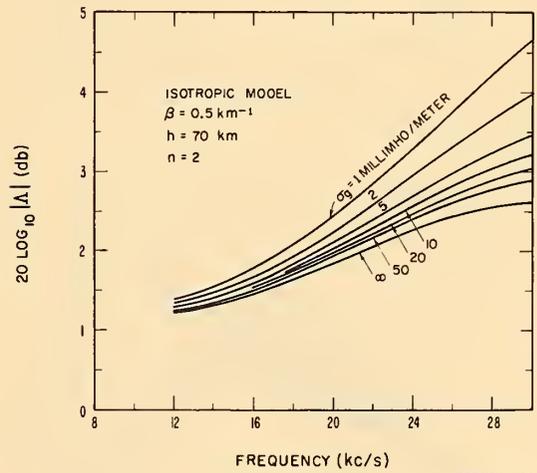
FIGURE 24b

MAGNITUDE OF EXCITATION AS A FUNCTION OF
FREQUENCY SHOWING EFFECT OF GROUND CONDUCTIVITY

7-10
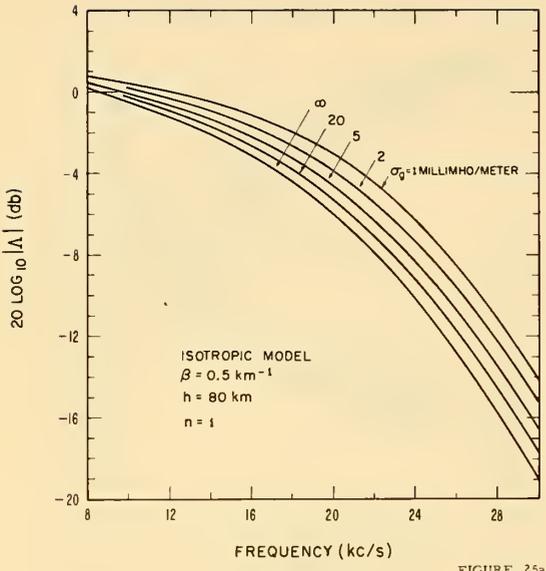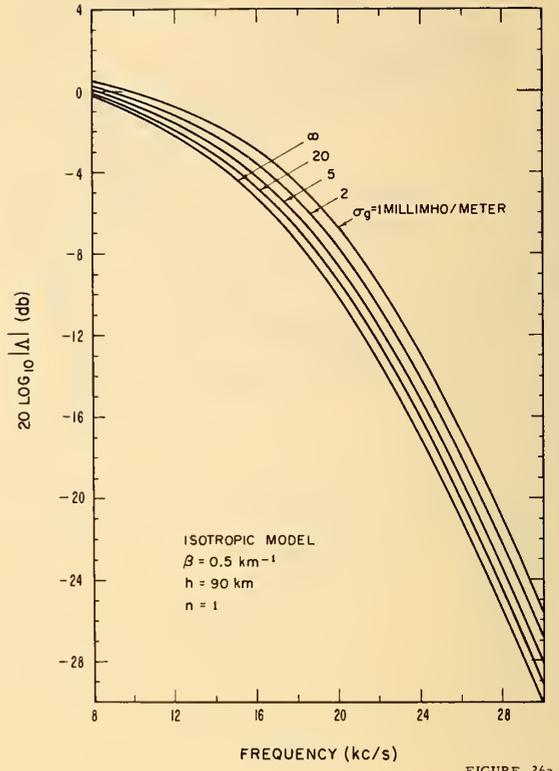
FIGURE 25a

FIGURE 26a
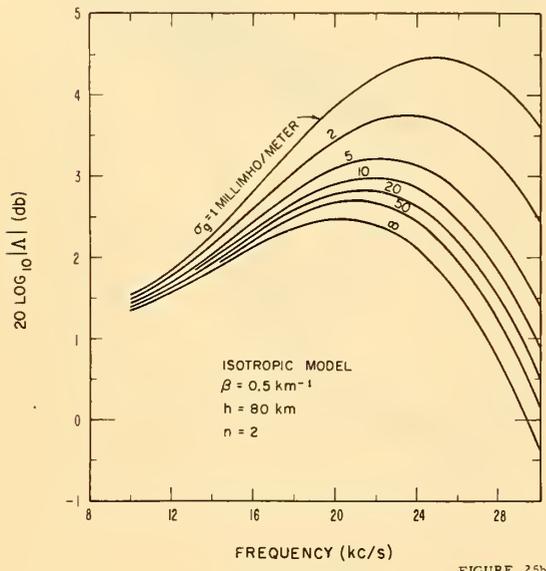
FIGURE 25b
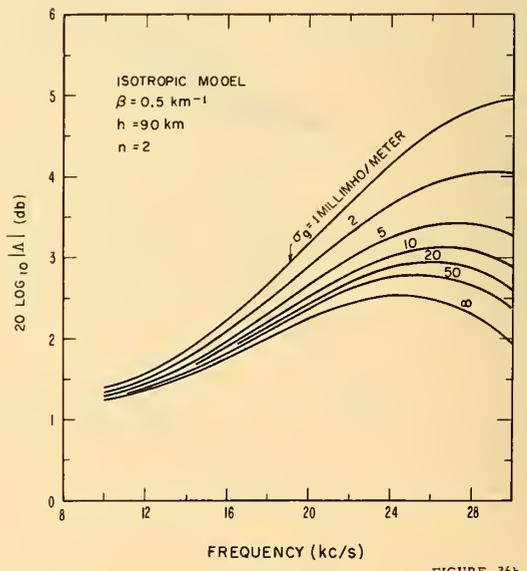
FIGURE 26b

MAGNITUDE OF EXCITATION FACTOR AS A FUNCTION
OF FREQUENCY SHOWING EFFECT OF GROUND CONDUCTIVITY
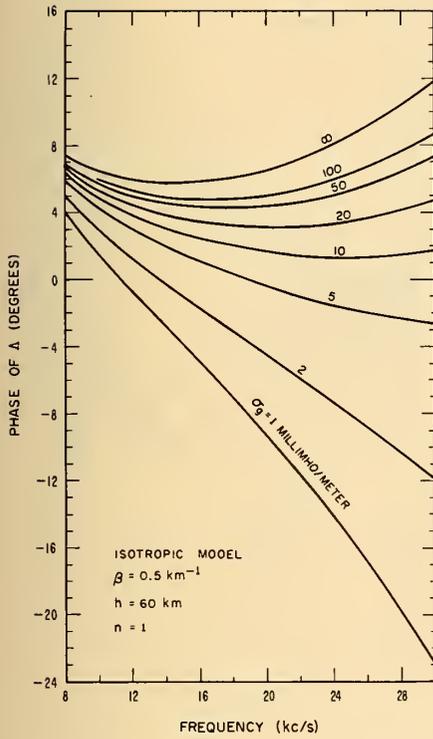
FIGURE 27a
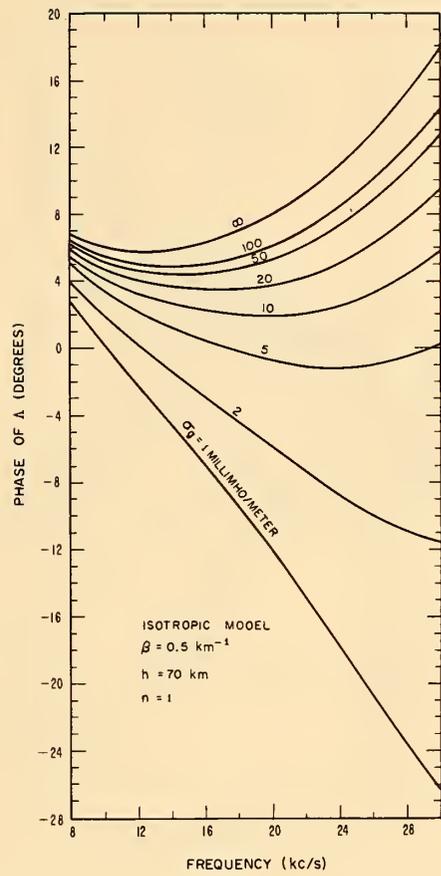
FIGURE 28a
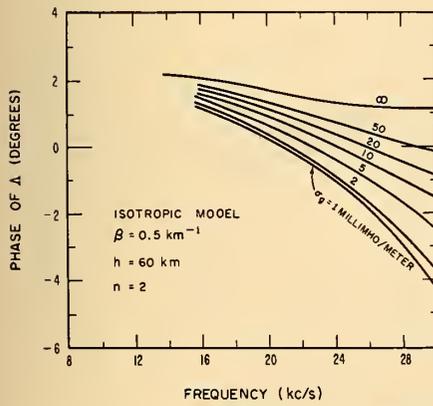
FIGURE 27b
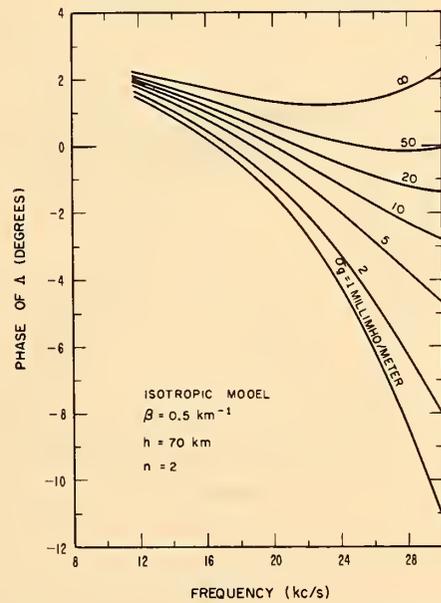
FIGURE 28b

PHASE OF EXCITATION FACTOR AS A FUNCTION OF
FREQUENCY SHOWING EFFECT OF GROUND CONDUCTIVITY

7-12
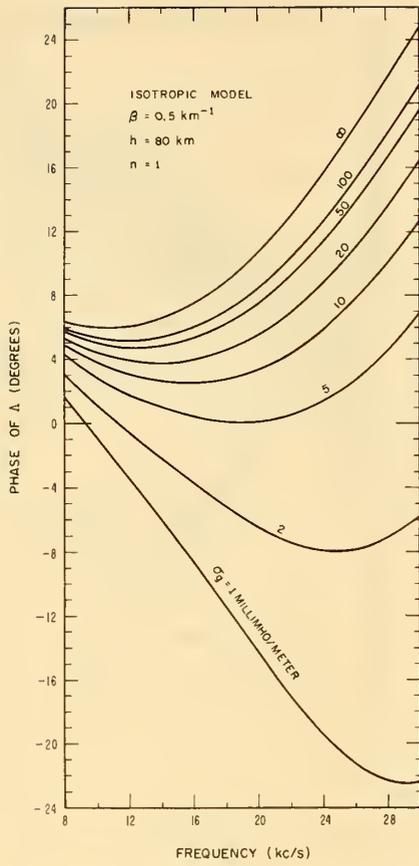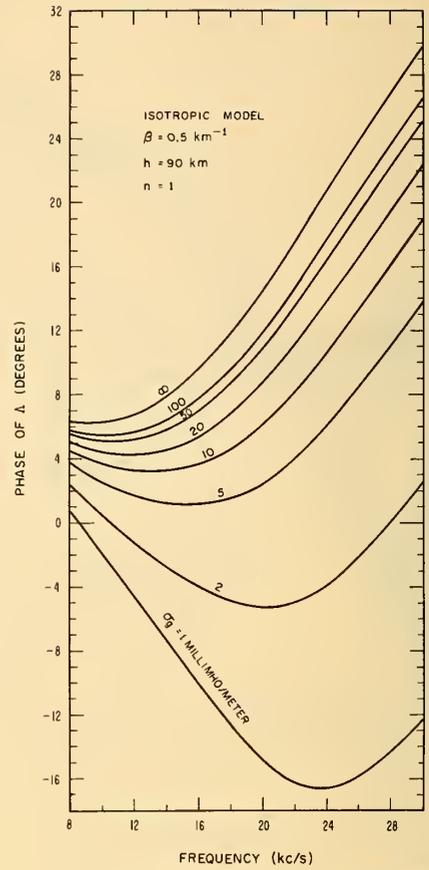
FIGURE 29a

FIGURE 30a
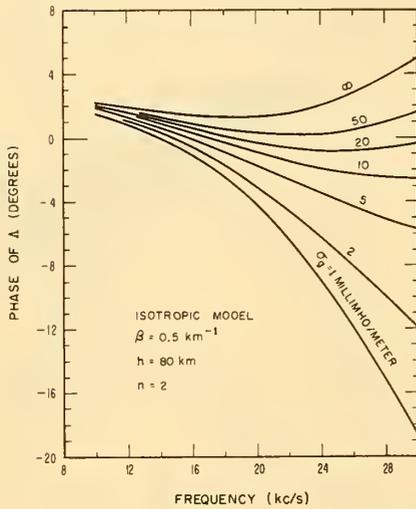
FIGURE 29b
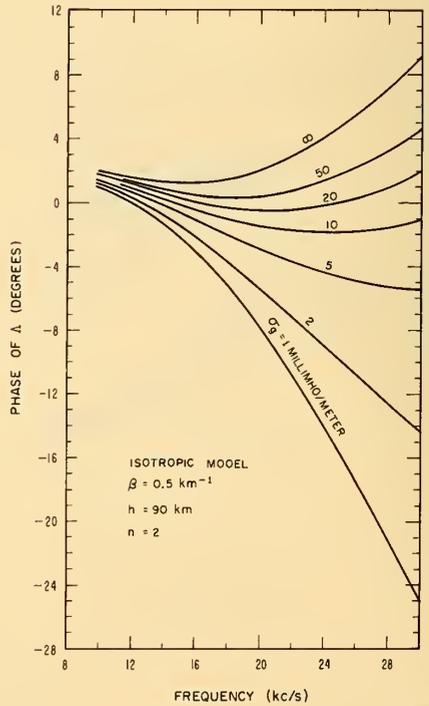
FIGURE 30b

PHASE OF EXCITATION FACTOR AS A FUNCTION OF
FREQUENCY SHOWING EFFECT OF GROUND CONDUCTIVITY

7-13
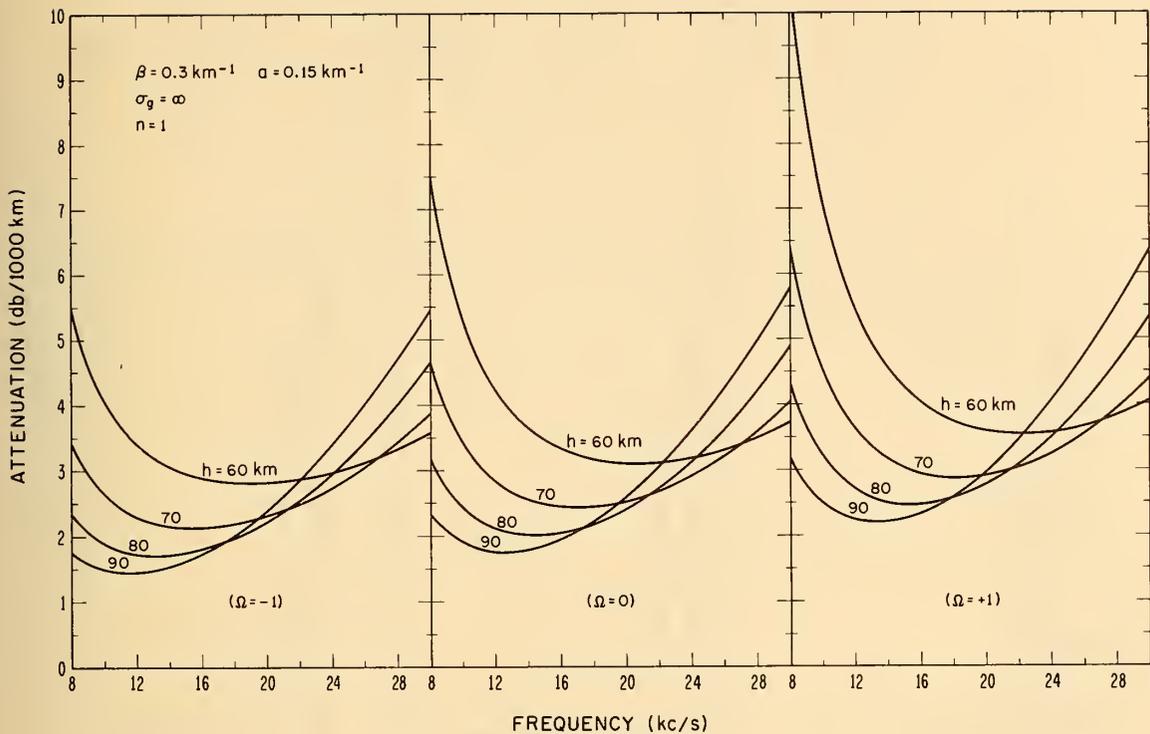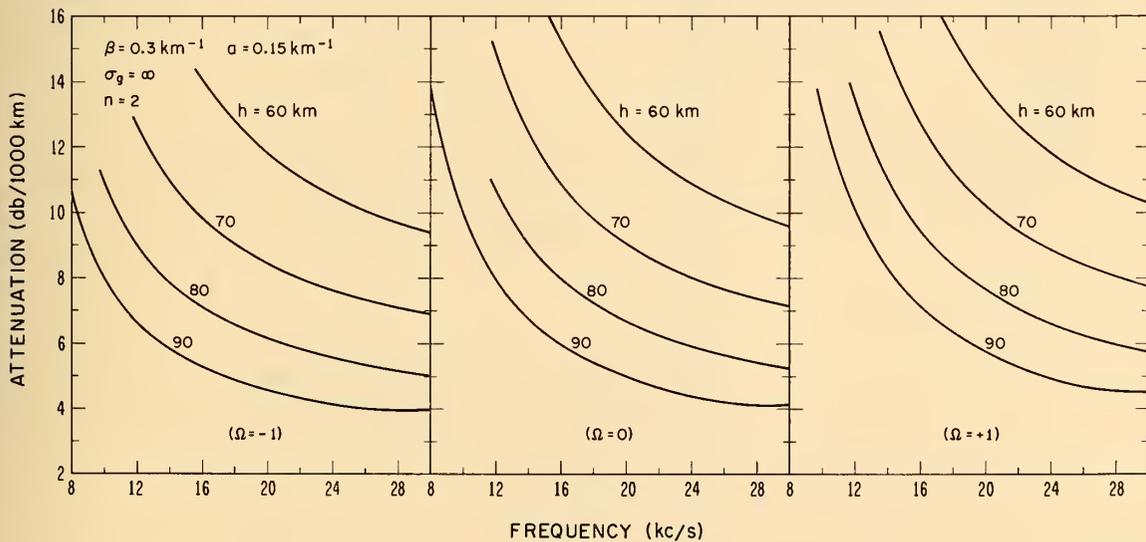
FIGURE 31a

FIGURE 31b

ATTENUATION AS A FUNCTION OF FREQUENCY SHOWING
EFFECT OF REFLECTING HEIGHT AND MAGNETIC FIELD
(NEGATIVE VALUES OF Ω CORRESPOND TO PROPAGATION
TOWARDS THE EAST)
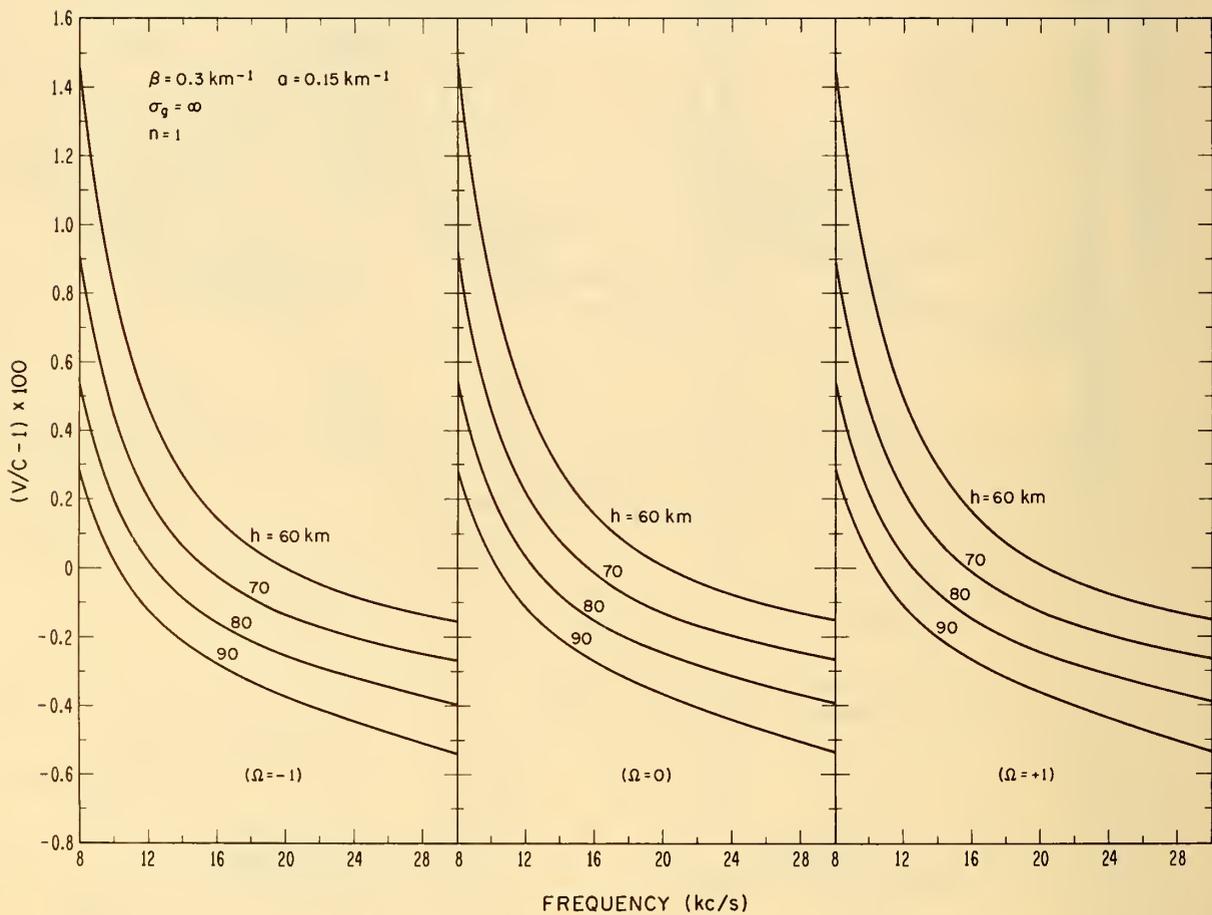
FIGURE 32

PHASE VELOCITY AS A FUNCTION OF FREQUENCY SHOWING
EFFECT OF REFLECTING HEIGHT AND MAGNETIC FIELD
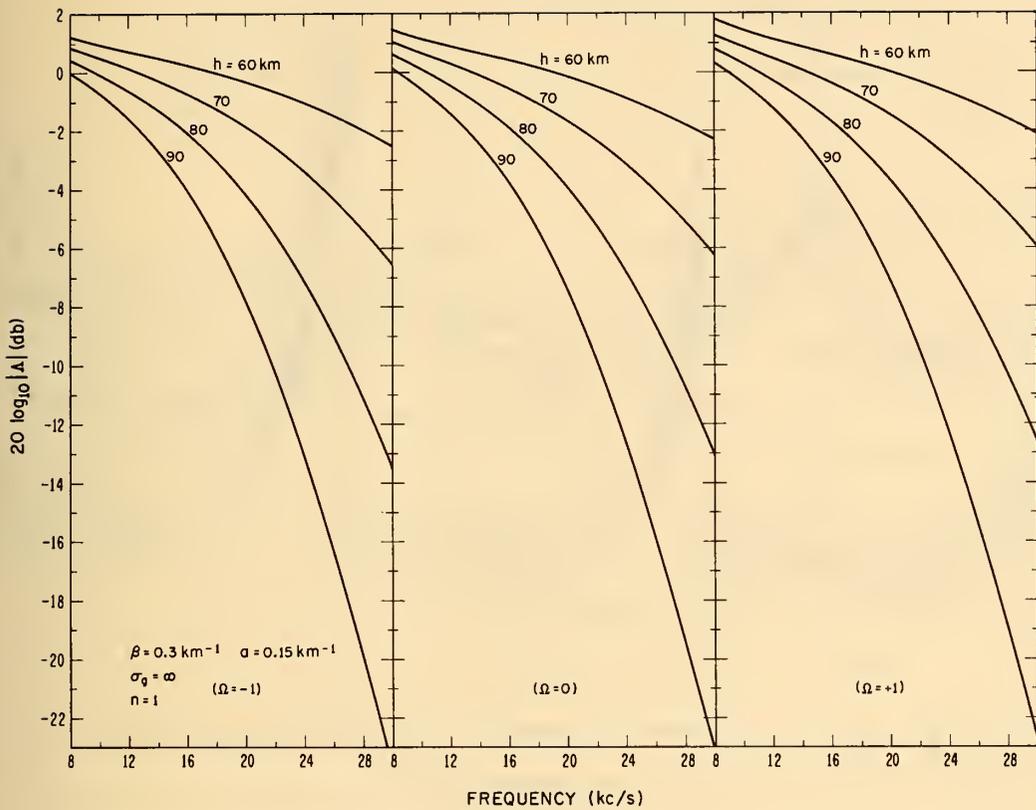
FIGURE 33
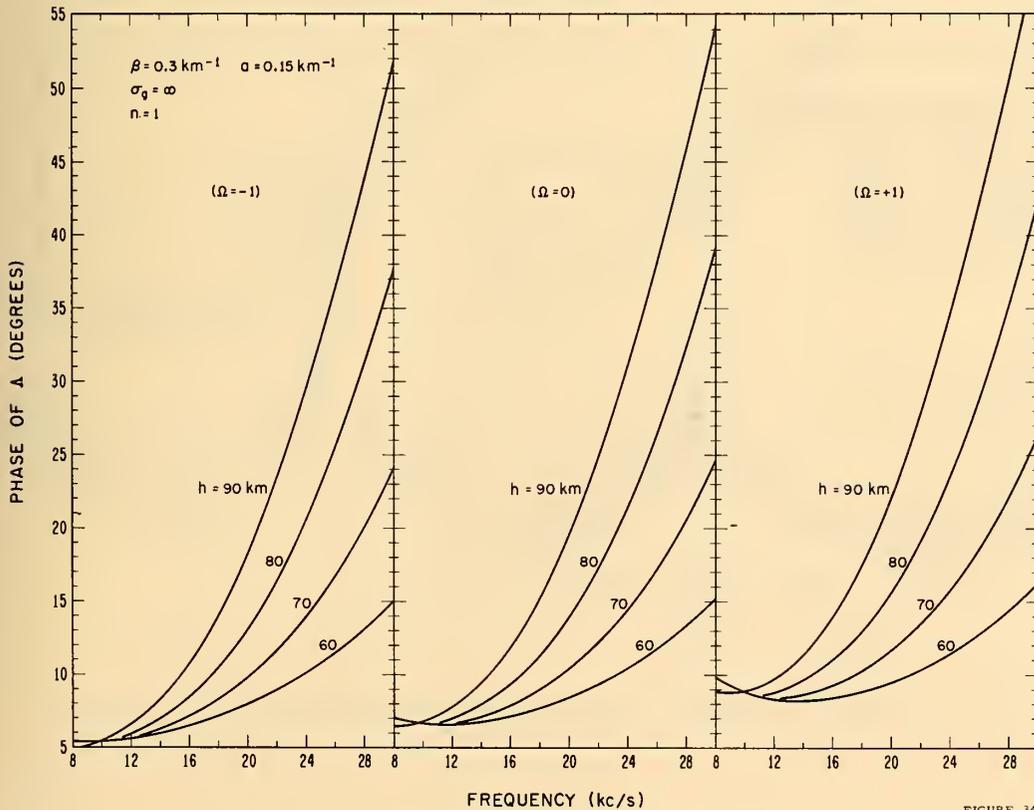
FIGURE 34

EXCITATION FACTOR AS A FUNCTION OF FREQUENCY SHOWING
EFFECT OF REFLECTING HEIGHT AND MAGNETIC FIELD

7-16
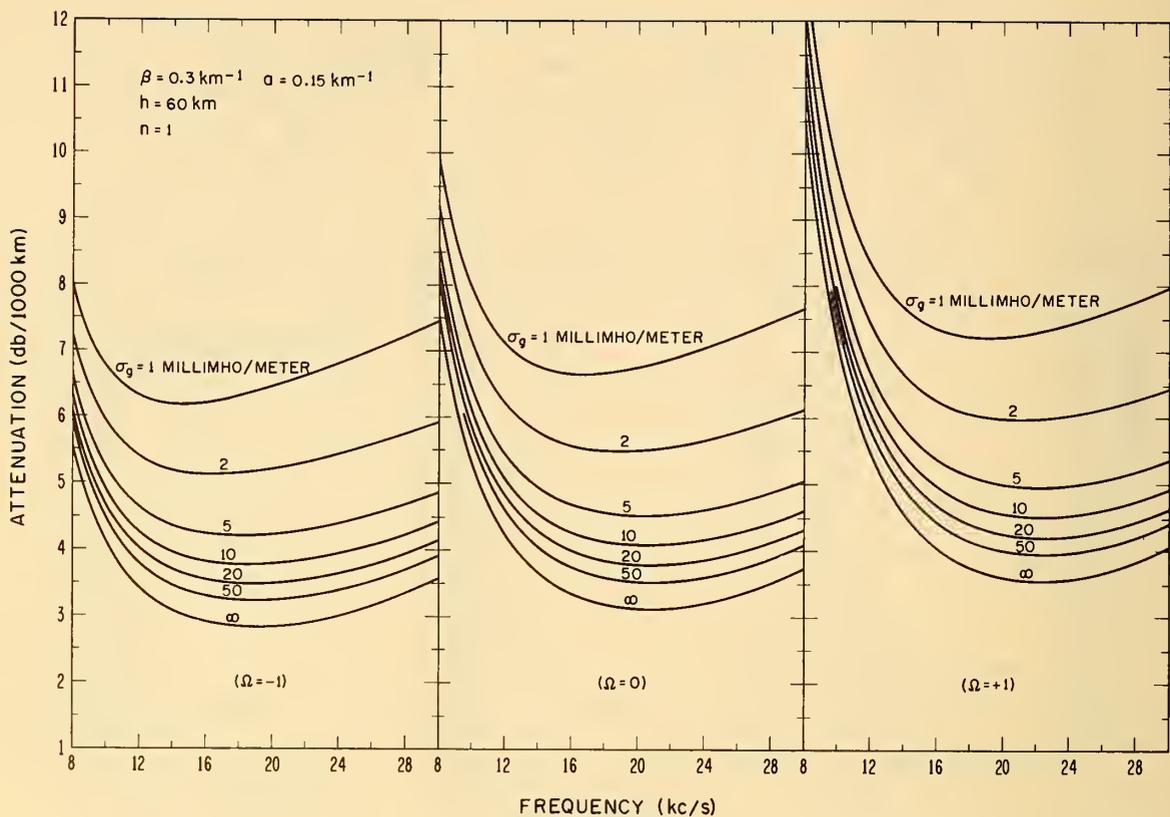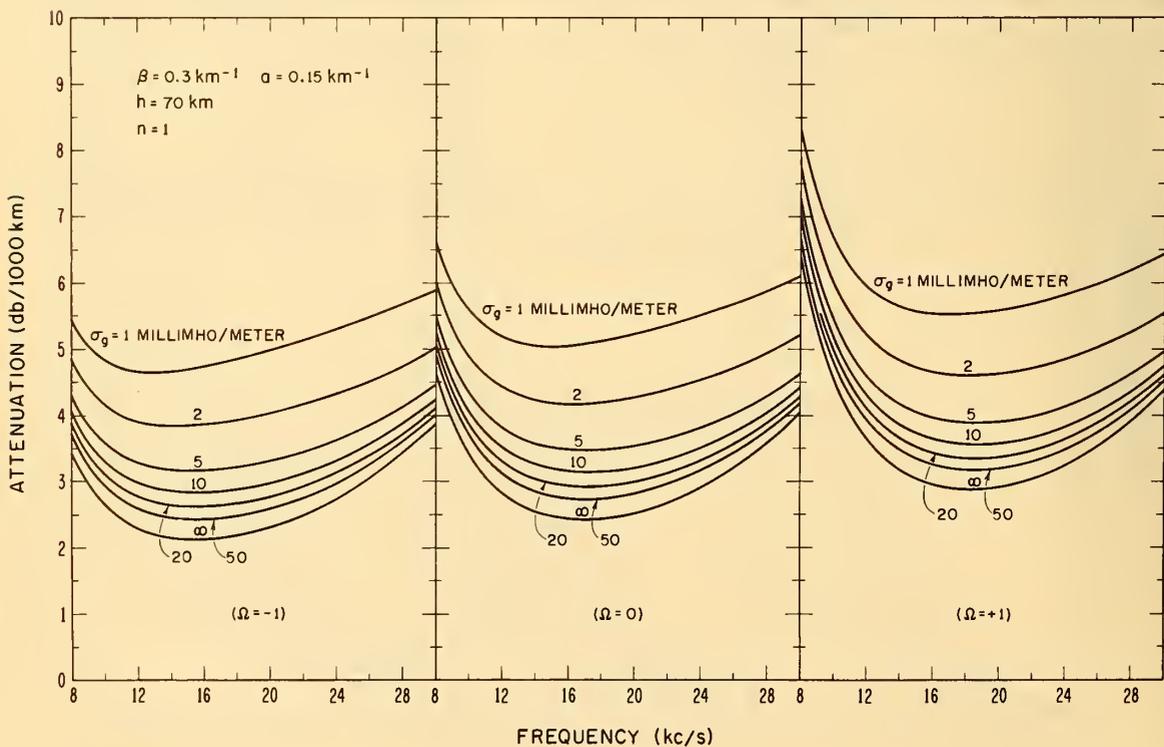
FIGURE 35

FIGURE 36

ATTENUATION AS A FUNCTION OF FREQUENCY SHOWING
EFFECT OF GROUND CONDUCTIVITY AND MAGNETIC FIELD

7-17
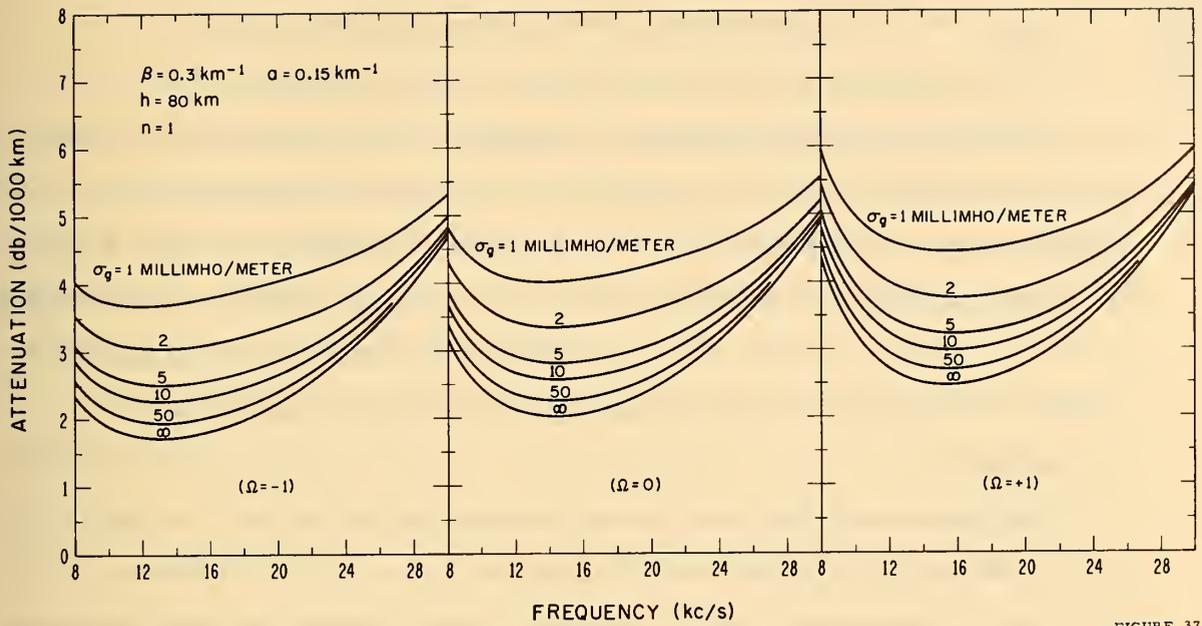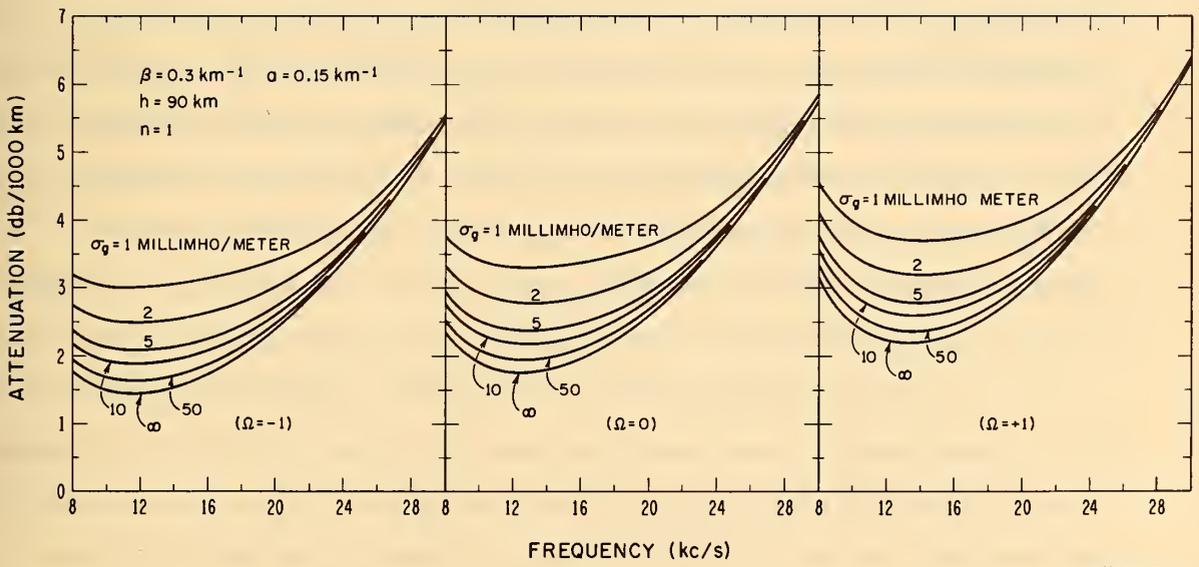
FIGURE 37

FIGURE 38

ATTENUATION AS A FUNCTION OF FREQUENCY SHOWING
EFFECT OF GROUND CONDUCTIVITY AND MAGNETIC FIELD

8. Comparison with Some Experimental Data

It is of interest to compare some of the calculated curves with appropriate experimental data as reported in the literature. There are two distinct sources of such data. These are recordings of field strengths of distant VLF transmitters and the observations of the waveforms of atmospherics which originate in lightning discharges. Up-to-date and comprehensive surveys of the various experimental methods are given in recent papers by Watt and Crogan [1964] and Horner [1964].

The phase velocity is a rather crucial characteristic in the theory of the propagation of VLF radio waves. The U.S. Navy Electronics Laboratory (N.E.L.) has obtained some valuable experimental data for phase velocity in the frequency range from 9.2 kc/s to 15.2 kc/s. The results [Tibbals, 1960; Pierce and Nath, 1961] are shown in figure 39 for both daytime and nighttime paths predominantly over sea. The vertical bars encompass the range of several independent measurements for the frequencies indicated. These results were obtained by employing an ingenious technique which combined the results observed from widely spaced transmitting stations operating in sequence. As a consequence, the data for east-to-west and west-to-east paths are averaged in a sense.

In a recent investigation (during July 1963), Steele and Chilton [1964] conducted an experiment to measure phase velocity by utilizing frequency stabilized signals radiated in sequence from transmitters NPG and NBA at frequencies of 18 kc/s. They measured the phase in Colorado, Alaska, Hawaii, and Argentina. From a combined analysis, they deduced the average phase velocities for night and day indicated in figure 39.

Theoretical curves are shown in figure 39 which correspond to

the calculations for an exponential ionosphere with $\beta = 0.5$, $\sigma_g = \infty$, $n = 1$, and heights $h = 70$km and 90 km. Also shown is a similar pair of calculated curves for a homogeneous and sharply bounded isotropic ionosphere characterized by $\omega_r = 2 \times 10^5$ sec^{-1}. It is evident that the agreement between the experimental points and the calculated curves is quite good. Here, there is not much to choose between the two theoretical models.

A comparison between theory and experiment showing the effect of finite ground conductivity is shown in figure 40. The two indicated experimental points, for propagation over sea and land, at 10.2 kc/s are quoted from the work of Pierce and Nath [1960]. The difference between these, expressed as a ratio to c, corresponds to about 5×10^{-4}. Corresponding theoretical curves for earth conductivities of ∞, 5 and 1 millimhos per meter are also shown. As somewhat of a coincidence, the $\sigma_g = \infty$ curve passes through the experimental point for sea water and the $\sigma_g = 5$ curve passes through the point for land. Thus, the theoretical prediction that the finite ground conductivity slows the wave down is confirmed experimentally.

The excitation factor Λ is a rather elusive quantity which is not always understood. Fortunately, Watt and Crogan [1964], in a noble effort, have taken a vast amount of experimental daytime data for VLF propagation over sea-water paths and extrapolated it back to zero distance in such a manner that experimentally deduced values of $|\Lambda|$ may be estimated. In some cases, they required a knowledge of effective radiated power of the transmitting antenna. The vertical bars indicated in figure 41 indicate rather crudely the range of the data points which they deduced for mode 1. As indicated, it seems to fall on a theoretical curve calculated for $h = 80$ km and $\beta = 0.5$. It would have been more satisfying to see closer agreement

with the $h = 70$ km curve which is several decibels higher. How-
ever, two factors might contribute to this apparent discrepancy. In
the first place, the assumed radiated powers might be lower than
claimed. Secondly, the effect of conversion of energy from mode 1
to higher modes would also tend to reduce the apparent excitation
efficiency.

Experimental data on attenuation rates relating to nighttime
propagation over sea are indicated in figure 42. The vertical bars
indicate the range of data points quoted by Taylor and Lange [1958]
who analyzed the waveforms of atmospherics observed simultaneously
at several stations. The dashed curve at the bottom of figure 42 is
quoted directly from Watt and Crogan [1964] who deduced it mainly
from the early data of Round, et al. [1925]. Calculated curves are
shown for mode 1 and $h = 90$ km for exponential ionospheres with
both $\beta = 0.3$ km^{-1} and 0.5 km^{-1}. It is apparent that the $\beta = 0.5$
curve is certainly more representative for nighttime propagation,
as suggested back in section 2. The theoretical curve for mode 2
and $\beta = 0.5$ is also shown, which indicates that modal interference
will be significant at frequencies above 20 kc/s. The spread of the
experimental data points attests to this fact. Also, for comparison,
the curve for an ionosphere with $\beta = 1$ is shown in figure 42. It
appears to be quite near the experimental curve attributed to Watt
and Crogan [1964]. Finally, a calculated attenuation curve for a
homogeneous sharply bounded and isotropic ionosphere (with
$h = 90$ km and $\omega_r = 2 \times 10^5$) is shown on figure 42 which is in
only fair agreement with the experimental data.

Measured daytime attenuation rates [Watt and Crogan, 1964] for
propagation over sea are shown in figure 43 by a curve which is the
average for north-to-south paths at temperate latitudes. This is seen

to agree reasonably well with a calculated curve for an exponential ionosphere with $h = 70$ km and $\beta = 0.3$ km^{-1}. The calculated curve for $\beta = 0.5$ is decidedly too low, which is also the case for the homogeneous sharply bounded model for $h = 70$ km.

The measured dependence of attenuation rate on direction of propagation is indicated in figure 44 for daytime propagation over sea. The data attributed to Watt and Crogan [1964] are based on the analysis of field strength for paths at temperate latitudes which are predominantly west to east, north to south, or east to west. Again, some of their data are taken from the classic paper by Round, et al. [1925]. Corresponding attenuation data deduced from atmospheric waveforms by Taylor [1960a, 1960b] are also shown in figure 44. These data are also for paths at temperate latitudes over sea water in daytime.

Calculated attenuation curves for mode 1 with $\beta = 0.3$ km^{-1}, $a = 0.15$ km^{-1}, $\sigma_g = \infty$, and $h = 70$ km are shown in figure 44 for comparison with the experimental curves. As indicated, the values of Ω given by -1, 0 and +1 seem to be quite appropriate. Any other choice of the magnitude of Ω would not give the right amount of non-reciprocity.

Added Note

After this technical note was written, Mr. E. R. Swanson communicated to us experimental results which he describes in more detail in Report No. 1239 of the U.S. Navy Electronics Laboratory. For example, for propagation at 10.2 kc/s over the sea in daytime and in summer, he finds attenuation rates as follows: 2.5 db/1000 km for west-to-east, 3.4 db/1000 km for north-to-south or south-to-north, and 4.1 db/1000 km for east-to-west. These may be compared with the respective values in figure 44 of 2.65, 3.33, and

4.28 db/1000 km.   The dip angle for these measurements was of
the order of 55°, whereas the calculations are for a purely hori-
zontal magnetic field.   The good agreement is attributed to the
fortuitous choice of the magnitude of the parameter Ω.   Mr. Swan-
son also found that, for the same conditions, at night the attenuation
rate at 10.2 kc/s was 1.6 db/1000 km for north-south propagation,
while figure 42 indicates a calculated value of 1.5 db/1000 km when
$\beta = 0.5$ km^{-1},   n = 1, $\Omega = 0$,   and   h = 90 km.   Furthermore, he
quotes the average non-reciprocal variation at night of ± 0.5 db/1000
km which is certainly consistent with the calculated variation in-
dicated in figure 38.   At the same time, Mr. Swanson comments
that the N.E.L. data in figure 39 for 10.2 kc/s now indicates that
$(v/c) - 1 \cong 0.34 \times 10^{-2}$ for day and $\cong -0.06 \times 10^{-2}$ for night --
for propagation over sea water in the temperate latitudes during
the summer.
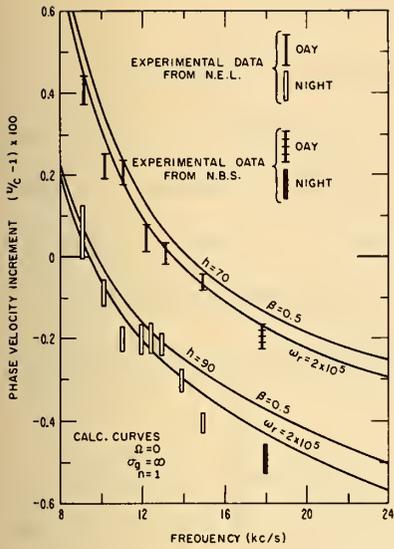
FIGURE 39
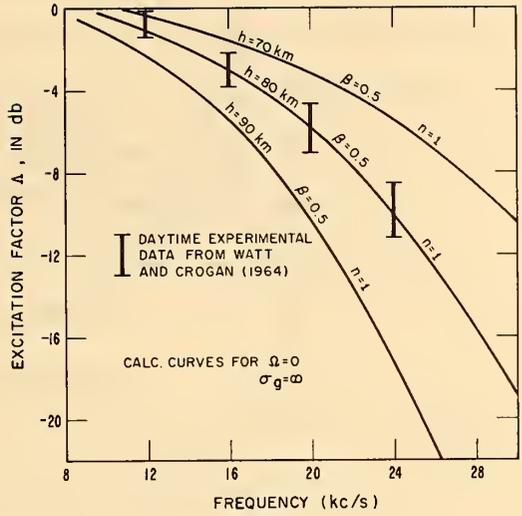
FIGURE 41
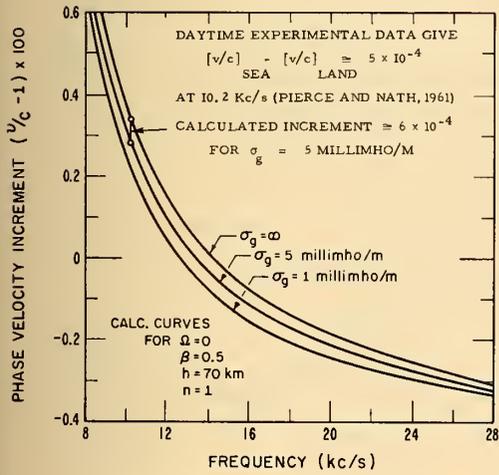
FIGURE 40
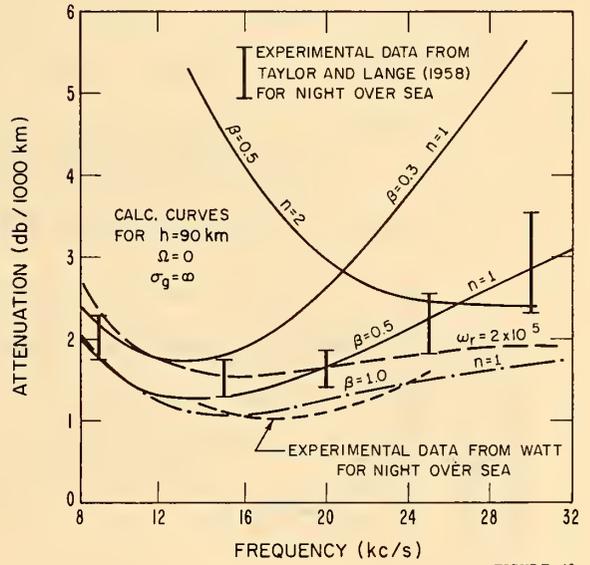
FIGURE 42

EXPERIMENTAL DATA FROM VARIOUS SOURCES
AND PERTINENT THEORETICAL CURVES
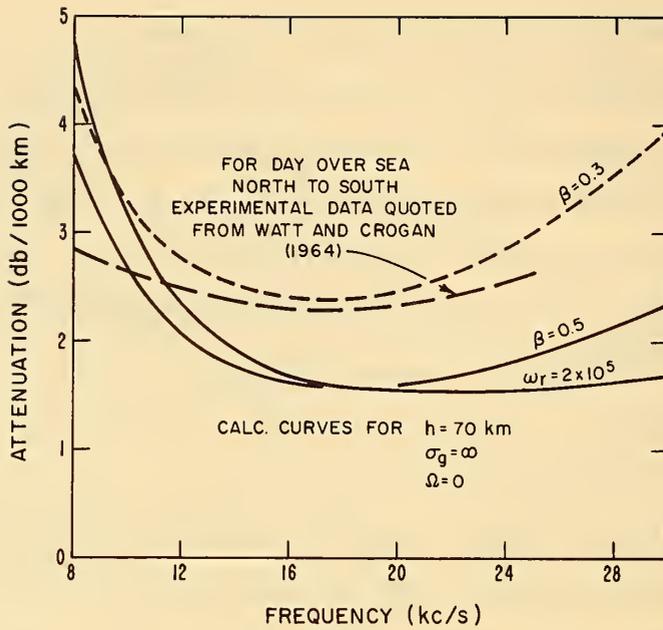
FIGURE 43
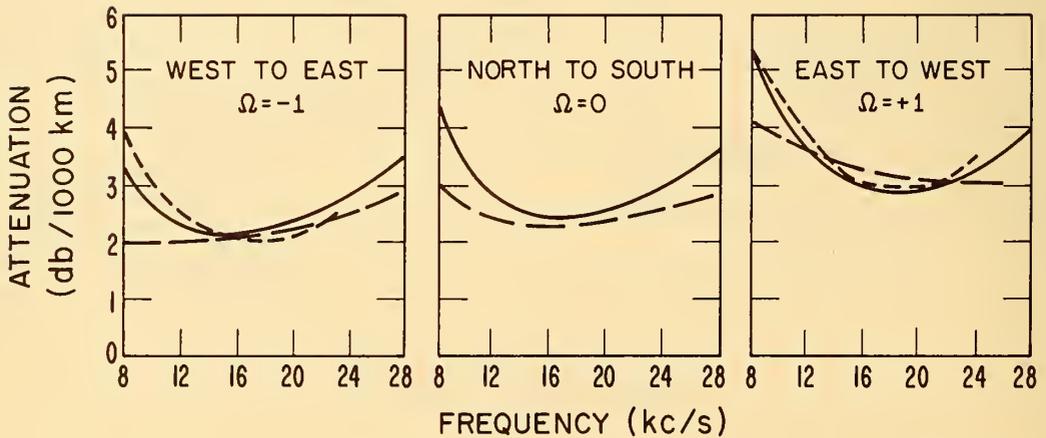
FIGURE 44

EXPERIMENTAL DATA FOR ATTENUATION RATES
WITH PERTINENT THEORETICAL CURVES

8-7

9. Concluding Remarks

The results given in this technical note, while not entirely exhaustive, should be of value in interpreting further experimental data. It would seem that much additional theoretical work in this field is not warranted until the experimentalists broaden their investigations to ascertain the actual direction and geographical dependences on the propagation parameters.

10. Acknowledgement

11. References

Arnold, H. R. (Feb. 1964), Comments on a paper "Collisional de-
    tachment and the formation of an ionospheric" by E. T. Pierce,
    Radio Sci. J. Res. NBS/USNC-URSI 68D, No. 2, 215-217.

Barber, N. F., and D. D. Crombie (1959), VLF reflections from the
    ionosphere in the presence of a transverse magnetic field, J.
    Atmos. Terrest. Phys. 16, 37-45.

Barrington, R. E., E. V. Thrane, and B. Bjelland (1963), Diurnal and
    seasonal variations in D-region electron densities derived from
    observations of cross modulation, Can. J. Phys. 41, 271-285.

Belrose, J. S. (1964), Present knowledge of the lowest ionosphere,
    p. 3-24, in Propagation of radio waves at frequencies below
    300 kc/s, ed. W. T. Blackband (Pergamon Press, Oxford).

Belrose, J. S., and M. J. Burke (1964), Study of the lower ionosphere
    using partial reflection, J. Geophys. Res. 69, 2799-2818.

Belrose, J. S., L. R. Bode, and L. W. Hewitt (Dec. 1964), Physical
    properties of the polar winter mesosphere obtained from low
    frequency propagation and partial reflection studies, Radio Sci.
    J. Res. NBS/USNC-URSI 68D, No. 12, 1319-1323.

Budden, K. G. (1961), Radio waves in the ionosphere (Cambridge
    Univ. Press, Cambridge).

Ferraro, A. J., and J. J. Gibbons (1959), Polarization computations
    by means of the multi-slab approximation, J. Atmos. Terrest.
    Phys, 16, 136-144.

Galejs, J. (Sept. 1, 1964), Propagation of VLF waves below a curved
    and stratified ionosphere, J. Geophys. Res. 69, 3639-3650.

Gossard, E. E. (Sept. 1963), U. S. Navy Electronics Lab., San Diego,
    Calif. (private communication).

Horner, F. (1964), Radio noise from thunderstorms, in Advances in
    radio research, vol. 2, ed. J. A. Saxton (Academic Press, London).

Johler, J. R. (1963), Radio wave reflections at a continuously strati-
fied plasma with collisions proportional to energy and arbitrary
magnetic induction, pp. 436-445, Proc. International Conference
on the Ionosphere (Chapman and Hall, London).

Johler, J. R., and J. D. Harper, Jr. (Mar. 1963), On plasma
collision frequencies proportional to energy in the radio wave
reflection and transmission process, NBS Tech. Note No. 164.

Kane, J. A. (1961), Re-evaluation of ionospheric electron densities
and collision frequencies derived from rocket measurements of
refractive index and attenuation, J. Atmos. Terrest. Phys. $\underline{23}$,
338-347.

Krasnushkin, P. E. (1962), On the propagation of long and very-long
radio waves around the earth, Nuovo Cimento $\underline{26}$, Series 10,
50-112.

Nicolet, M., and A. C. Aikin (1960), The formation of the D-region
of the ionosphere, J. Geophys. Res. $\underline{65}$, 1469-1483.

Phelps, A. V., and J. L. Pack (1959), Electron collision frequencies
in nitrogen and in the lower ionosphere, Phys. Rev. $\underline{3}$, 340-342.

Pierce, E. T., and H. R. Arnold (July, 1963), Final report -- Sudden
ionospheric disturbances and the propagation of VLF radio waves,
Part I, Stanford Research Institute, Stanford, California.

Pierce, J. A., and S. C. Nath (1961), VLF propagation, Annual
progress report No. 60, 1-6, Cruft Laboratory, Harvard University.

Round, H. J. T., T. L. Eckersley, K. Tremellen, and F. C. Lunnon,
(1925), Report on measurements made on signal strength at great
distances during 1922 and 1923 by an expedition sent to Australia,
J. I. E. E. (London) $\underline{63}$, 933-1011.

Spies, K. P., and J. R. Wait (Jul. 17, 1961), Mode calculations for
    VLF propagation in the earth-ionosphere waveguide, NBS Tech.
    Note No. 114 (PB-161615).

Steele, F. K., and C. J. Chilton (Dec. 1964), The measurement of the
    phase velocity of VLF propagation in the earth-ionosphere wave-
    guide, Radio Sci. J. Res. NBS/USNC-URSI 68D, No. 12,
    1269-1274.

Taylor, W. L. (Jul.-Aug. 1960a), Daytime attenuation rates in the
    VLF band using atmospherics, J. Res. NBS 64D (Radio Prop.),
    No. 4, 349-355.

Taylor, W. L. (1960b), VLF attenuation for east-west and west-east
    propagation using atmospherics, J. Geophys. Res. 65, 1933-1938.

Taylor, W. L., and L. J. Lange (1958), Some characteristics of VLF
    propagation using atmospheric waveforms, pp. 609-617, Proc.
    Second Conference on Atmospheric Electricity (Pergamon Press,
    London).

Tibbals, M. L. (1960), U. S. Navy Electronics Lab., San Diego, Calif.
    (private communication)

Wait, J. R. (Jan.-Feb. 1961), A new approach to the mode theory of
    VLF propagation, J. Res. NBS 65D (Radio Prop.), No. 1, 37-46.

Wait, J. R. (1962a), Electromagnetic waves in stratified media,
    chapter VII (Pergamon Press, Oxford, New York).

Wait, J. R. (1962b), Electromagnetic waves in stratified media,
    chapter IX (Pergamon Press, Oxford, New York).

Wait, J. R. (Jul.-Aug, 1963), Influence of the lower ionosphere on
    propagation of VLF waves to great distances, J. Res. NBS 67D
    (Radio Prop.), No. 4, 375-381.

Wait, J.R., and K. Spies (Aug. 1960), Influence of earth curvature and the terrestrial magnetic field on VLF propagation, J. Geophys. Res. 65, No. 8, 2325-2331.

Wait, J.R., and L.C. Walters (1963), Reflection of VLF radio waves from an inhomogeneous ionosphere, J. Research NBS 67D (Radio Prop.), Part I. Exponentially varying isotropic model, No. 3, 361-367 (May-Jun. 1963); Part II. Perturbed exponential model, No. 5, 519-523 (Sept. -Oct. 1963); Part III. Exponential model with hyperbolic transition, No. 6, 747-752 (Nov. -Dec. 1963.)

Wait, J.R., and L.C. Walters (Jan. 1964), Reflection of electromagnetic waves from a lossy magnetopoasma, Radio Sci. J. Res. NBS/USNC-URSI 68D, No. 1, 95-101. (See also, by same authors, Numerical calculations for reflection of electromagnetic waves from a lossy magnetoplasma, NBS Tech. Note No. 205, Nov. 21, 1963.)

Watt, A.D., and R.D. Crogan (Jan. 1964), Comparison of observed VLF attenuation rates and excitation factors with theory, Radio Sci. J. Res. NBS/USNC-URSI 68D, No. 1, 1-9.

Additional References

Barrington, R.E., and E. Thrane (1962), The determination of D-region electron densities from observations of cross modulation, J. Atmos. Terrest. Phys. 24, 31-42.

Bates, H.F., and P.R. Albee (Jul. 1964), High latitude VLF propagation, Final report on N.B.S. Contract CST-7388 from the University of Alaska.

Berry, L.A. (Jan. 1964), Some remarks on the Watson transformation and mode theory, Radio Sci. J. Res. NBS/USNC-URSI 68D, No. 1, 59-66.

Blackband, W. T. (Feb. 1964), The first mode coupling factor for VLF aerials, Tech. Note No. RAD-860, Royal Aircraft Establishment, Ministry of Aviation, London.

Burgess, B. (Jan. 1964), Some experimental results concerning non-reciprocal east-west VLF wave propagation, Radio Sci. J. Res. NBS/USNC-URSI 68D, No. 1, 17-18.

Crombie, D. D. (1958), Differences between east-west and west-east propagation over long distances, J. Atmos. Terrest. Phys. 12, 110-117.

Crombie, D. D. (Sept.Oct.1961), Reflection from a sharply bounded ionosphere for VLF propagation perpendicular to the magnetic meridian, J. Res. NBS 65D (Radio Prop.), No. 5, 455-464.

Crombie, D. D., and A. G. Jean (May, 1964), The guided propagation of ELF and VLF radio waves between the earth and the ionosphere, Radio Sci. J. Res. NBS/USNC-URSI 68D, No. 5, 584-588.

Galejs J. (Jun. 1964), ELF and VLF waves below an inhomogeneous anisotropic ionosphere, Radio Sci. J. Res. NBS/USNC-URSI 68D, No. 6, 693-707.

Hanselman, J. C., C. J. Casselman, M. L. Tibbals, and J. E. Bickel (Jan. 1964), Field intensity measurements at 10.2 kc/s over reciprocal paths, Radio Sci. J. Res. NBS/USNC-URSI 68D, No. 1, 11-14.

Jean, A. G., W. L. Taylor, and J. R. Wait (Mar. 1960), VLF phase characteristics deduced from atmospheric waveforms, J. Geophys. Res. 65, No. 3, 907-912.

Johler, J. R. (Jan. 1964), Concerning limitations and further corrections to geometric-optical theory for LF, VLF propagation between the ionosphere and the ground, Radio Sci. J. Res. NBS/USNC-URSI 68D, No. 1, 67-78.

Johler, J.R., and L.C. Walters (May-June 1960), On the theory of reflection of low- and very-low radiofrequency waves from the ionosphere, J. Res. NBS 64D (Radio Prop.), No. 3, 269-285.

Pierce, J.A., W. Palmer, A.D. Watt, and R.H. Woodward (1 June 1964), Omega, a world wide navigation system, Publication No. 886, Pickard and Burns Electronics (Company), Waltham, Mass.

Rhoads, F.J., W.E. Garner, and J. E. Rogerson (1963), Some experimental evidence of directional effects on VLF propagation (private communication).

Volland, H. (Mar. 1964), Zur Theorie der Aubreitung langer elektromagnetischer Wellen, Archiv der Elektrischen Uebertragung 18, 181-188.

Wait, J.R. (1958), A study of VLF field strength data: Both old and new, Geofis. Pura e Appl. (Milano) 41, 73-85.

Wait, J.R. (Sept. 1962), Excitation of modes at very low frequency in the earth-ionosphere waveguide, J. Geophys. Res. 67, No. 10, 3823-3828.

Wait, J.R. (Jan. 1, 1963), A note on diurnal phase changes of very-low frequency waves for long paths, J. Geophys. Res. 68, No. 1, 338-340.

Wait, J.R., and K. P. Spies (Mar. 1961), A note on phase velocity of VLF radio waves, J. Geophys. Res. 66, No. 3, 992-993.

Watt, A.D. (1965), VLF Handbook (Pergamon Press, Oxford).

Westfall, W.D. (Nov. 1, 1964), Simultaneous measurement of phase and amplitude of NAA very low frequency east-west and west-east radio transmission at San Diego, J. Geophys. Res. 69, 4523-4529.

12. Appended Contour Plots

The graphical propagation data given in this technical note are only valid for a limited range of ionospheric parameters. Such a restriction is imposed by the nature of the physical problem and the economics of the situation.

In order to facilitate calculation for additional parameters, some of the solutions of the waveguide problem have been presented in the form of contour plots in this appendix. The preparation of these graphical presentations is rather time consuming even when the numerical data is available. Thus, even these are limited in scope.

Briefly, the plots in figures 45-62 are designed so that, given the surface impedance Z of the waveguide boundary, the propagation and excitation factors for the dominant modes may be determined by reading the values from the appropriate contours. Following the notation in section 4, the impedance parameters A and B are related to the surface impedance by

$$Z/\eta_o = \Delta = -2(iA - B)^{-1} \quad .$$

Then, on specifying the height h of the reflecting boundary, the contour plots may be used to obtain the attenuation rate, phase velocity, and excitation factor for a given mode. For the curves shown in this appendix, the ground conductivity σ_g is assumed to be infinite. Thus, these results should only be used for propagation over sea water.

In figure 63, similar contour plots are shown to facilitate the conversion from the parameter $\alpha = \alpha_1 + i\alpha_2$ to the parameter $\hat{\alpha} = \hat{\alpha}_1 + i\hat{\alpha}_2$ where $\hat{\alpha}_1 = -B$ and $\hat{\alpha}_2 = A$. These are based simply on the solution of (24) which is described in section 4.

The manner in which the contour plots may be used is explained best by using a few examples:

Case 1; sharply bounded isotropic model with $\omega_r = 2 \times 10^5$, $h = 70$ km, $\sigma_g = \infty$, $f = 20$ kc/s.

Using (19), it is found that

$$A \cong \sqrt{2} \left[\left(\frac{\omega_r}{\omega} \right)^{\frac{1}{2}} - \left(\frac{\omega}{\omega_r} \right)^{\frac{1}{2}} \right] = 0.67$$

and

$$B = \sqrt{2} \left[\left(\frac{\omega_r}{\omega} \right)^{\frac{1}{2}} + \left(\frac{\omega}{\omega_r} \right)^{\frac{1}{2}} \right] = 2.91 \ .$$

From figure 50, it is seen that the attenuation is 1.50 db/1000 km when the phase velocity relative to c is -0.224 percent for $n = 1$. Similarly, using figure 52, it is seen that the attenuation is 5.7 db/1000 km, while the phase velocity relative to c is +0.82 percent for $n = 2$. These compare very well with similar calculations for the same model published elsewhere [Wait, 1963].

Case 2; sharply bounded isotropic model with $\omega_r = 4.9 \times 10^4$, $h = 64$ km, $\sigma_g = \infty$, $f = 10$ kc/s. In order to make use of the contour plots for $h = 70$ km, we note that $A(64)$ for a reference height of 64 may be transformed approximately to the corresponding value $A(70)$ for a reference height of 70 km by the simple relation

$$A(70) \cong A(64) + (4\pi/\lambda)(70 - 64) \cong 2.21 \ , \quad \text{while,}$$

within a good first approximation, B remains unchanged. Thus,

$$B = 2.8$$

Using figure 50, it is readily found that the attenuation rate is 3.2 db/1000 km for n = 1, while the phase velocity relative to c is 0.34 percent also for n = 1. These values compare well with the computations for this situation as quoted by Krasnushkin [1962] who used an entirely different method of calculation.

As indicated in the latter example, the contour plots, while prepared for a fixed reflecting height, may be used somewhat approximately for other heights. Such interpolation (or extrapolation) is valid when the reflection coefficient may be approximated by the form $-\exp(\alpha C')$ for a reference height h. Thus, if the reference height is changed to $h - \Delta h$, then the new form of the reflection coefficient must be $-\exp[(\alpha - i 4\pi \Delta h/\lambda) C']$, provided C', the local angle of incidence, does not change significantly. Thus, as suggested above, the value of $\alpha(h)$ for a reference height h is related to the value of $\alpha(h - \Delta h)$ by the simple formula

$$\alpha(h) \cong \alpha(h - \Delta h) + 4\pi i \Delta h/\lambda \quad .$$

A rather stringent test of this concept is to transfer data from say a height of 80 km to a height of 70 km. For example, if we are given $\alpha_1 = -3.0$, $\alpha_2 = 0$, h = 70 km, f = 20 kc/s, and $\sigma_g = \infty$, how could we estimate the appropriate propagation factors if only the h = 80 km contour plots were available? To answer this question, we note that

$$\alpha_2(80) = \alpha_2(70) + 40\pi/15 = 8.4 \quad .$$

Now, using the contour plots in figure 63, we would find that for
h = 80 km, B = 4.4 and A = 9.1 . From the h = 80 km con-
tour plots in figure 50, it is thus found that the attenuation and phase
velocity factors are 1.6 db/1000 km and -0.23 %, respectively. With-
in this accuracy, these are identical to values read directly from the
corresponding contour plots for h = 70 km where we use the original
values $\alpha_1 \cong -B = -3.0$ and $\alpha_2 \cong A \cong 0$.

It would appear from the above tests and other ones not described
here, that the contour plots for fixed heights of h = 70, 80, and
90 km may be used for interpolation to other heights and to a certain
amount of extrapolation below the 70 km level (say, down to 60 km).

Another important feature of the contour plots is the one-to-one
correspondence, for a given mode between impedance parameters A
and B and propagation factors such as attenuation rate and phase
velocity. This raises the possibility that the observed characteristics
of the propagation may be inverted to yield the impedance parameters
at the reference boundary of the waveguide. This aspect of the prob-
lem is outside the scope of the present technical note.

f = 10 kc/s, h = 70 km, $\sigma_g = \infty$, n = 1
ATTENUATION IN db/1000 km
PHASE VELOCITY RELATIVE TO c IN %

f = 10 kc/s, h = 80 km, $\sigma_g = \infty$, n = 1
ATTENUATION IN db/1000 km
PHASE VELOCITY RELATIVE TO c IN %

f = 10 kc/s, h = 90 km, $\sigma_g = \infty$, n = 1
ATTENUATION IN db/1000 km
PHASE VELOCITY RELATIVE TO c IN %

FIGURE 45

12-5

f = 10 kc/s, h = 80 km, $\sigma_g = \infty$, n = 1
PHASE OF Λ IN DEGREES Λ IN db

f = 10 kc/s, h = 90 km, $\sigma_g = \infty$, n = 1
PHASE OF Λ IN DEGREES Λ IN db

FIGURE 46

12-6

FIGURE 47

12-7

f = 16 kc/s, h = 70 km, $\sigma_g = \infty$, n = 1
PHASE OF Δ IN DEGREES Δ IN db

f = 16 kc/s, h = 80 km, $\sigma_g = \infty$, n = 1
PHASE OF Δ IN DEGREES $|\Delta|$ IN db

f = 16 kc/s, h = 90 km, $\sigma_g = \infty$, n = 1
PHASE OF Δ IN DEGREES Δ IN db

FIGURE 48

f = 16 kc/s, h = 80 km, $\sigma_g = \infty$, n = 2
ATTENUATION IN db/1000 km
PHASE VELOCITY RELATIVE TO c IN %

f = 16 kc/s, h = 90 km, $\sigma_g = \infty$, n = 2
PHASE OF Λ IN DEGREES Λ IN db

FIGURE 49

f=20 kc/s, h=70 km, $\sigma_g = \infty$, n=1
ATTENUATION IN db/1000 km
PHASE VELOCITY RELATIVE TO c IN %

f=20 kc/s, h=80 km, $\sigma_g = \infty$, n=1
ATTENUATION IN db/1000 km
PHASE VELOCITY RELATIVE TO c IN %

f= 20 kc/s, h= 90 km, $\sigma_g = \infty$, n=1
ATTENUATION IN db/1000 km
PHASE VELOCITY RELATIVE TO c IN %

FIGURE 50

12-10

f = 20 kc/s, h = 70 km, $\sigma_g = \infty$, n = 1
PHASE OF Δ IN DEGREES Δ IN db

f = 20 kc/s, h = 80 km, $\sigma_g = \infty$, n = 1
PHASE OF Δ IN DEGREES $|\Delta|$ IN db

f = 20 kc/s, h = 90 km, $\sigma_g = \infty$, n = 1
PHASE OF Δ IN DEGREES Δ IN db

FIGURE 51

12-11

f = 20 kc/s, h = 70 km, $\sigma_g = \infty$, n = 2
ATTENUATION IN db/1000 km
PHASE VELOCITY RELATIVE TO c IN %

f = 20 kc/s, h = 70 km, $\sigma_g = \infty$, n = 2
PHASE OF Λ IN DEGREES Λ IN db

f = 20 kc/s, h = 80 km, $\sigma_g = \infty$, n = 2
ATTENUATION IN db/1000 km
PHASE VELOCITY RELATIVE TO c IN %

FIGURE 52

12-12

f=24 kc/s, h=70 km, σ_g=∞, n=1
ATTENUATION IN db/1000 km
PHASE VELOCITY RELATIVE TO c IN %

f=24 kc/s, h=90 km, σ_g=∞, n=1
ATTENUATION IN db/1000 km
PHASE VELOCITY RELATIVE TO c IN %

FIGURE 53

12-13

f=24 kc/s, h=70 km, $\sigma_g=\infty$, n=1
PHASE OF Λ IN DEGREES Λ IN db

f=24 kc/s, h=90 km, $\sigma_g=\infty$, n=1
PHASE OF Λ IN DEGREES Λ IN db

FIGURE 54

12-14

f=24 kc/s, h=70 km, $\sigma_g = \infty$, n=2
ATTENUATION IN db/1000 km
PHASE VELOCITY RELATIVE TO c IN %

f=24 kc/s, h=70 km, $\sigma_g = \infty$, n=2
PHASE OF Λ IN DEGREES
$|\Lambda|$ IN db

FIGURE 55

f=24 kc/s, h=80 km, $\sigma_g = \infty$, n=2
ATTENUATION IN db/1000 km
PHASE VELOCITY RELATIVE TO c IN %

f=24 kc/s, h=80 km, $\sigma_g = \infty$, n=3
ATTENUATION IN db/1000 km
PHASE VELOCITY RELATIVE TO c IN %
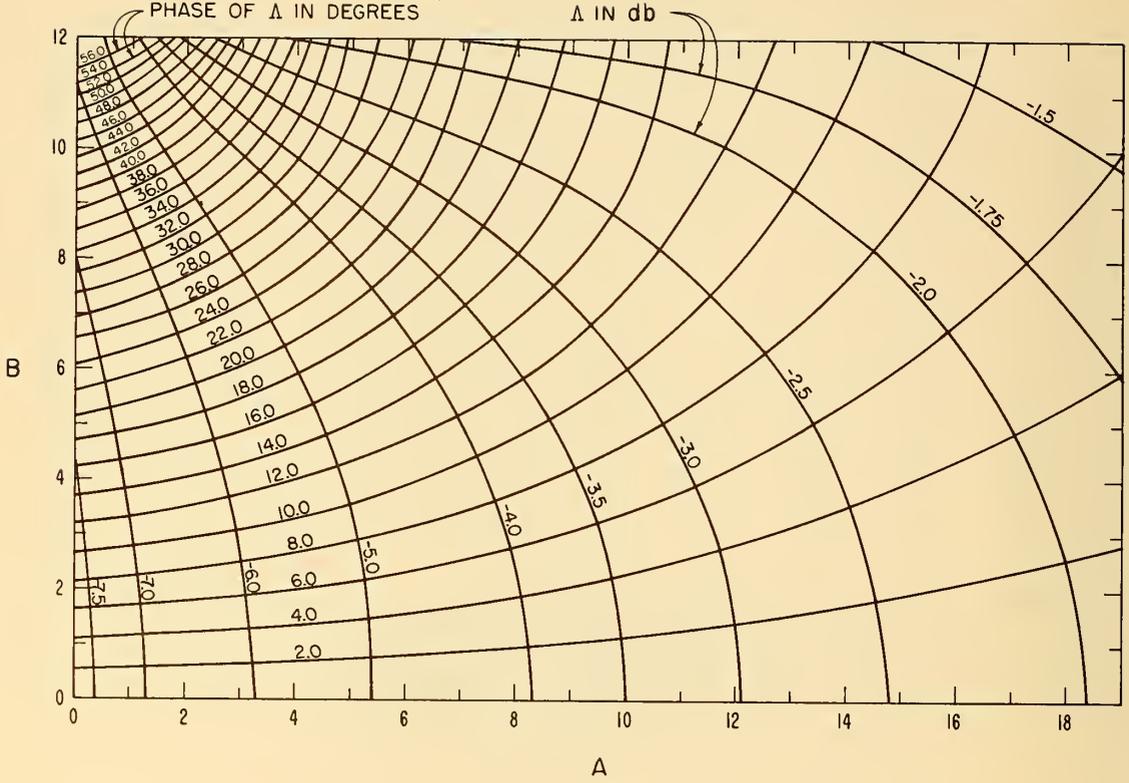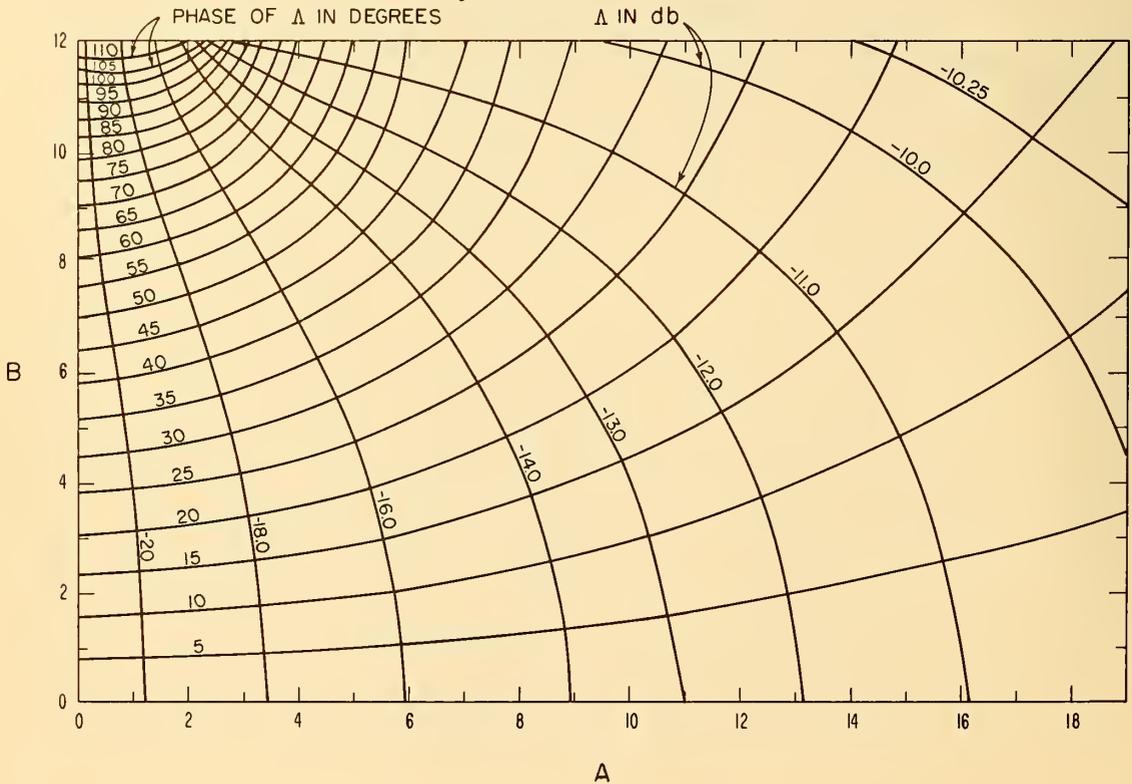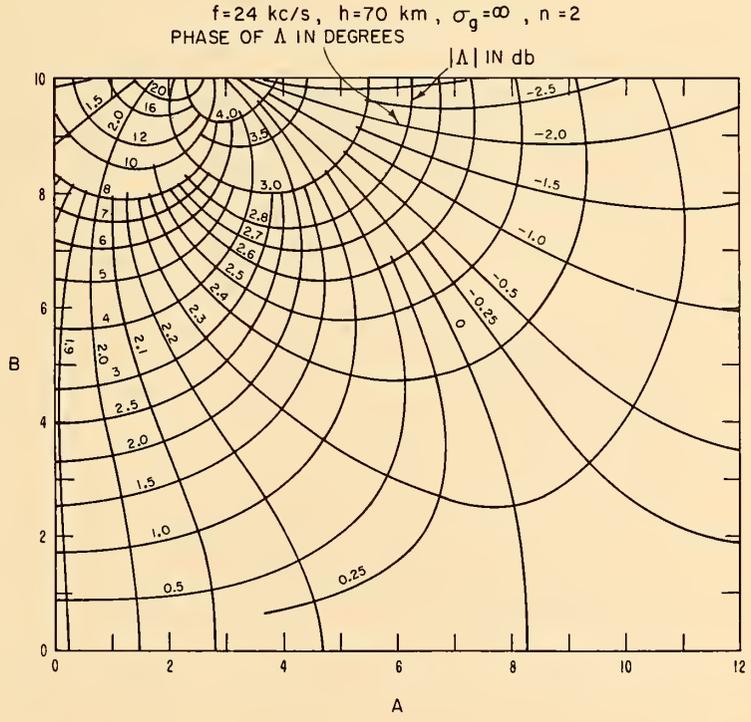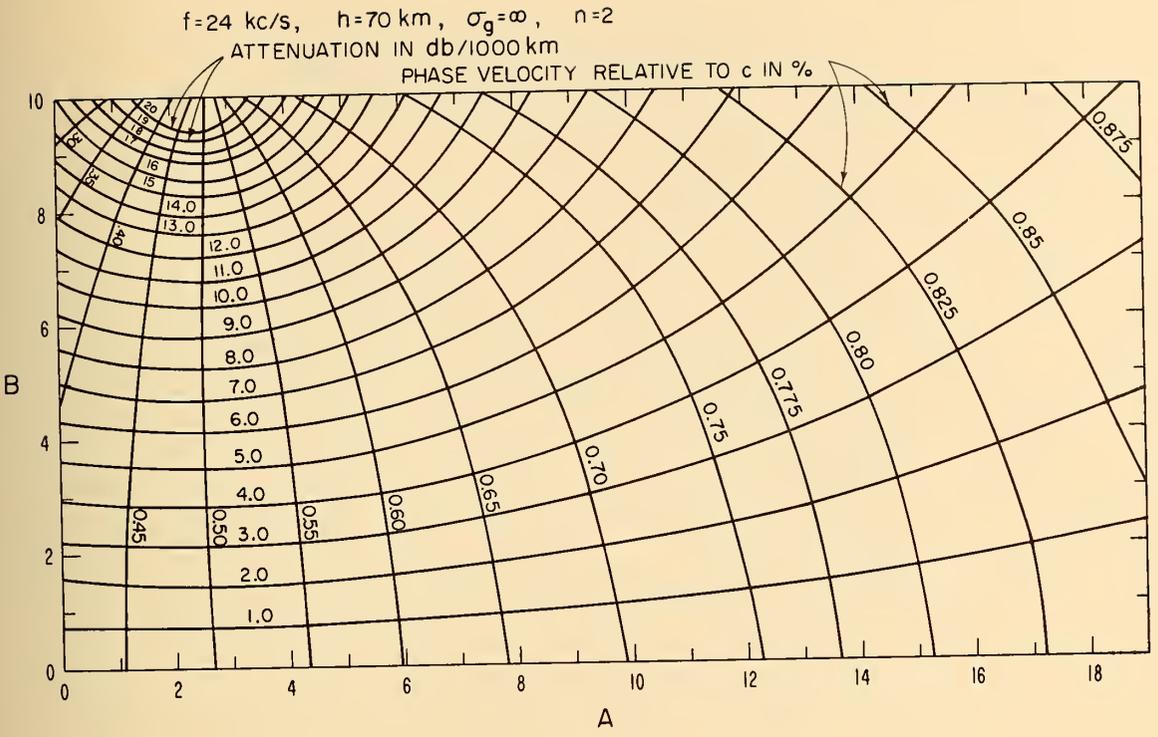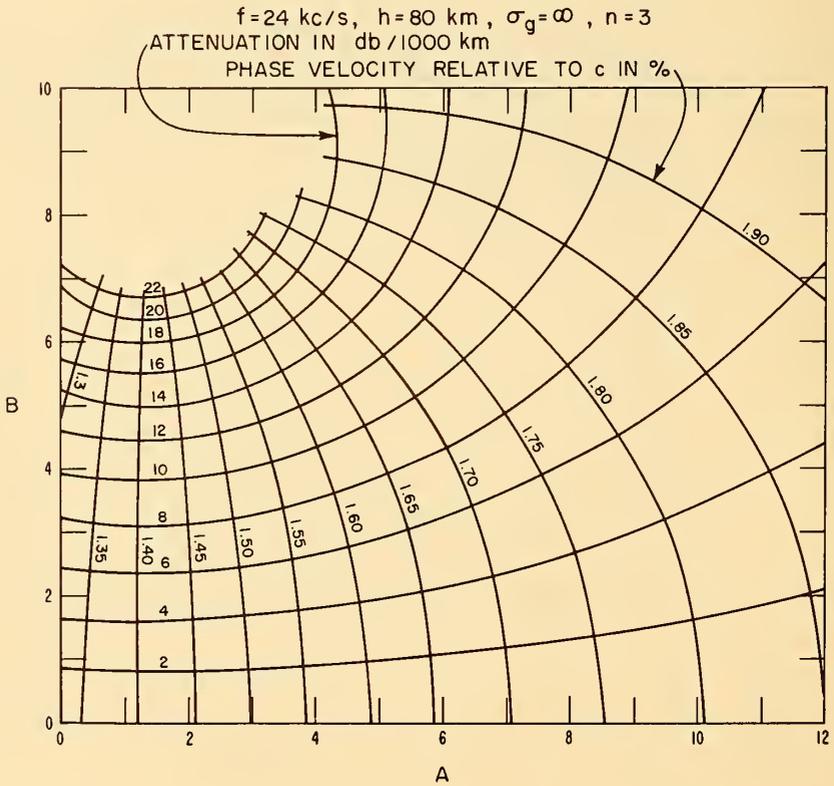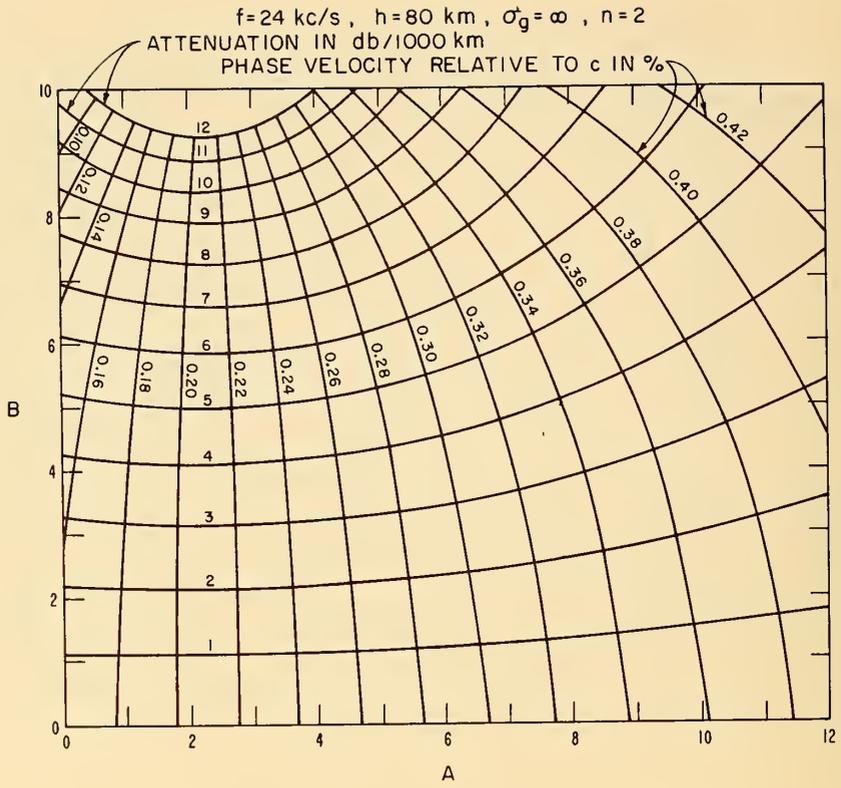
FIGURE 56

12-16

f=24 kc/s, h=90 km, $\sigma_g = \infty$, n=3

ATTENUATION IN db /1000 km

PHASE VELOCITY RELATIVE TO c IN %

FIGURE 57

f = 30 kc/s, h = 70 km, $\sigma_g = \infty$, n = 1
ATTENUATION IN db/1000 km
PHASE VELOCITY RELATIVE TO c IN %

f = 30 kc/s, h = 90 km, $\sigma_g = \infty$, n = 1
ATTENUATION IN db/1000 km
PHASE VELOCITY RELATIVE TO c IN %

FIGURE 58

12-18

f=30 kc/s, h=70 km, $\sigma_g = \infty$, n=1
PHASE OF Λ IN DEGREES Λ IN db

f=30 kc/s, h=90 km, $\sigma_g = \infty$, n=1
PHASE OF Λ IN DEGREES Λ IN db

FIGURE 59

12-19
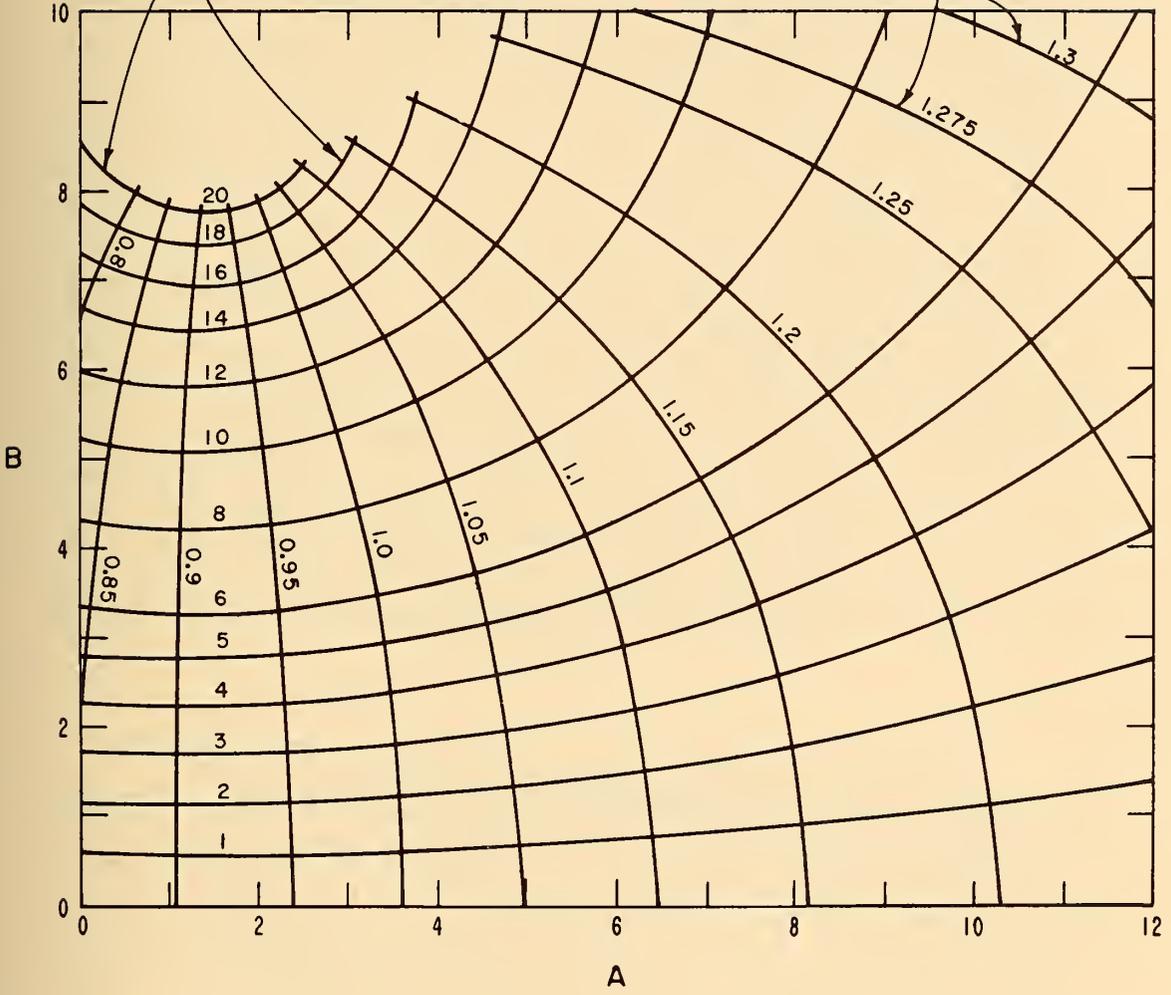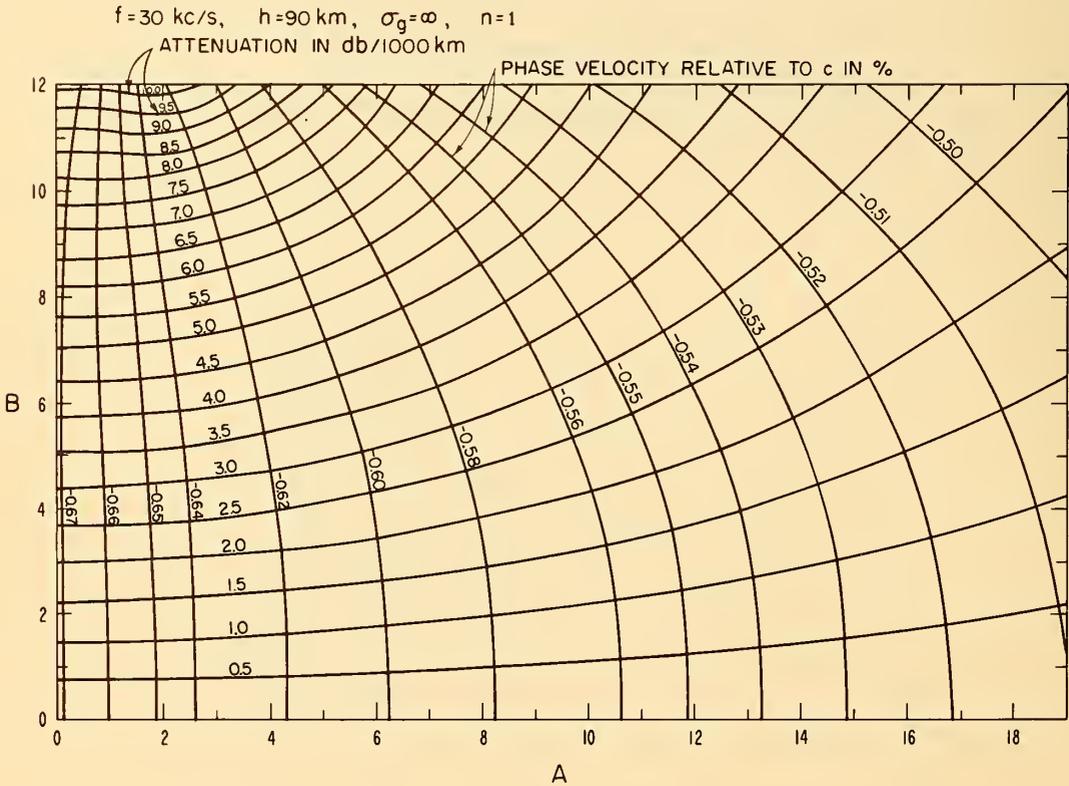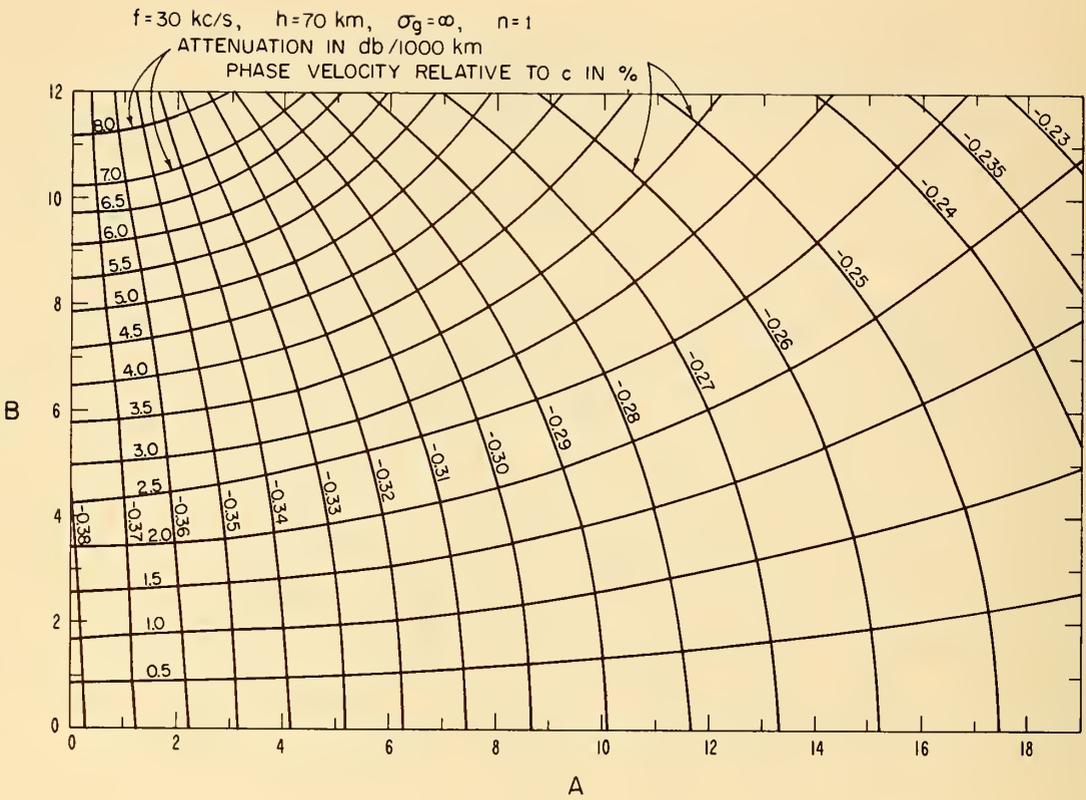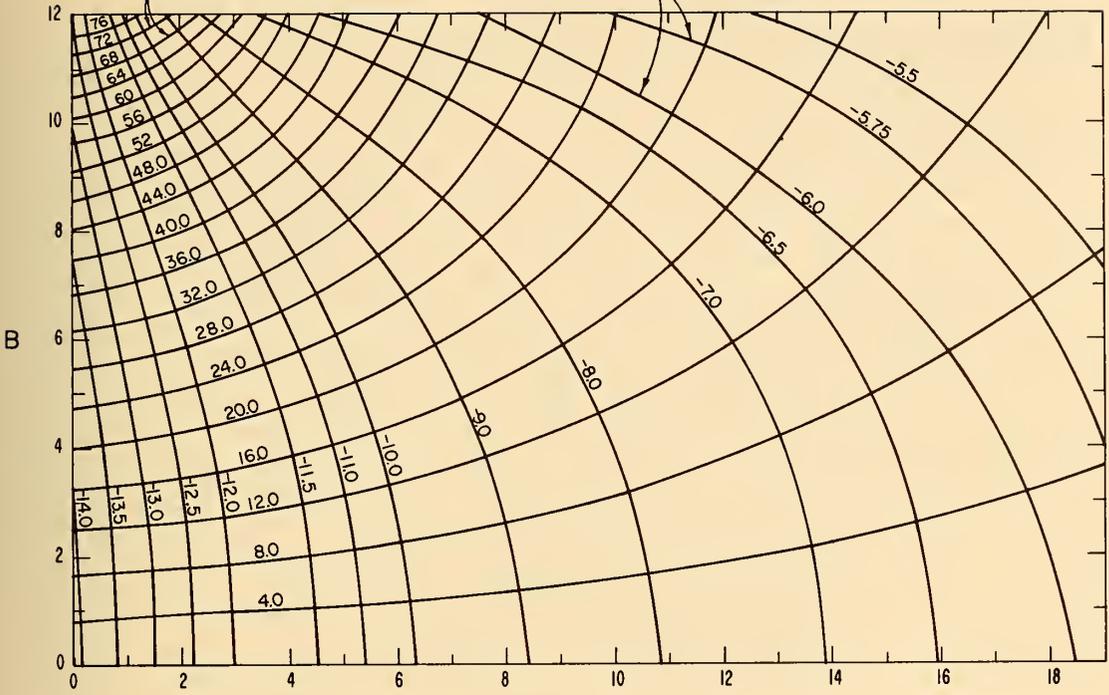
f = 30 kc/s, h = 70 km, $\sigma_g = \infty$, n = 2
ATTENUATION IN db /1000 km
PHASE VELOCITY RELATIVE TO c IN%
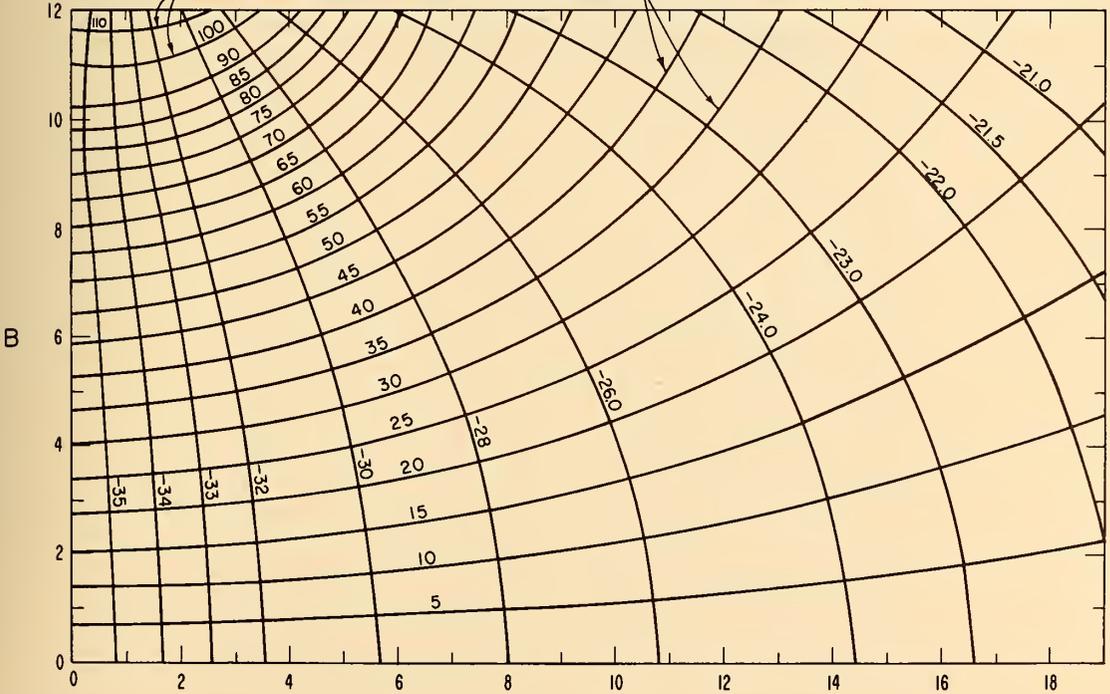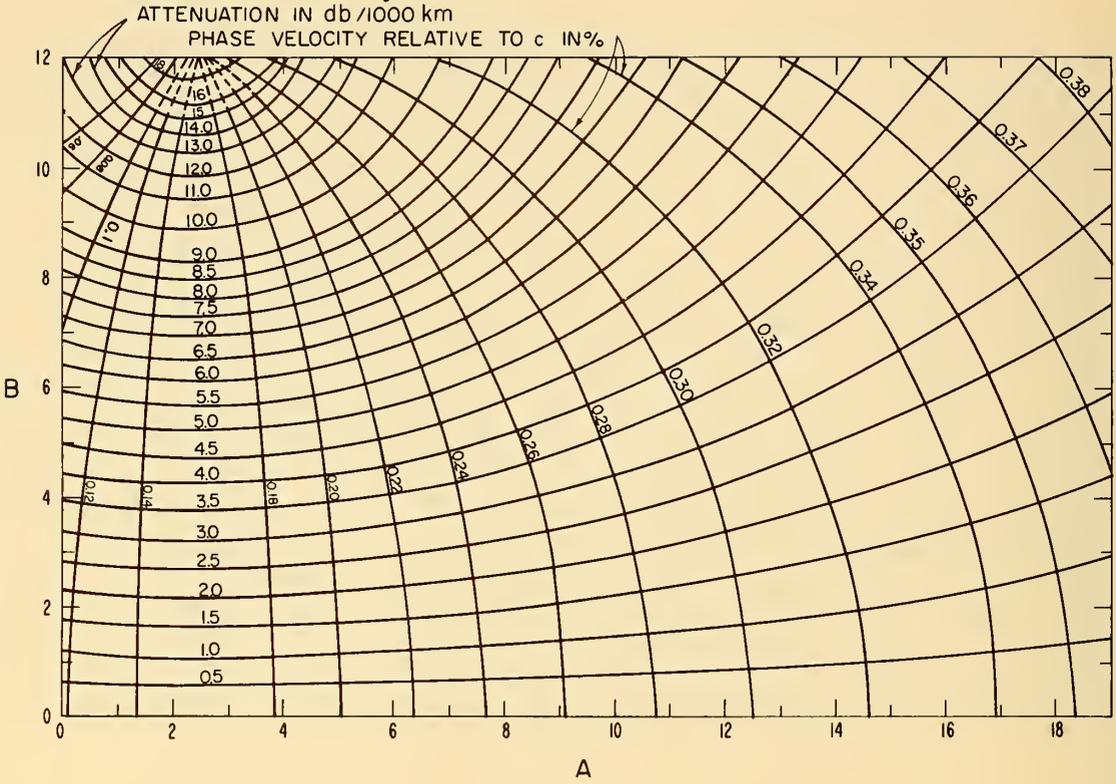
f = 30 kc/s, h = 90 km, $\sigma_g = \infty$, n = 2
ATTENUATION IN db /1000 km
PHASE VELOCITY RELATIVE TO c IN %

FIGURE 60

12-20

$f = 30\ kc/s,\ h = 70\ km,\ \sigma_g = \infty,\ n = 2$
PHASE OF Λ IN DEGREES Λ IN db

FIGURE 61

12-21

f=30 kc/s, h=70 km, $\sigma_g = \infty$, n=3
ATTENUATION IN db/1000 km
PHASE VELOCITY RELATIVE TO c IN %

f=30 kc/s, h=80 km, $\sigma_g = \infty$, n=3
ATTENUATION IN db/1000km
PHASE VELOCITY RELATIVE TO c IN %

f=30 kc/s, h=90 km, $\sigma_g = \infty$, n=3
ATTENUATION IN db/1000 km
PHASE VELOCITY RELATIVE TO c IN %
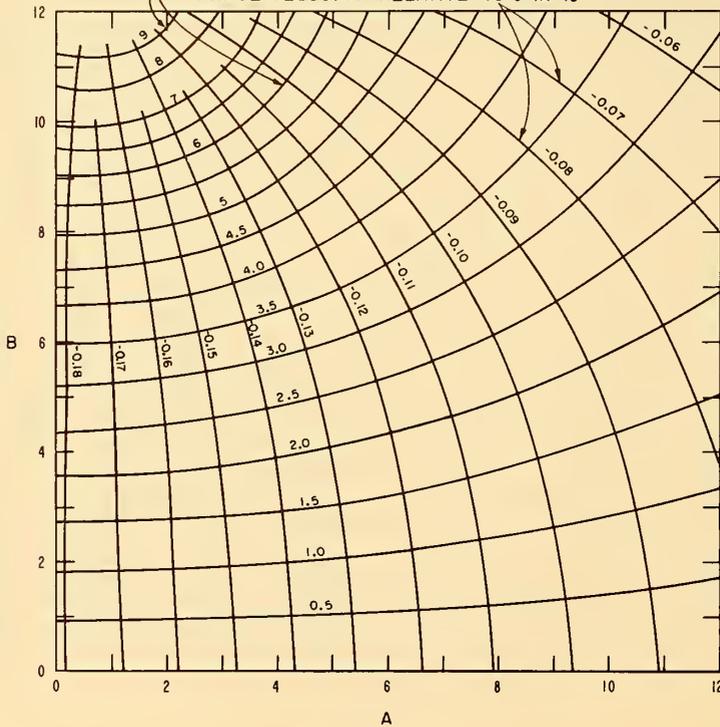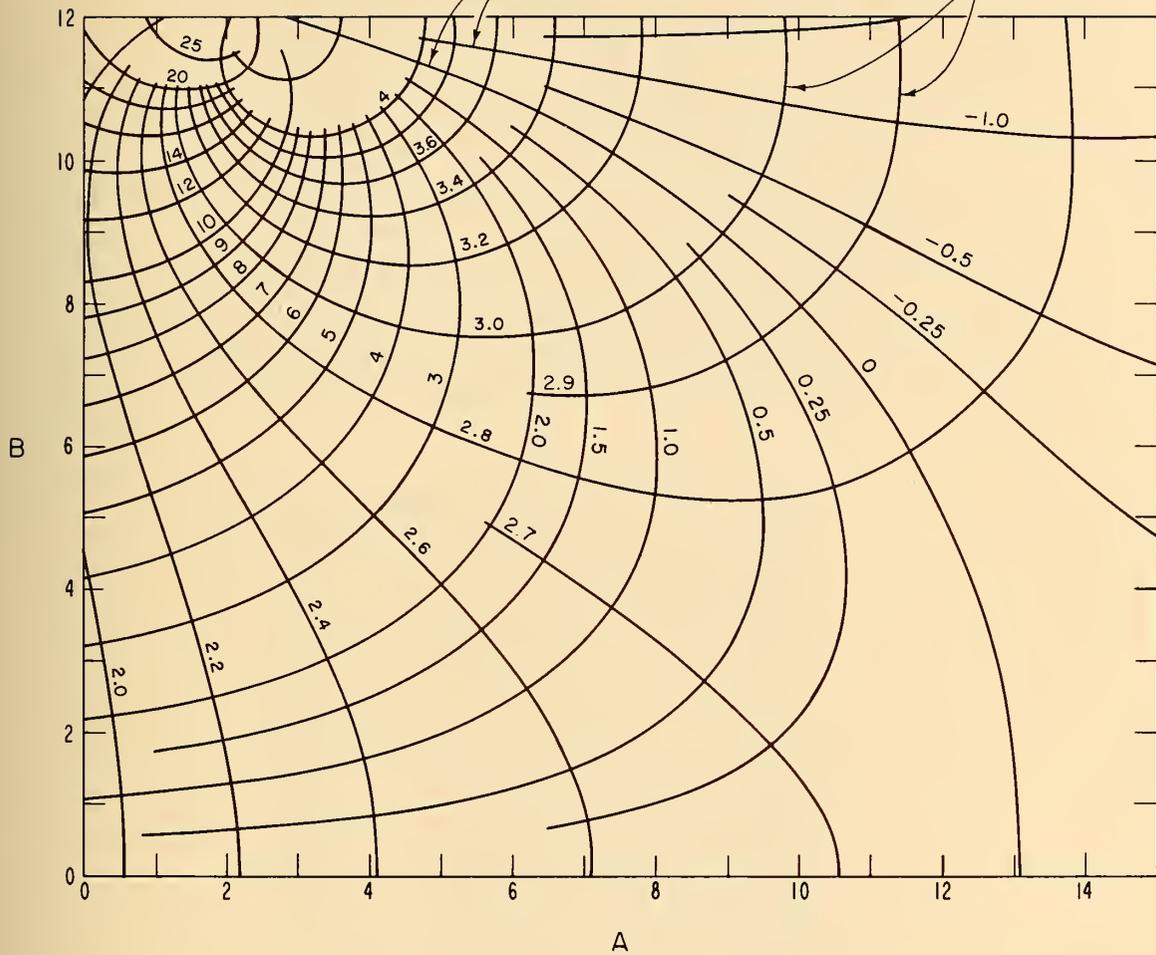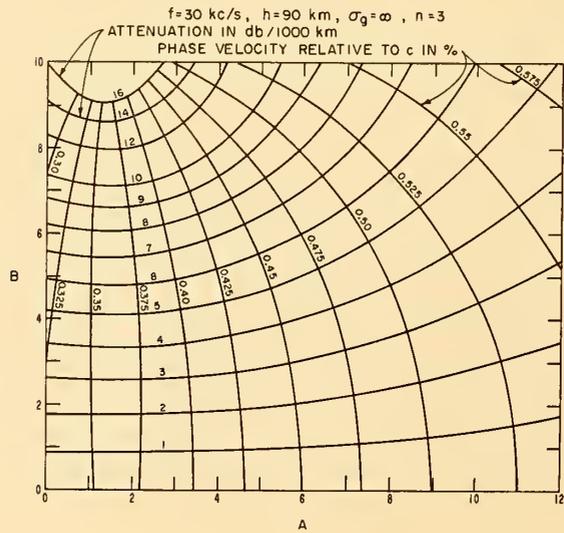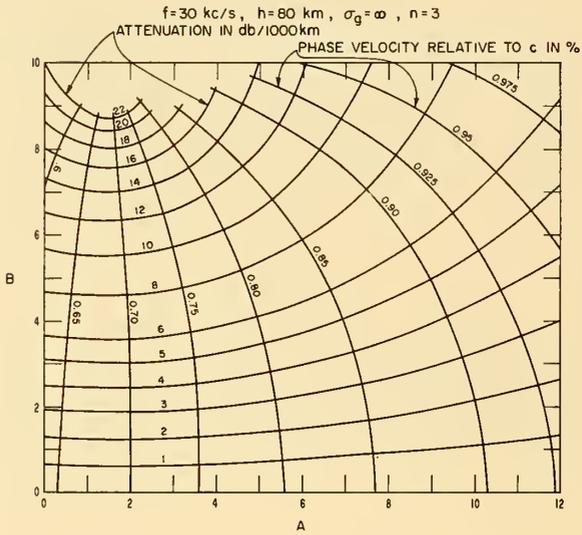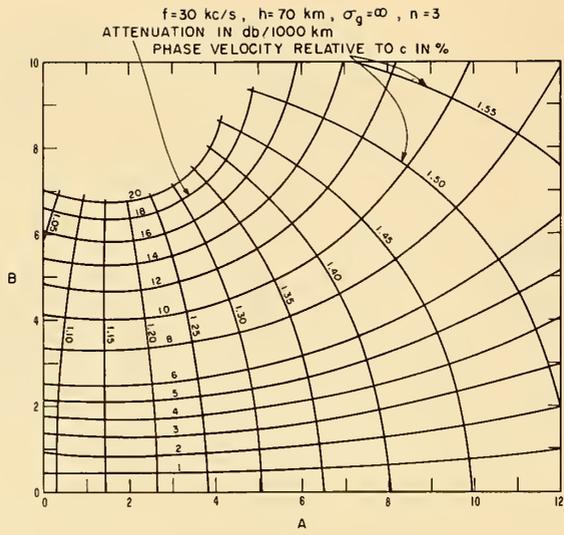
FIGURE 62

12-22
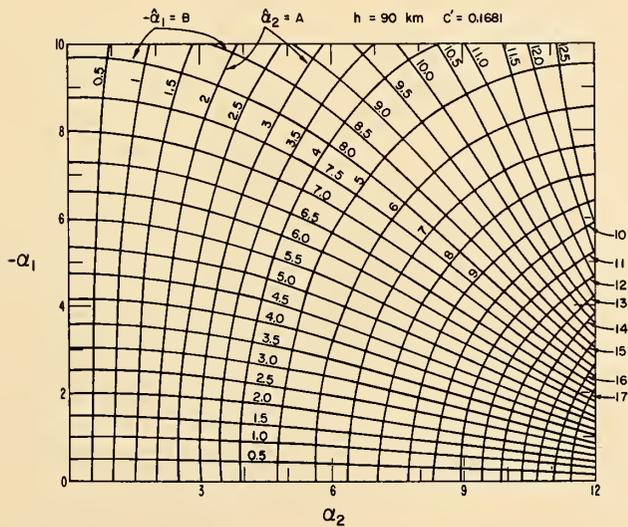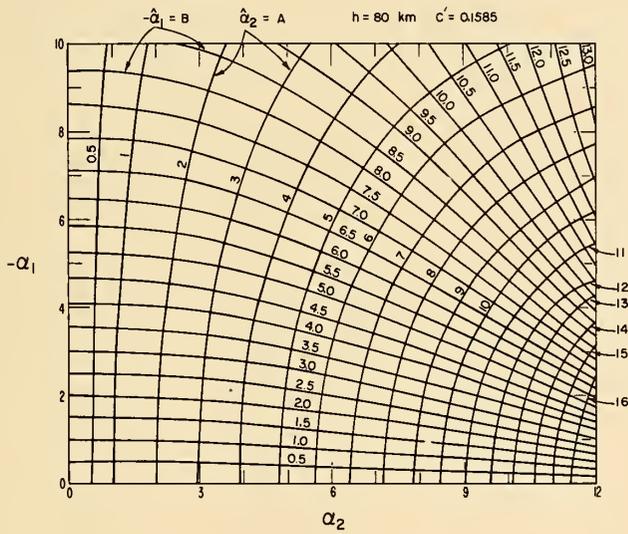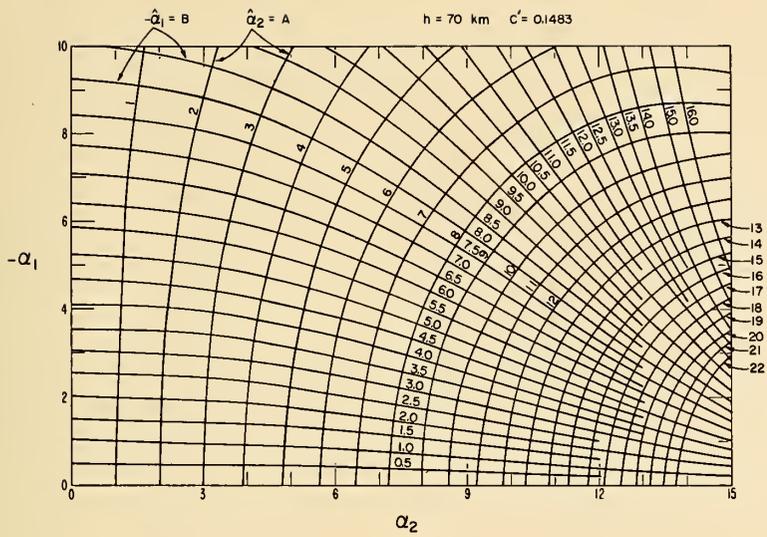
RELATION BETWEEN $\alpha_1 + i\alpha_2$ AND $-B + iA$ FIGURE 63

12-23